AD-A097 297 TEXAS A AND M UNIV COLLEGE STATION MECHANICS AND MAT--ETC F/G 11/4
COMPOSITE MATERIALS FOR STRUCTURAL DESIGN.(U)
FEB 81 R A SCHAPERY, W L BRADLEY, W E HAISLER F49620-78-C-0034
UNCLASSIFIED MM-3724-81-5 AFOSR-TR-81-0326 NL

1 of 2
AD
A097297

AFOSR-TR- 81-0326

Mechanics and Materials Center
TEXAS A&M UNIVERSITY
College Station, Texas

4

LEVEL III

AD A097297

COMPOSITE MATERIALS
FOR
STRUCTURAL DESIGN

(THIRD ANNUAL TECHNICAL REPORT)

DTIC
ELECTE
APR 0 3 1981
S D
F

AIR FORCE OFFICE OF SCIENTIFIC RESEARCH
OFFICE OF AEROSPACE RESEARCH
UNITED STATES AIR FORCE
CONTRACT NO. F49620-78-C-0034

MM 3724-81-5 FEBRUARY 1981

APPROVED FOR PUBLIC RELEASE: DISTRIBUTION UNLIMITED

81 4 2 041

UNCLASSIFIED

SECURITY CLASSIFICATION OF THIS PAGE (When Data Entered)

REPORT DOCUMENTATION PAGE	READ INSTRUCTIONS BEFORE COMPLETING FORM
1. REPORT NUMBER AFOSR-TR-81-0326 2. GOVT ACCESSION NO. AD-A097297	3. RECIPIENT'S CATALOG NUMBER
4. TITLE (and Subtitle) COMPOSITE MATERIALS FOR STRUCTURAL DESIGN, AD83721	5. TYPE OF REPORT & PERIOD COVERED INTERIM 1 Jan [redacted] – 31 Dec 80
	6. PERFORMING ORG. REPORT NUMBER MM-3724-81-5
7. AUTHOR(s) R. A. Schapery, W. L. Bradley, W. E. Haisler, J. S. Ham, K. L. Jerina, Y. Weitsman	8. CONTRACT OR GRANT NUMBER(s) F49620-78-C-0034
9. PERFORMING ORGANIZATION NAME AND ADDRESS TEXAS A&M UNIVERSITY MECHANICS & MATERIALS CENTER COLLEGE STATION, TX 77843	10. PROGRAM ELEMENT, PROJECT, TASK AREA & WORK UNIT NUMBERS 61102F 2307/B1
11. CONTROLLING OFFICE NAME AND ADDRESS AIR FORCE OFFICE OF SCIENTIFIC RESEARCH/NA BLDG 410 BOLLING AIR FORCE BASE, D C 20332	12. REPORT DATE Feb[redacted]81
	13. NUMBER OF PAGES 125
14. MONITORING AGENCY NAME & ADDRESS(if different from Controlling Office)	15. SECURITY CLASS. (of this report) UNCLASSIFIED
	15a. DECLASSIFICATION DOWNGRADING SCHEDULE

16. DISTRIBUTION STATEMENT (of this Report)

Approved for public release; distribution unlimited.

17. DISTRIBUTION STATEMENT (of the abstract entered in Block 20, if different from Report)

18. SUPPLEMENTARY NOTES

19. KEY WORDS (Continue on reverse side if necessary and identify by block number)

COMPOSITE MATERIALS; THERMOMECHANICAL BEHAVIOR OF RESINS; PROCESSING OF LAMINATES; THERMOMECHANICAL BEHAVIOR OF COMPOSITES; RESINS; DELAMINATION; ADHESIVES; FINITE ELEMENTS; VISCOELASTICITY; AGING OF RESINS; FRACTURE

20. ABSTRACT (Continue on reverse side if necessary and identify by block number)

Summarized are research activities related to polymer-matrix composite materials in the areas of processing and dynamic mechanical testing, physical aging, delamination fracture characterization, temperature and moisture effects, finite element modelling, and fracture and damage analysis of nonlinear viscoelastic materials. Also included are Abstracts of seven M.S. theses and six papers describing several recently completed experimental and analytical research investigations of factors which pertain to processing, testing, and analysis of composite structures.

DD FORM 1 JAN 73 1473

UNCLASSIFIED

SECURITY CLASSIFICATION OF THIS PAGE (When Data Entered)

COMPOSITE MATERIALS FOR STRUCTURAL DESIGN

Third Annual Technical Report

by the

Professional Staff

of the

TEXAS A&M UNIVERSITY

MECHANICS AND MATERIALS CENTER

Submitted to the

Air Force Office of Scientific Research

Office of Aerospace Research

United States Air Force

MM 3724-81-5

Contract No. F49620-78-C-0034

February 1981

TABLE OF CONTENTS

1. INTRODUCTION

1.1 Summary

Primary activities during the third year consisted of (i) expanding the laboratory capabilities for processing and testing of composites, (ii) conducting research in accordance with the Statement of Work given in Section 1.3, (iii) preparing thirteen technical papers and M.S. theses, and (iv) various interactions of the faculty with the technical community through presentation of papers, participation as members of technical committees, etc.

Sections 2 - 4 summarize the research activities. The professional personnel associated with the project and the outside activities of the faculty related to composites are given in Section 5. Papers completed and/or published during the year are reproduced in Appendix A. A brochure describing the student activities is in Appendix B.

We provide only a brief discussion of most activities, as they are detailed in existing reports (Appendix A) or theses, or are in early stages of development. However, the processing and testing facility has been greatly expanded in 1980, but its increased capability is not described elsewhere; thus a relatively detailed description is given (Section 2.1).

1.2 Discussion

The general objective of the research program is to develop improved understanding of fibrous composite material as a basis for improving its structural performance. Integral to achievement of this objective is the determination of constitutive equations and time (or cycles) to fracture for complex loading patterns and hostile environments such as high relative humidity. This in turn requires a better understanding of the viscoelastic deformation and mechanisms of damage growth and fracture in composites including delamination, cumulative damage via microcrack initiation and growth, and global fracture criteria.

The importance of micromechanisms of viscoelastic deformation and fracture of resin matrix composites has only recently become widely appreciated; for example, graphite/epoxy composites are quite sensitive to processing and to service environments, especially moisture [1].* Furthermore, because curing is seldom taken to completion in the epoxies used in graphite/epoxy composites [2], the degree of cure is a processing variable. Physical aging (densification) of the epoxy matrix may occur in service, giving significant changes in mechanical properties [3]. The post-cure cool-down path affects the magnitude of residual stresses in a composite [4]. Moisture absorption can change the glass transition temperature, giving a significant change in mechanical properties [1]. The rate of moisture absorption appears to depend on the degree of curing and physical aging, and moisture content may itself affect the rate of physical aging. The lack of consistency in experimental results and micromechanistic modelling appearing in the composite materials literature today is believed a consequence of the fact that much of the earlier experimental research was conducted without fully controlling all of the important variables which affect resin matrix composites.

It is anticipated that the continuing research program at Texas A&M University described herein will make a major contribution toward more unified methods of characterizing behavior of composite materials by

---

*Numbers in brackets indicate References on p. 48.

identifying and accounting for the important variables. In view of the large number of variables to be considered experimentally, it is essential that the mechanical testing be guided by mechanistic modelling to keep the total amount of experimental work at a manageable level. A considerable part of the effort at Texas A&M University is being so directed. Additionally, some of the theoretical research is leading to analytical methods of predicting deformation and fracture behavior of laminates for use in design analysis of those structures that must withstand severe environments over long periods of time.

1.3 Statement of Work

"a. Investigate the effects of cure cycle parameters on the mechanical characteristics of resins, composites and composite structural specimens:

(1) Study the curing process.

(2) Investigate the effects of cure cycle parameters on physical aging.

(3) Investigate generation, relief and effects of residual stresses in laminates.

b. Investigate deformation, damage growth and fracture behavior for resins, composites and composite structural specimens:

(1) Develop and verify constitutive equations.

(2) Develop and verify ply damage and delamination models.

(3) Develop an automated structural material property characterization system and data base."

2. Processing and Testing of Resins and Composites

2.1 New Equipment and Software*

During the year 1980, several pieces of new equipment were acquired for expansion of the experimental research laboratory to broaden the capability in processing and testing of composite materials. The majority of this equipment was purchased with funds from the Texas Engineering Experiment Station; supplemental funds were provided by AFOSR. The following equipment was purchased, delivered, and installed in the composite materials experimental research laboratory (McNew Building) during the year:

curing oven
vacuum oven
process controller
cold stage for differential scanning calorimeter
diamond tools
humidity monitor
digital thermometer
laboratory oscilloscope and modules
closed loop servohydraulic mechanical test system
MINC-11 laboratory data acquisition and control computer
HP-45 desktop computer
digital oscilloscope
ultrasonic C-scan system
charge amplifier
HP digital plotter
HP-85 desktop computers (2)
data acquisition and control units (2)
synthesizer/function generator

*Prepared by Dr. K. L. Jerina

The laboratory oscilloscope and modules are for general purpose laboratory use and the other equipment has been incorporated into specific functional systems for processing and testing of composite materials.

The capacity for processing and machining of test samples has been enchanced by the addition of a vacuum oven and convection oven. These ovens are used to cure and post cure resins, adhesives and composites fabricated from prepreg systems. An assortment of new diamond tools for the Micromech cutting machine has increased the capacity and quality of machining specimens with hard fibers such as glass and graphite.

The processing press has been used extensively in glass/epoxy and graphite/epoxy specimen fabrication for student and faculty research projects. During the reporting period, a microprocessor-based process controller was installed on the press and control parameters optimized. The process controller makes it possible to generate a wide variety of temperature, vacuum and pressure profiles for cure cycles. New cure cycles are easily programmed in an automatic fashion. Heating or cooling rates of 3°F/min. are possible while controlling within an absolute temperature reading of ±3°F. The best accuracy and control for an arbitrary temperature profile is obtained at a rate of 3°F/Min., although the press is capable of higher heating and cooling rates. The control scheme, Fig. 1, consists of a primary control loop on laminate temperature and two secondary control loops on the upper and lower platen temperatures. The actual laminate temperature is blended with the command temperature profile in a cascade control scheme to command the upper and lower platen heaters and cooling water valves. Optimization of the controller was accomplished through an empirical process of ad-

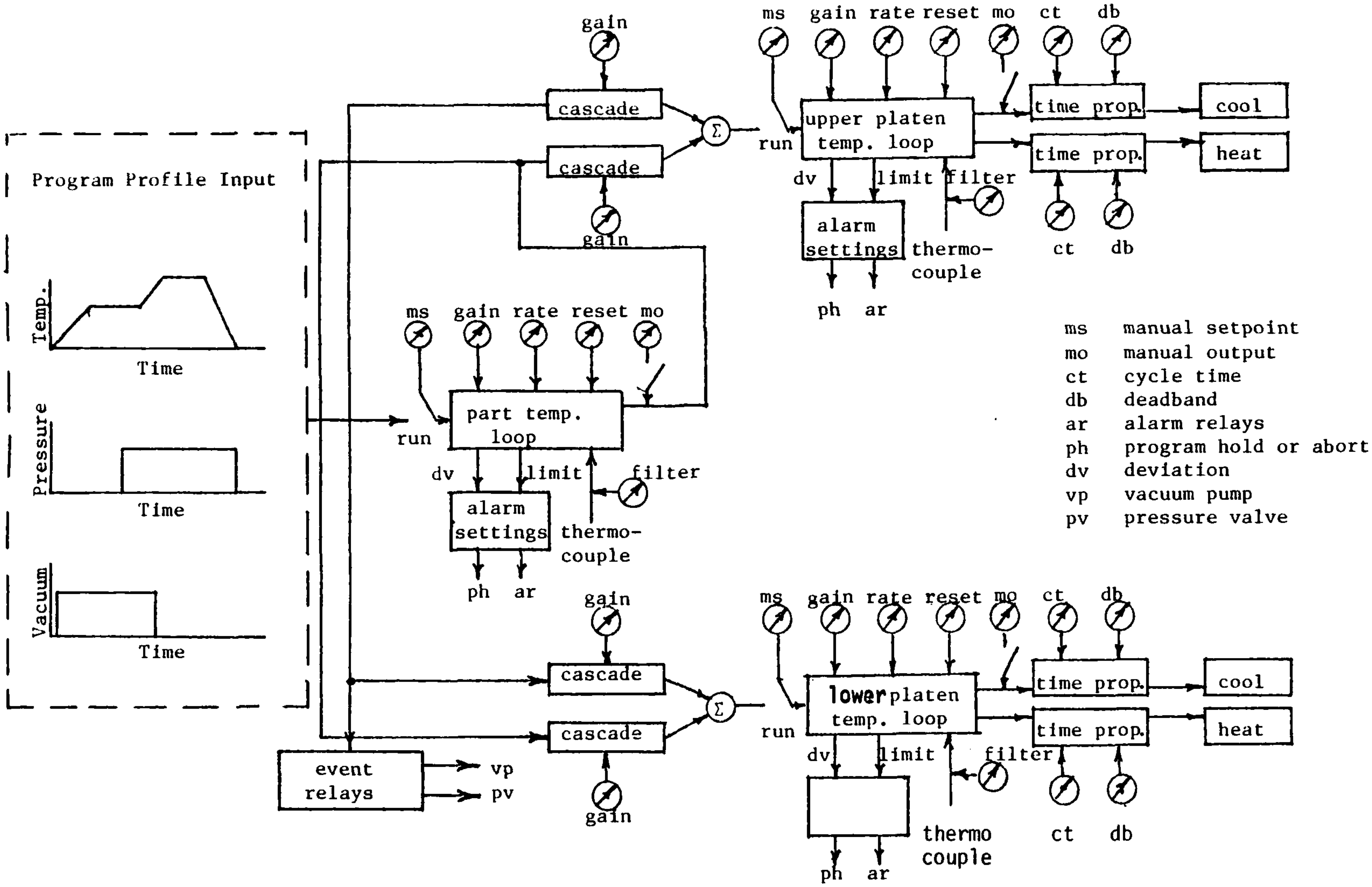

Fig. 1 Block Diagram of Press Controller

justing the individual loop parameters for gain, rate and reset. The controller is interlocked so that an orderly shut down occurs on an error such as over temperature or thermocouple burn out. The press controller has proven successful in increasing production of laminate samples and in improving the accuracy and repeatability of cure cycles. Additionally, the ability to study the effects of cure cycle variation is greatly enchanced by the press controller.

The Perkin Elmer Differential Scanning Calorimeter II has an extended temperature range made possible through the addition of a liquid nitrogen cold stage. Also a MINC-11 laboratory data acquisition and control computer has been interfaced to the DSC, Fig. 2. The temperature and specific heat signals from the DSC are now acquired by the computer through a digital input module and analog-to-digital converter. Under control of a real time computer program the specific heat of a resin sample can be monitored as a function of temperature. Once acquired by the computer, the data can be easily manipulated to subtract baseline calibrations and then permanently stored as part of a data base on floppy disk for later review and analysis. The data can be plotted on a video-graphics terminal or digital plotter. Automation of the DSC has increased the accuracy and repeatability of experiments involving glass transition temperature studies of resins used in composite materials.

New instrumentation has aided the project in development of the piezoelectric "duomorph" complex modulus gage. A charge amplifier, digital oscilloscope, function synthesizer and desktop computer have been incorporated into the instrumentation, Fig. 3. The task of data acquisition and reduction for a typical experiment has been reduced from several weeks to less than a day through automation. The electrical excitation and

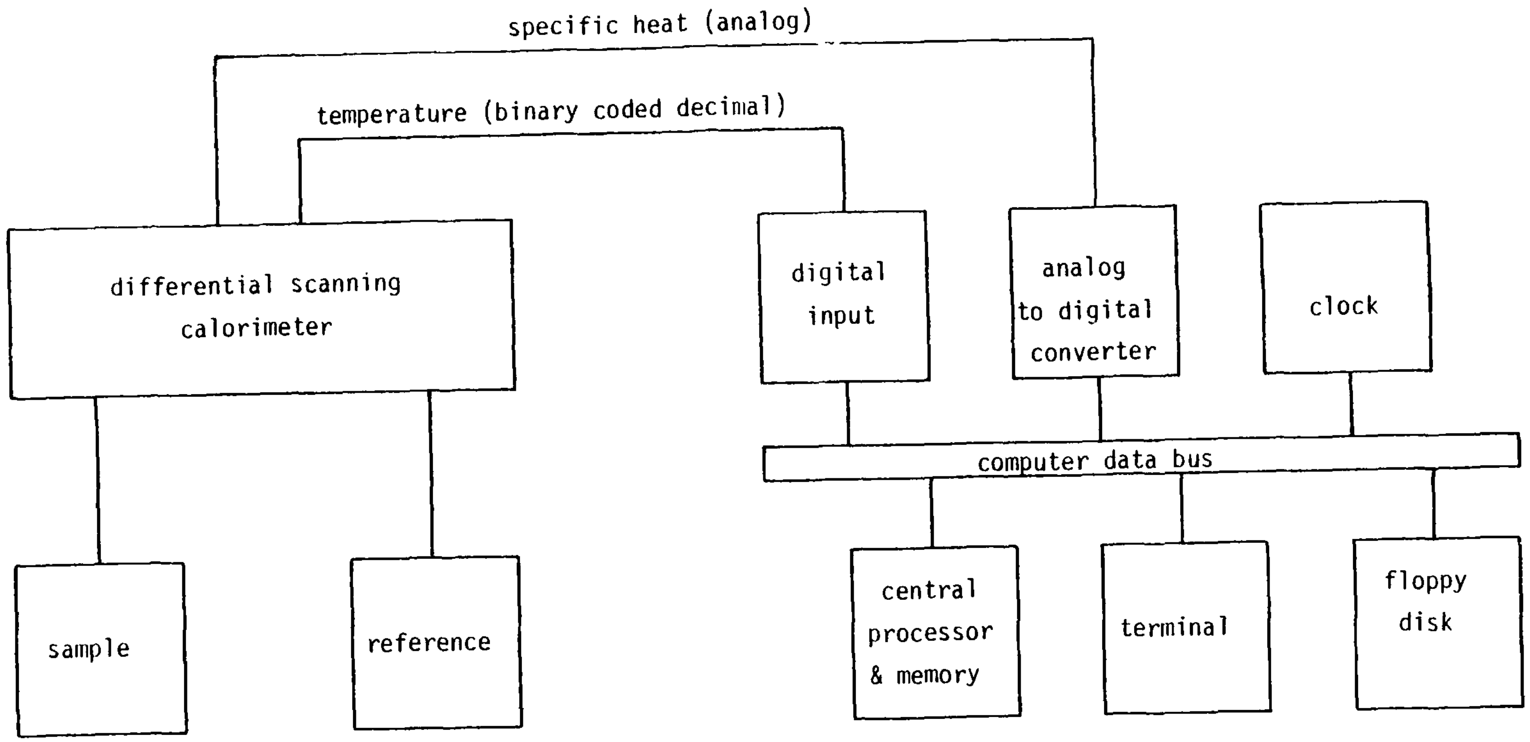

Figure 2 Block diagram of differential scanning calorimeter and laboratory instrument computer

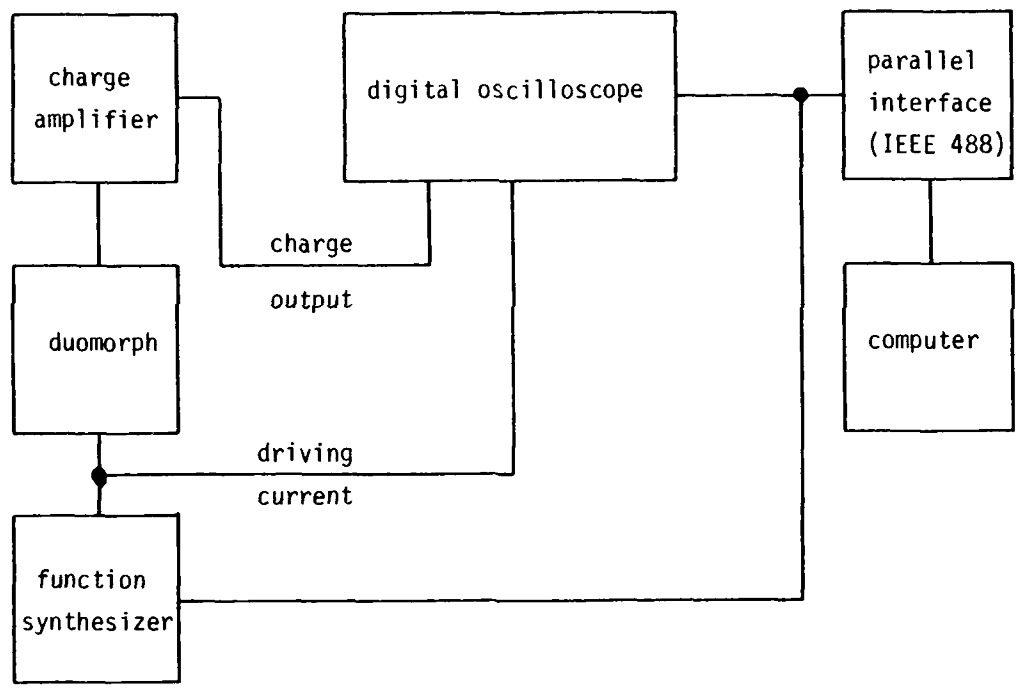

Figure 3 Block diagram of duomorph instrumentation

response of the duomorph are monitored by the digital oscilloscope. Under control of a real time program on the HP-85 desktop computer, excitation frequency is automatically programmed on the function synthesizer and sampled values of the gage excitation and response are transferred to the computer for amplitude and phase angle analysis, Fig. 4. Automation has reduced the data acquisition and analysis time for the duomorph gage, making it possible to consider the duomorph as a real-time cure process monitor if feasability studies are successful.

Management of a mechanical property data base and the analysis of experimental data has been enchanced by an HP-45 desktop computer and HP 9872B digital plotter, Fig. 5. The system is designed to allow analysis of experimental data stored in a data base with a powerful computational capability, video graphics, digital plotter, hard copy graphics, and communications to other laboratory instrument computers. This system has been installed during the reporting period and software is currently being developed to bring the system up to its full usefulness and potential as an interactive graphics system. Fig. 6 shows the graphics capability of the system for a $[\pm 45°]_{2s}$ graphite/epoxy creep experiment. The greatest utility of this data analysis system will be to allow interactive access and analysis of data base information with high quality graphics capability.

Data acquisition for the five channel temperature/humidity creep/recovery system has been accomplished with an HP-85 desktop computer and an HP-3497A data acquisition and control unit, Fig. 7. Also, a multi-point digital thermometer and humidity gage monitor the environmental conditions in the test chambers. Creep and recovery data are acquired by the data acquisition unit under program control from the computer. The program samples two

Figure 4 Data analysis of duomorph excitation and response for amplitude and phase angle (theta)

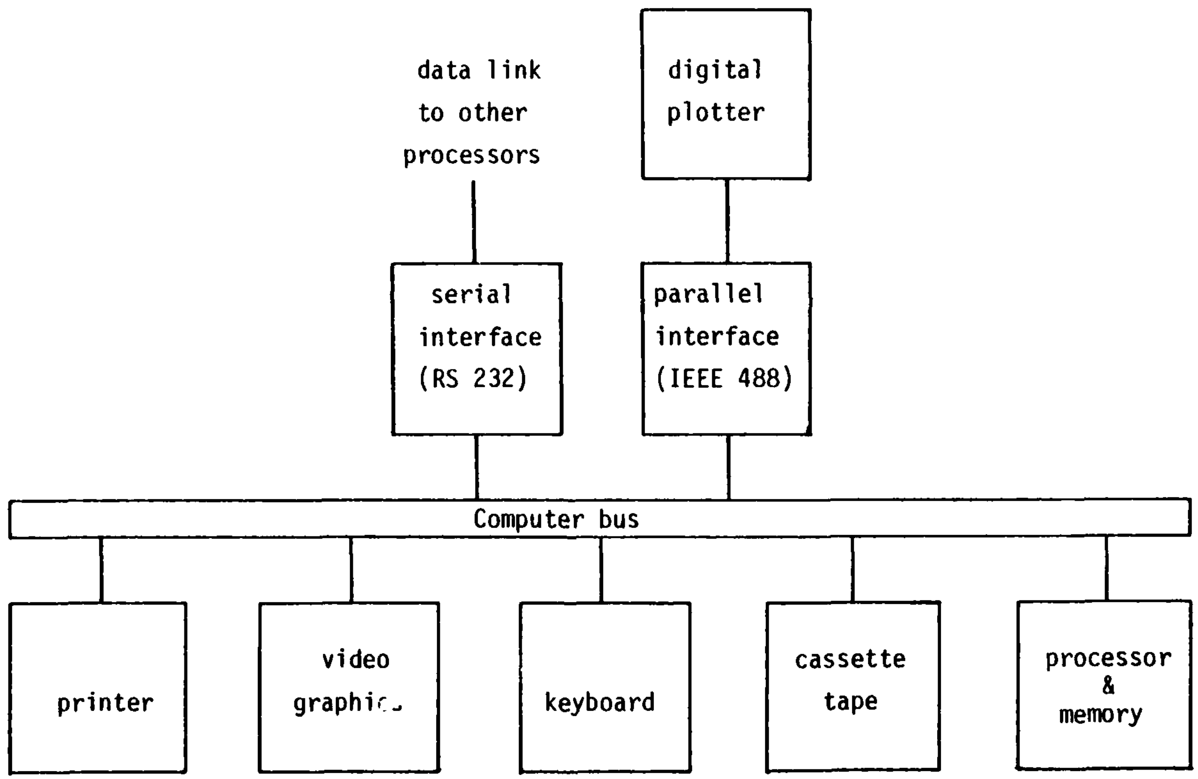

Figure 5 Block diagram of interactive graphics data analysis system

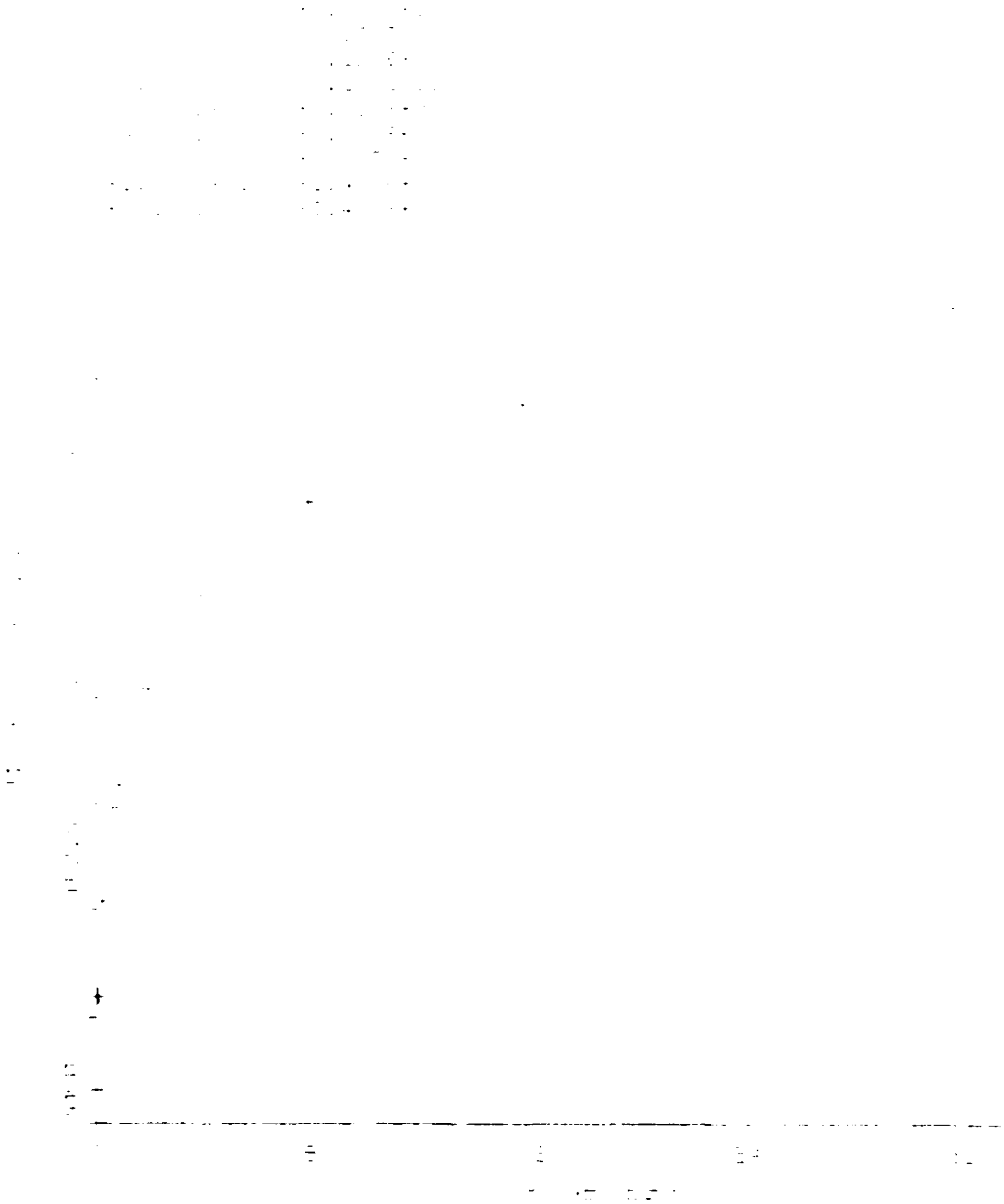

Figure 6 Creep of $[\pm 45]_{2S}$ graphite/epoxy

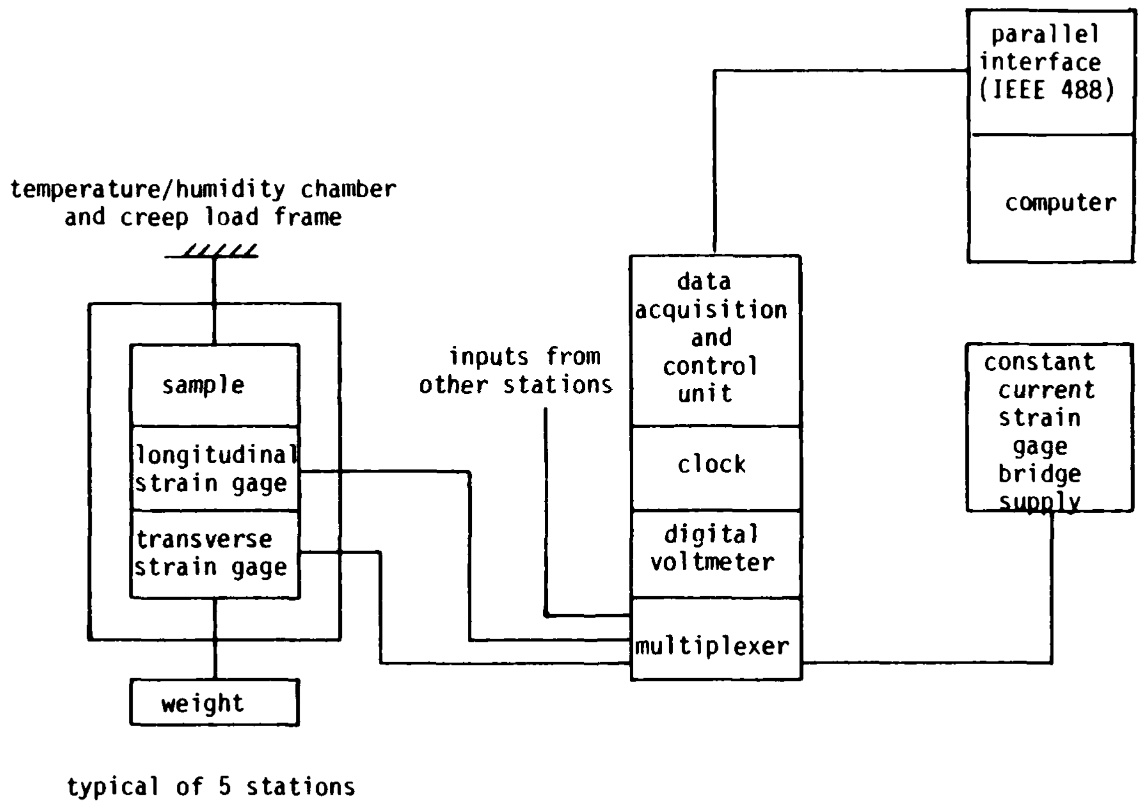

Figure 7 Block diagram of five-station automated creep/recovery temperature/humidity apparatus

channels of strain data from each creep station at logarithmic time intervals. The data are tabulated, Fig. 8, and stored as a file as part of the laboratory data base. Implementation of this hardware configuration has allowed more cost effective and efficient use of laboratory instrumentation.

Capability for non-destructive inspection of composites has been added to the laboratory during the reporting period. A Testtech scanning bridge, tank, and plotter, Panametrics transducers and tranducer conditioner, and an HP delayed sweep oscilloscope give the laboratory an NDT capability for composite laminates, Fig. 9. A selection of transducers in the range of 2.5 to 25 MHz allow inspection of graphite/epoxy and glass/epoxy laminates. Initial tests of the system show that it is possible to detect small density changes, such as an extra roving, in cured laminates. The system is being used for both instructional purposes in the composite materials curriculum and inspection of research material.

Capability for static and fatigue testing of composites has been added during the reporting period. An MTS Systems Corporation 20,000 pound capacity servohydraulic testing machine and a MINC-11 laboratory instrument computer have been intergrated, Fig. 10. Data acquisition and control programs have been developed so far for static tests and single cycle (load and unload) tests. Structuring of a data base has been initiated with test data from fracture tests on a short glass fiber/polyester composite at different temperatures and strain rates. This initial data base will be used as a guide for structuring and developing data base concepts. Fortran software for general purpose data analysis, including curve fitting and graphic plotting (both video and hard copy), has been developed for the system. The program reads data files from the data base (these files are written by real-time data acquisition and control programs),

[illegible]

Figure 8 Tabulation of creep and recovery data for an epoxy resin. Column 1 is time (sec), Column 2 longitudinal strain, and Column 3 transverse strain.

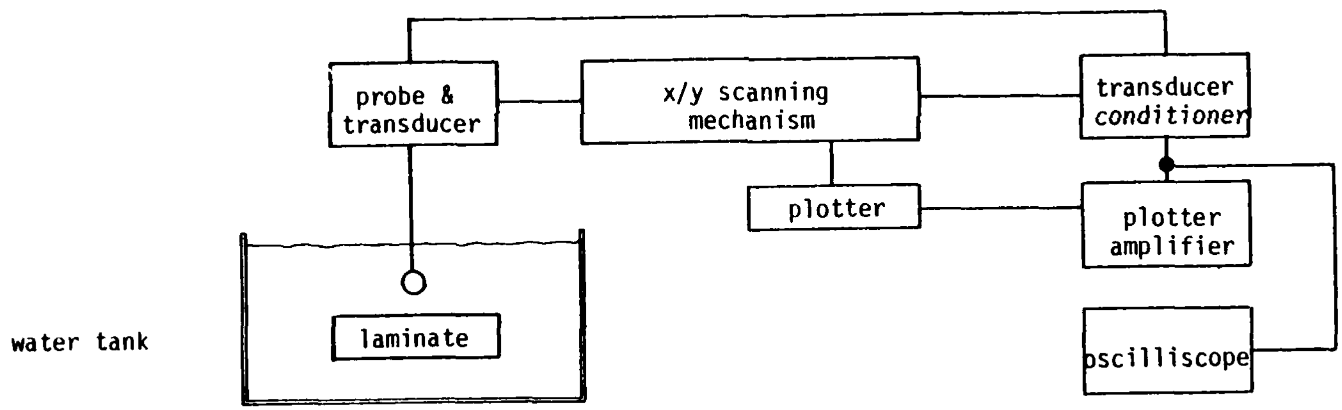

Figure 9 Block diagram of ultrasonic C-scan nondestructive inspection system

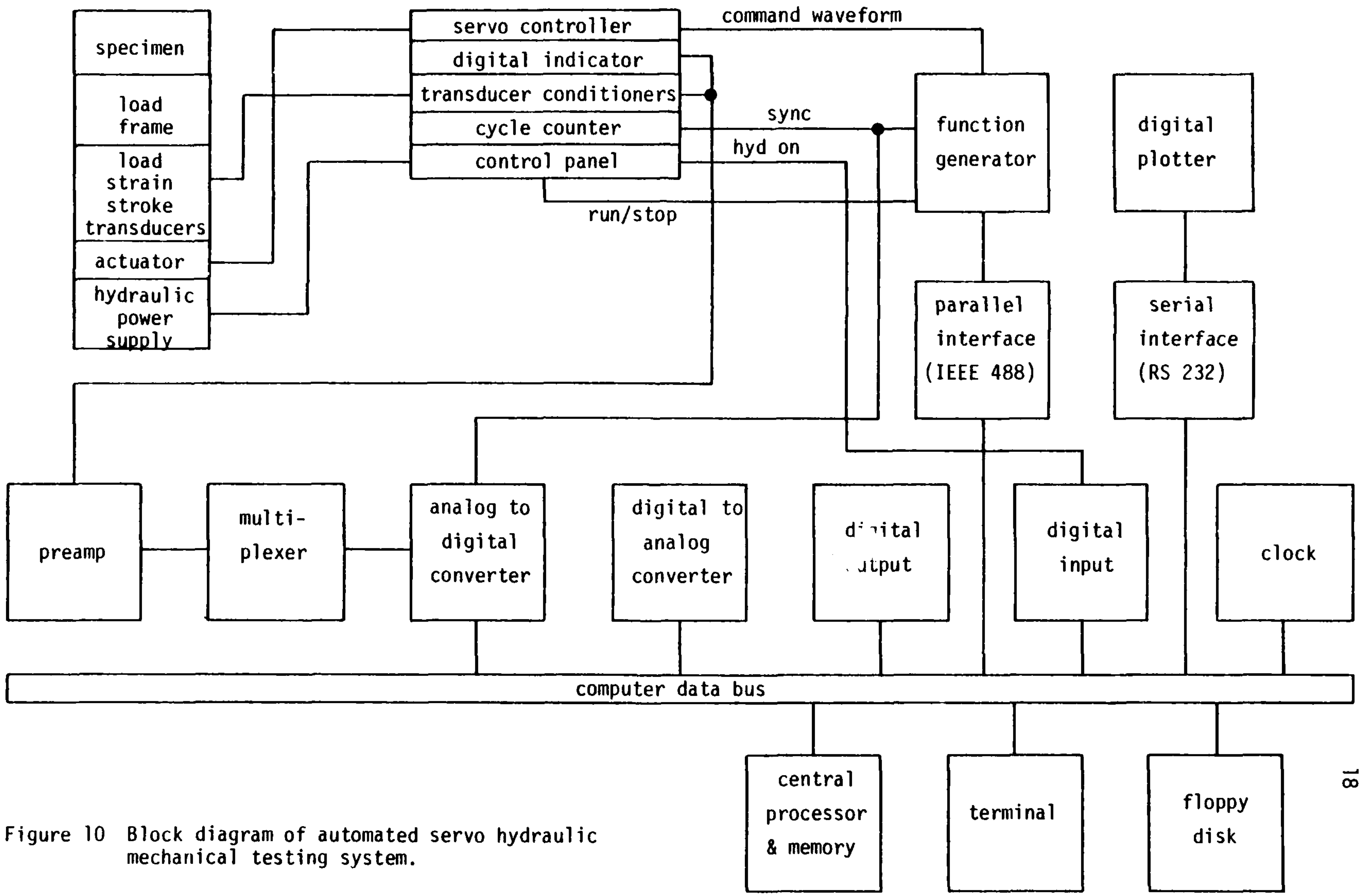

Figure 10 Block diagram of automated servo hydraulic mechanical testing system.

provides interactive curve fitting and data editing and provides graphics output (video or hard copy) of actual data and curve fit parameters.

An algorithm and Fortran software were developed to fit creep data to a power law for creep compliance, $D(t) = D_0 + D_1 t^n$, using a minimum squared error criterion. Current effort involves development of data acquisition and control software for fatigue experiments and related expansion of the laboratory experimental data base and analysis capability.

2.2 Delamination Fracture*

Recently completed work on delamination fracture of a glass/epoxy composite (Scotchply) and a graphite/epoxy composite (AS/3502) is described in the following paper (cf. Appendix A) and thesis (cf. Section 4 for Abstract), respectively:

(i) Devitt, D. F., Schapery, R. A., and Bradley, W. L., "A Method for Determining the Mode I Delamination Fracture Toughness of Elastic and Viscoelastic Composite Materials", Journal of Composite Materials, Vol. 14, Oct. 1980, pp. 270-285.

(ii) Hulsey, R. C., "Delamination Fracture Toughness of a Unidirectional Graphite/Epoxy Composite", M.S. Thesis, Texas A&M University, Dec. 1980.

Delamination in the opening mode of fracture was investigated using a split laminate loaded as a double cantilever beam, which is shown in the inset in Fig. 11; the fibers are parallel to the beam axis. Here we shall discuss primarily the graphite/epoxy study, as the investigation on Scotchply is detailed in Appendix A (Ref. (i)).

Initial experiments on the graphite/epoxy composite were conducted at ambient temperature and humidity, and consisted of measuring load, P, versus displacement, 2Δ, for various crack lengths, a. The beam analysis,

---

*Prepared by Drs. W. L. Bradley and R. A. Schapery

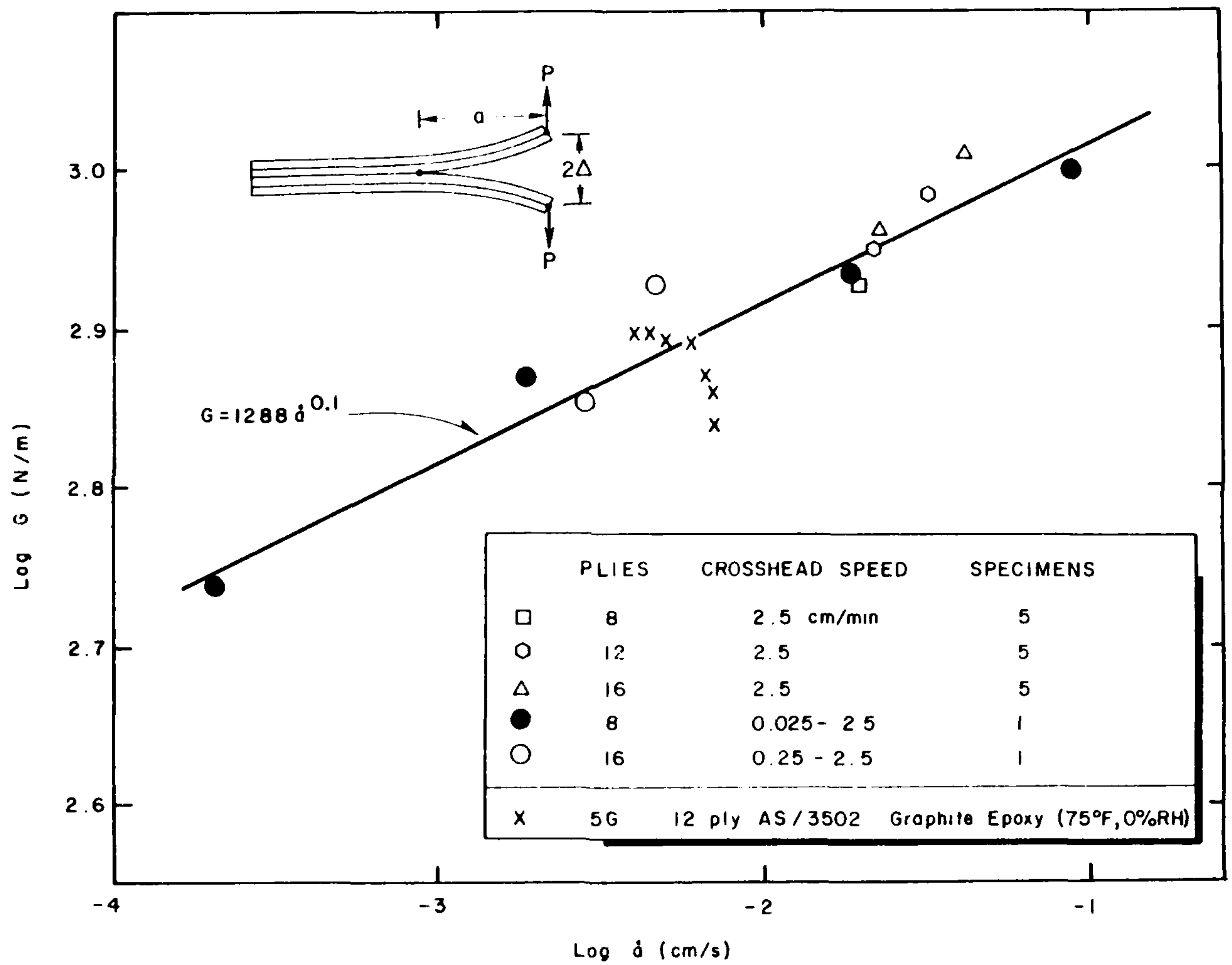

Figure 11. Energy release rate for Scotchply (1002) versus delamination crack speed (dry, 75°F). Graphite/epoxy data plotted for comparison; note that the actual G is one-fifth that shown.

which includes geometric nonlinearity due to large rotations, was verified using two of the measured quantities to predict the third, which was also measured. Subsequent experiments were then run at higher temperatures in a controlled atmosphere where measurement of instantaneous crack length was not convenient; the analysis was used with P - Δ data to predict crack length as a function of time. The results of these experiments indicated a critical energy release rate of approximately 1 in-lb/in^2 except at the highest temperature and humidity (200°F and 95%RH) (cf. Fig. 12) where a 20% increase in the critical energy release rate was observed. This increased toughness at higher temperature and relative humidity could be interpreted as resulting from a softening of the matrix as the glass-transition temperature, T_g, approached the test temperature, T; thus, with much more deformation taking place in the vicinity of the crack tip, more energy would be dissipated as the crack propagated. A significant variation in energy release rate, G, with crack growth rate, $\dot{a}$, was not observed. However, a somewhat serrated load-time record as well as fractographic analysis of the broken specimens in the scanning electron microscope suggested strongly the possibility of discontinuous crack extension which might obscure the true G versus $\dot{a}$ relationship.

Although more energy may be dissipated in the material surrounding the crack tip with an increase in temperature and moisture level, as noted above, the more severe environment may in some cases reduce the total amount of external work required for the local resin fracture process; e.g. crack propagation in a thermorheologically simple elastomer is facilitated by an increase in temperature [5]. Consequently, there could be competing processes, and without a good understanding of all

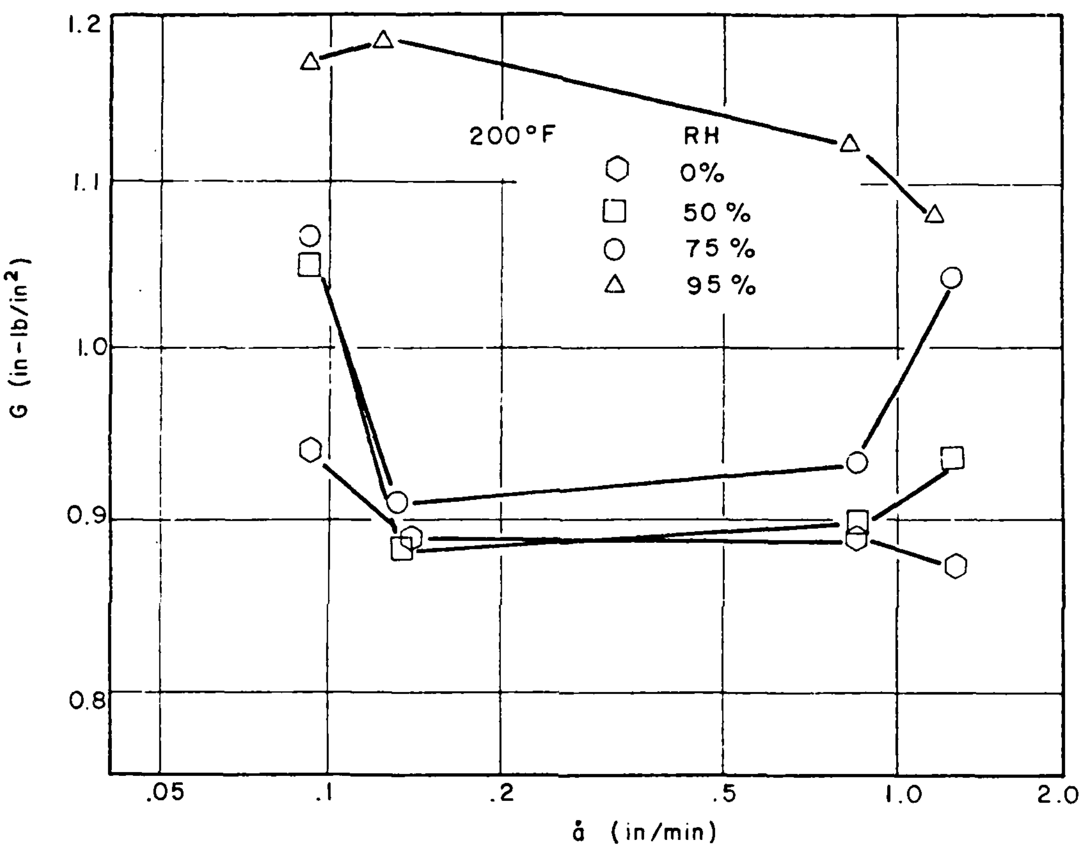

Figure 12. Energy release rate versus delamination crack speed for graphite/epoxy (AS/3502) in various environments (saturated state).

significant phenomena related to crack growth, one cannot predict behavior with any real confidence. In order to address this question, a preliminary theoretical viscoelastic analysis of delamination crack growth was made using the approximate method in [6], and the results are shown in Fig. 13. (The model is that of a thin cracked resin layer bonded between orthotropic beams.) The energy release rate G is plotted against the resulting crack speed $\dot{a}$ using dimensionless ratios. The intrinsic fracture energy required for material separation, Γ, was assumed constant, and the resin was assumed to be thermorheolocally simple; therefore, all temperature-dependence of the value of G required to produce any given speed $\dot{a}$ is due to the effect of the familiar time-temperature shift factor a_T on the resin's creep compliance [5]. Recognizing that a major effect of moisture in epoxy (and many other polymers) on mechanical response is analogous to that of temperature, we have indicated in Fig. 13 the predicted effect of an increase in both temperature and moisture.

The existence of a maximum in the G - $\dot{a}$ curve and the subsequent negative slope shown in Fig. 13 for graphite/epoxy is due entirely to the mechanical interaction of resin and fibers. In order to illustrate the effect of fiber modulus, we predicted the G - $\dot{a}$ curve for glass/epoxy, in which the same resin and fracture properties were employed; the G - $\dot{a}$ slope turned out to be nonnegative (cf. Fig. 13). However, other reasonable choices for resin properties indicate that the slope for glass/epoxy can be negative in some speed ranges.

The analysis was based on continuous crack growth. However, when the G - $\dot{a}$ curve has a negative slope, one can show the actual behavior is unstable. As the actual overall specimen geometry and

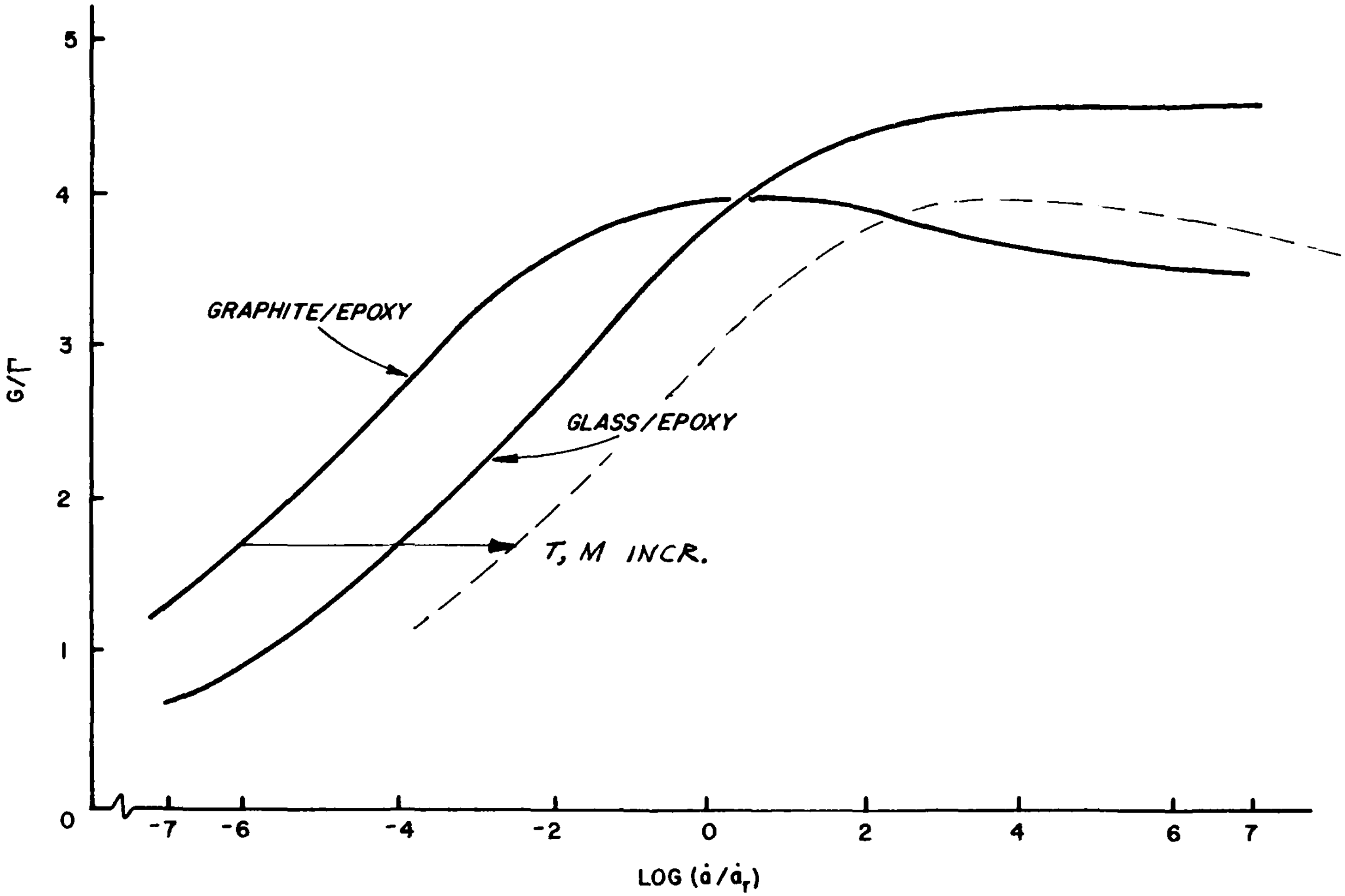

Figure 13. Theoretical prediction of normalized energy release rate versus normalized delamination crack speed based on representative fiber/matrix properties; the same matrix properties used for both composites.

loading condition (constant crosshead rate) employed in our tests is such that average crack growth is stable (cf. Ref. (i)), one can expect crack growth to occur in very small steps of high speed propagation and arrest. Further, at any given speed, the energy release rate is predicted theoretically to increase with an increase in moisture and temperature whenever the intrinsic G - $\dot{a}$ curve has a negative slope, as indicated in Fig. 13.

These preliminary theoretical findings are fully consistent with the experimental results for graphite/epoxy discussed previously. Figure 11 compares graphite/epoxy and glass/ epoxy results; the data shown for the former composite are from one test sample, but are typical. The noticeable decrease in G with crack speed for graphite/epoxy occurs over a very small speed range compared to that in Fig. 13. This latter difference may be due to the actual step-growth phenomenon, in which each small step consists of very slow to very high speed propagation, whereas the theory assumed continuous growth.

Finally, it should be added that epoxy resins (without reinforcement) in some cases exhibit unstable, step-growth [7]. Such behavior may be predicted from a viscoelastic fracture model in which the material in the neighborhood of the crack tip is very soft compared to the surrounding continuum. We should emphasize that the theoretical models discussed here are only tentative representations of the actual material, and much more theoretical and experimental work is needed in order to achieve an acceptable level of understanding of time-dependent fracture in resins and composites.

Further work to clarify the delamination fracture process in the graphite/epoxy composite is currently underway; a large portion of this research activity is leading to Master's theses for some of the current M.S. students. Included in this effort is a study of delamination under axial compression, as a follow-up to work reported in the thesis by C. D. Poniktera (cf. Section 4). Also, mixed mode fracture toughness testing has been initiated; the split-beam geometry in Fig. 11 is used, but the left end is held in place and different loads are applied to the top and bottom beams. More extensive fractographical analysis of specimens broken at TAMU and at General Dynamics is planned for this year also. Furthermore, a special stage has been ordered for the scanning electron microscope, which will allow composite specimens to be broken in the microscope while under observation; this should greatly assist the modelling efforts currently underway.

2.3 Effect of Physical Aging on Creep and Recovery of Resin*

The recent work on physical aging is discussed in the M.S. thesis by D. H. Metz (cf. Section 4); it is a continuation of an investigation started in 1979 [8]. The changes in mechanical properties of 3502 epoxy resin†, as measured by creep/recovery tests, were determined as a function of time after quench from above the short-time glass transition temperature. Quench rate and aging temperature were also varied. Aging occured most rapidly for a high quench rate, a higher aging temperature and short times after quenching. The physical aging was observed to cause a 10 - 20% change in the compliance of the epoxy (with the material getting stiffer with aging time) at the fastest cooling rate (100°F/min) and the highest aging temperature (300°F). At cooling rates more typical

---

*Prepared by Dr. W. L. Bradley

†Provided by Hercules, Inc., Magna, Utah.

of some commercial processing cycles (5°F/min) and at ambient aging temperature such as one might also expect commercially, a neglibly small amount of physical aging was observed. The epoxy material was thought to physically age much less than thermoplastic materials and many other thermosetting materials because the very high degree of chemical crosslinking constrains the material on a molecular level such that less free volume expansion is observed above T_g; thus, less excess free volume is trapped on subsequent cooling. Since physical aging is associated with time-dependent free volume collapse, this effectively reduces the effect.

2.4 Molecular Structure - Property Studies of Resin*

The resin in glass and graphite fiber composites is the source of most of the time-dependent and ambient sensitive properties and so studies of the resin properties are very basic to an understanding of composite properties. An important interface between the studies on molecular structure and those on the mechanical properties of glassy resins is in the study of the glass transition temperature and related effects. Here one hopes to be able to relate the phenomena simultaneously to both the molecular structure and to the mechanical properties. We have been studying these effects on 3502 epoxy resin with the differential scanning calorimeter (DSC) in an effort to improve our understanding of the effects of curing conditions, aging, moisture and molecular structure upon the resin properties.

Most of our effort has been spent in an attempt to improve the reproducibility and quality of the DSC runs since the intended studies seem to push the instrument to the limit of its capabilities.

---

*Prepared by Dr. J. S. Ham

It is often observed that the first trace on a DSC sample is ragged and so cannot be used, while subsequent traces are of high quality. For many purposes, the later scans are adequate, but to study aging phenomena the first trace must be used. This raggedness seems to be due to moisture evaporating from the sample so we are now trying to keep our samples extremely dry with some success.

One of the problems considered is how to measure the glass transition temperature of the proprietary resins (e.g., 3502 and others used in advanced composites) which is above the decomposition temperature. One concept is to lower T_g by dissolving moisture into the sample and then measure the lowered T_g. Unfortunately, escaping moisture obscures the trace, so that we cannot maintain the desired level of moisture while measuring T_g. If the moisture level is uncertain, then the value of T_g is uncertain so that the changes we seek are lost.

The experimental procedure that offers the most practical method to determine T_g in these samples is to scan rapidly to a high temperature and then immediately cool back down before much decomposition has taken place. If one can do this with different scan rates, both up and down, one should be able to correct for a small rate of thermal decomposition. This approach requires some data analysis which accounts for the time constant of the response of the equipment.

In principle, there are a variety of response time constants since the heater, thermometer and cell are geometrically separated and each has its own heat capacities and thermal conductivies to other parts and the surroundings. Since all of the decay times are exponential, we are concerned primarily with the longest one. We have measured the response rate constants under various conditions in an effort to develop a method to unfold the data so that much of the data is saved while the equipment is approaching a steady state. This work is continuing.

In related work, I spent the summer (1980) at the Materials Laboratory, Air Force Wright Aeronautical Laboratories, investigating problems associated with composites. The Materials Laboratory has underway a program to develop acetylene terminated polymers for use as high temperature adhesives and composite matrices. The thermal stability of these materials is excellent and the chemistry is very flexible so that many different polymers may be made. Unfortunately, there are few guidelines as to which polymer will best satisfy the eventual end uses. Since the cost is very high to develop the relevant chemistry, there is a danger that a premature choice will be made, resulting in a material far from optimum. Therefore, they have developed a program to collect a variety of data on each polymer or version of the polymer, utilizing extremely small amounts of material. One of the many items measured is the fracture toughness. While this information cannot yet be tied with precision to the properties of the adhesive or composite matrix, it is clear that there is a relationship and that one seeks a material with high fracture toughness.

My task was to seek methods to enhance the fracture toughness of resins so that appropriate monomers will be produced to be studied in detail. My conclusions are that while a heterogeneous material may be the eventual solution, the development of such a material is difficult and lacks clear guideposts along the way. On the other hand, it should be possible to loosen the crosslinked network of the polymer by introducing some dangling ends so that the fracture toughness is improved. This will reduce certain properties, such as the glass transition temperature, but this temperature is already so high that some tradeoff probably can be made. (The length of these loose ends was estimated by the entanglement length determined from viscous flow in the corresponding thermoplastic material). The materials being developed have an extremely short entanglement length so that only short dangling chains should suffice. To enhance fracture toughness, this work will be pursued at AFWAL this summer, where it is hoped that my concepts can be tested. Work conducted during the summer 1980 will soon be published as a Materials Laboratory report.

3. ANALYSIS OF COMPOSITES

3.1 Effects of Environment on Response of Composites*

The investigations include studies of the deformation of non-symmetric laminated plates due to thermal cool-down, the diffusion of moisture into laminates under fluctuating ambient environments, and optimization of cool-down time-temperature paths in cross-ply laminates. The latter study accounts for the temperature dependence of the coefficients of thermal expansion.

The following papers and theses on this work were prepared:

(i) Douglass, D.A. and Weitsman, Y., "Stresses Due to Environmental Conditioning of Cross-Ply Graphite/Epoxy Laminates." In Advances in Composite Materials (Proceedings of 3rd International Conference on Composite Materials, Paris, France). A. R. Bunsell et al., Editors, Vol. 1, pp. 529-542, Pergamon Press (1980).

(ii) Harper, B.D. and Weitsman, Y., "Residual Thermal Stresses in an Unsymmetrical Graphite/Epoxy Laminate". To appear in the proceedings of the 22nd SSD & Materials Conference, Atlanta, GA, April 6-8, 1981.

(iii) Weitsman, Y., "A Rapidly Convergent Scheme to Compute Moisture Profiles in Composite Materials Under Fluctuating Ambient Conditions", Texas A&M University Report No. MM3724-81-6.

(iv) Harper, B.D., "Residual Thermal Stresses in an Unsymmetrical Cross-Ply Graphite/Epoxy Laminate", M.S. Thesis, Aug. 1980.

(v) Lott, R.S., "Moisture and Temperature Effects on Curvature of Anti-Symmetric Cross-Ply Graphite/Epoxy Laminates", M.S. Thesis, Dec. 1980.

An additional investigation on "Optimal Cooling of Cross-Ply Laminates and Adhesive Joints" is presently in preparation by Y. Weitsman and B.D. Harper.

---

*Prepared by Dr. Y. Weitsman

The essential finding of Ref. (i) are illustrated in Figs. 3-5 therein (Appendix A). If we consider in particular the state of the residual stresses upon termination of moisture and temperature conditioning, we note that the stress profile depends most significantly on the conditioning history. When we observe the solid and dashed curves at the times when our laminate was "Returned to Room Temperature", we note that the stresses are of entirely reversed sign, in spite of the fact that the current levels of moisture and temperature are indentical. The significance of the time-dependent material response is illustrated in Fig. 5, which demonstrates that elastic predictions may be different in both sign and magnitude.

In Ref. (ii), we managed to demonstrate that the time-dependent behavior is amenable to experimental detection. In addition, we also observe that the residual stresses can reach critical values, sufficient to produce large cracks in composite laminates. Additional analytical and experimental work is currently in progress, extending the findings of Ref. (ii).

Reference (iii) exhibits the coupling between the moisture diffusion process and temperature in composite materials. Figure 1 therein (Appendix A) demonstrates that when exposed to identical, fluctuating, ambient relative humidities, entirely different internal moisture profiles can develop within laminates under different temperature histories.

3.2 Analysis by the Finite Element Method: Constitutive Models and Fracture Mechanics*

The nonlinear viscoelastic constitutive model developed during previous years hasbeen incorporated into the finite element program, AGGIE. The model has been implemented and tested for the plane stress, plain strain, and axi-symmetric cases. The 3/D model has been written but has not been tested yet. A number of isothermal and nonisothermal creep and creep-plasticity problems have been investigated and results compared to available experiments. A report on this work should be completed by June, 1981.

Related experimental work on the nonlinear viscoelastic characterization of composites was initiated; it is described in the thesis (Section 4):

Kerstetter, M.S., "Nonlinear Viscoelastic Characterization of AS/3502 Graphite/Epoxy Composite Material," M.S. thesis, Texas A&M University, Dec. 1980.

The finite element program has been modified to calculate nodal forces in the vicinity of crack tips and the resulting intensity factors and/or J-integral values. Three-dimensional calculations of Mode I, II, and III cracking are thus possible with the program. Although not yet tested, elastic-plastic calculations for the J integral may be possible with the program.

3.3 Damage Growth and Fracture of Composites†

Recently completed work on theoretical models for damage growth and fracture is described in the following two papers (cf. Appendix A):

---

*Prepared by Dr. W. E. Haisler
†Prepared by Dr. R. A. Schapery

(i) Schapery, R.A., "On Constitutive Equations for Viscoelastic Composite Materials with Damage," Proc. NSF Workshop on Damage, Cincinnati, April, 1980.

(ii) Schapery, R.A., "Nonlinear Fracture Analysis of Viscoelastic Composite Materials based on a Generalized J Integral Theory", Proc. 1st Japan--U.S. Conference on Composite Materials, Tokyo, Jan., 1981.

In Reference (i), the material is assumed to be linearly viscoelastic for a fixed state of damage. A rigorous derivation is then given to obtain the effect of microcracking and rejoining of crack surfaces (with or without healing) on the macroscopic constitutive equation. Residual stress effects due to temperature and/or moisture are included. The results have served to provide guidelines for the development of more general nonlinear viscoelastic constitutive equations with damage and a new theory for the prediction of initiation of crack growth and crack speed in such composites [9]. Some results and applications of this fracture theory are discussed in Ref. (ii).

Experimental work on microcrack growth in a viscoelastic composite (Scotchply) is described in the thesis (cf. Section 4),

Lehman, M.W., "An Investigation of Intra-Ply Microcrack Density Development in a Cross-Ply Laminate", M.S. Thesis, Texas A&M University, Dec. 1980.

The initial microcrack state and subsequent growth due to load application are described; a florescent dye penetrant is employed to help identify microcrack geometry. A comparison is made between theoretically and experimentally determined stiffness changes due to microcracking. This activity represents a portion of the work underway to develop analytical models of damage growth in viscoelastic composites through a combination of experimental and theoretical approaches.

4. GRADUATE RESEARCH ASSISTANT ACTIVITIES

4.1 Summary

The second group of graduate engineering students to participate in the AFOSR research project entered the program in September, 1979 and graduated with a Master of Science degree by December, 1980. Results of their research are reported in the following theses:

1. Harper, B.D., "Residual Thermal Stresses in an Unsymmetrical Cross-Ply Graphite/Epoxy Laminate."
2. Hulsey, R.C., "Delamination Fracture Toughness of A Unidirectional Graphite/Epoxy Composite."
3. Kerstetter, M.C., "Nonlinear Viscoelastic Characterization of AS-3502 Graphite/Epoxy Composite Material."
4. Lehman, M.W., "An Investigation of Intra-Ply Microcrack Density Development in a Crossply Laminate."
5. Lott, R.S., "Moisture and Temperature Effects on Curvature of Anti-Symmetric Cross-Ply Graphite/Epoxy Laminates."
6. Metz, D.H., "Experimental Investigation of Free Volume Concepts in Relationship to Mechanical Behavior of an Epoxy System Subjected to Various Aging Histories."
7. Poniktera, C.D., "Application of Energy Release Rate Principles to Compression Debonding."

Abstracts are given in Section 4.2. Copies of the theses will be provided upon written request to the Principal Investigator (R.A. Schapery).

The current group (starting September, 1980) consists of seven (7) M.S. students and one (1) Ph.D. student. The topics are listed below; most studies involve both experimental and theoretical work.

M.S. Theses--

1. Shear deformation effects in highly anisotropic laminates (Coulter/Weitsman).

2. Micromechanisms of delamination fracture (Williams/Bradley).

3. Mixed-mode delamination fracture (VanderKley/Bradley).

4. Compression-induced delamination (Earley/Jerina).

5. Delamination under complex loading histories (Cullen/Jerina).

6. Delamination fracture analysis including effect of matrix damage (Arenburg/Schapery).

7. The effect of elliptical hole shape on the design of pin loaded filament wound fiberglass tension lugs (Braswell/Alexander).

Ph.D. Dissertation--

8. Environmental effects in unbalanced laminates (Harper/Weitsman).

The next quarterly report will contain thesis proposals describing the research planned under each of these topics. Besides conducting this research, the students are involved in academic courses, as described in the brochure in Appendix B.

In addition to graduate students, a few select undergraduate students assist in the various research activities. The participation of these undergraduate students aids in the research and helps to acquaint them with composite materials prior to enrolling in the graduate program.

4.2 Abstracts of M.S. Theses Completed in 1980

ABSTRACT

Residual Thermal Stresses in an Unsymmetrical Cross-Ply
Graphite/Epoxy Laminate. (August 1980)
Brian Douglas Harper, B.S., Ag. En., Texas A&M University
Chairman of Advisory Committee: Dr. Y. Weitsman

This thesis presents a method for determining the residual thermal stresses in AS-3502 graphite/epoxy laminates due to cool-down from their cure temperature. Also included is a method for determining the optimal time-temperature path that will minimize these residual stresses.

The analysis considers the time-dependent behavior of the material and all calculations employ recent data on the thermo-viscoelastic response of the AS-3502 graphite/epoxy system.

The viscoelastic analysis is verified through curvature measurements of unsymmetric cross-ply plates fabricated from the AS-3502 graphite/epoxy material.

ABSTRACT

Delamination Fracture Toughness of A Unidirectional

Graphite/Epoxy Composite. (December 1980)

Roy Charles Hulsey, B.S., Texas A&M University

Chairman of Advisory Committee: Dr. Walter L. Bradley

The opening mode delamination fracture toughness of a graphite/epoxy composite under varied temperature, humidity and crack growth rates is investigated experimentally. Energy release rate for a stably growing crack (G_V) is determined using a double cantilever beam specimen and a linear elastic fracture mechanics analysis coupled with nonlinear beam theory. The temperature range of 75F to 200F and 0% RH to 95% RH has been studied. A significant effect of temperature and humidity on G_V is observed only at 200F and 95% RH for the system studied. G_V values of 0.955 in-lb/in^2 (standard deviation = 0.08) are determined in general with a value of 1.14 in-lb/in^2 determined at the 200F - 95% RH condition. The energy release rate is not found to be significantly affected by crack growth rates in the range 0.01 to 10.0 in/min.

ABSTRACT

Nonlinear Viscoelastic Characterization of AS-3502
Graphite/Epoxy Composite Material. (December 1980)
Michael Scott Kerstetter, B.S., Texas A&M University
Chairman of Advisory Committee: Dr. K.L. Jerina

The objective of this paper is to study the creep and recovery response of a composite subjected to several high stress levels in a high humidity environment. Strain versus time data obtained from uniaxial creep and recovery tests were used to characterize viscoelastic deformation in a $[\pm 45]_{2S}$ laminate. A description and examination of the effectiveness of two data collection schemes are presented along with a discussion of some important experimental aspects such as generation of the test environment and mechanical and humidity conditioning. Data were obtained from creep and recovery for several stress levels which were reduced using graphical shifting procedures from which nonlinear material parameters were determined. Conclusions and recommendations for future research are presented.

ABSTRACT

An Investigation of Intra-Ply Microcrack Density

Development in a Crossply Laminate. (December 1980)

Michael William Lehman, B.S., C.E., Texas A&M University

Chairman of Advisory Committee: Dr. R. A. Schapery

An investigative technique is qualified as an experimental tool to aid in the quest involving identification of parameters controlling damage accumulation in laminated composites. Specifically, the flaw state, encompassing geometry, size, and density as a function of a monotonic load history, is characterized for a $[90_3/0_4]_s$ glass epoxy test laminate. Founded upon direct and indirect experimental observations, a subjective description for flaw or crack development on both a local and global scale is also presented.

Theoretical bounds for strain energy change are established for the investigated test laminate. These bounds are used to compare and qualify the experimental data in the range for which the relationship between residual modulus and transverse crack density is linear. Finally, possible candidates controlling the global rate of strain energy change for accumulating damage are identified.

ABSTRACT

Moisture and Temperature Effects on Curvature of
Anti-Symmetric Cross-Ply Graphite/Epoxy Laminates. (December 1980)

Randall Stephen Lott, BAE, Georgia Institute of Technology

Chairman of Advisory Committee: Dr. Y. Weitsman

This thesis presents a method for analytically determining the mid-plane strains and curvatures of anti-symmetric cross-ply graphite/epoxy laminated plates which are exposed to high humidities at elevated temperatures.

The analysis considers temperature dependent moisture diffusion and time/temperature/moisture dependent stress relaxation. Recent data on the hygrothermal-viscoelastic behavior fo the AS/3502 graphite/epoxy system is employed in the calculations.

Results of both elastic and viscoelastic analyses are presented and compared to measured curvatures of anti-symmetric cross-ply plates fabricated from the AS/3502 system and exposed to high temperature/humidity environments.

ABSTRACT

Experimental Investigation of Free Volume Concepts in Relationship to Mechanical Behavior of an Epoxy System Subjected to Various Aging Histories. (December 1980)

Daniel Hugh Metz, B. S. University of Illinois

Chairman of Advisory Committee: Dr. W. L. Bradley

An epoxy resin commonly used in advanced composite materials for aerospace application was tested for changes in viscoelastic behavior after being quenched from above T_g to 300°F, 200°F and 75°F and then isothermally aged. The qualitative correlation between the changes in viscoelastic response and free volume is discussed. In general more total physical aging and a more rapid physical was observed at higher temperatures. Data obtained from these experiments is useful in contributing to an overall understanding of factors important to the optimization of processing parameters in the manufacture of composite material components.

ABSTRACT

Application of Energy Release Rate

Principles to Compression Debonding. (August 1980)

Christopher Dale Poniktera, B.A. Engineering Science with a

Specialization in Applied Mechanics, University of California

Chairman of Advisory Committee: Dr. K. L. Jerina

The objective of this research effort was to provide a critical assessment of the state-of-the-art of the analysis of compressive debonding of fiber-reinforced composite materials and to investigate the applicability of using an energy release rate approach as a means of analyzing this phenomenon.

The method developed utilizes linear beam-column theory and assumes prior knowledge of the critical strain energy release rate of the system analyzed.

An experimental program employing a polymethylmethacrylate (PMMA) model system was conducted to verify the proposed analytical technique. The model system consisted of a symmetrical beam-column arrangement subjected simultaneously to axial and lateral loads.

Results of the study indicated good agreement between experimental and theoretical model displacement predictions, but prediction of debond propagation, based on know Mode I critical strain energy release rate values (G_{IC}), was not obtained. The author offers several possible reasons for this apparent discrepancy.

5. PROFESSIONAL PERSONNEL INFORMATION

5.1 Faculty Research Assignments

Each participating faculty member is responsible for the research conducted in at least one specific area of investigation, as shown below. In addition, most serve as chairmen of one or more of the graduate advisory committees for M.S. students and, as such, direct their students' research project. The faculty also contribute to other research activities on the project by serving on student advisory committees, through technical meetings, informal discussions, and, in some cases, through specific research work.

The Principal Investigator (R. A. Schapery) has responsibility for overall technical direction and coordination and for project management. In addition he has direct responsibility for certain research work, as noted below.

Faculty Member/Departmental Affiliation	Primary Research Responsibility
Dr. Walter Bradley/Mechanical Engineering	Physical Aging Behavior, Delamination Fracture Properties.
Dr. Walter Haisler/Aerospace Engineering	Development of Finite Element Models.
Dr. Joe Ham/Physics	Curing and Aging Studies.
Mr. Bob Harbert/Civil Engineering	Duomorph Gage
Dr. Ken Jerina/Civil Engineering	Experimental Data Base, Mechanical and Failure Property Characterization.
Dr. Richard Schapery/Aerospace and Civil Engineering	Principal Investigator and Theoretical Models for Physical Aging, Damage Growth, and Fracture.
Dr. Jack Weitsman/Civil Engineering	Constitutive Relations, Environmental Effects.

5.2 Additional Professional Staff

Mechanics and Materials Center

Mr. Carl Fredericksen - Electronics Technician

Mr. William Eue - Computer Programmer

5.3 Spoken Papers and Lectures at Conferences and Other Professional Activities of the Faculty Related to Composite Materials (1 January 1980 - 31 December 1980):

W. L. Bradley

Invited Lectures and Conference Presentation:

"J-Integral Fracture Toughness Studies of Cast Iron," American Founderymen Society, Annual Meeting, St. Louis, April 1980.

"Fracture Toughness of Nodular Cast Iron," Sandia Laboratories, Sept. 1980.

"Size-Effect on Toughness Measurements of Nodular Cast Iron," American Institute of Metallurgical Engineers (AIME), Annual Meeting, Las Vegas, Feb. 1980.

Technical Committee Membership:

ASTM E-24 Committee on Fracture, Metal Properties Council, sponsored jointly by ASME, ASM, and ASTM.

Awards:

Best Materials paper of the year by the American Nuclear Society: "Corrosion and Mechanical Behavior of Iron in Liquid Lithium," Nuclear Technology, Vol. 39, 1978, pp. 75-83.

Named Haliburton Professor of Mechanical Engineering.

K. L. Jerina

Invited Lecture and Conference Presentation:

"Effective Moduli of Three Dimensionally Reinforced Fibrous Materials," Gordon Conference lecture on Composite Materials, Santa Barbara, Jan. 1980.

"Viscoelastic Characterization of a Random Fiber Composite Material Employing Micromechanics," Short Fiber Reinforced Composite Materials, ASTM, Minneapolis, May 1980.

Technical Committee Membership:

ASTM E-9 on Fatigue, Corresponding Secretary

ASTM E-24 on Fracture

ASTM D-30 on Composite Materials

SAE Fatigue Design and Evaluation Committee
Chairman of Task Force on Composite Materials

R. A. Schapery

Invited Lectures and Conference Presentations:

"Fracture and Fatigue of Viscoelastic Materials," University of Wyoming, Jan. 1980.

"On Constitutive Equations for Viscoelastic Composite Materials with Damage," NSF Workshop on Damage, Cincinatti, May 1980.

"A Complex Modulus Gage- The Duomorph", Annual Meeting of the Acoustical Society of America, Atlanta, April 1980.

"Nonlinear Approximate Analysis of Solid Propellant Grains", Structures and Mechanical Behavior Meeting of Rocket Propulsion Group, Sept. 1980.

"Composite Materials for Structural Design", Sixth Annual Mechanics of Composites Review Meeting, Oct. 1980.

"Application of a Generalized J Integral to Fracture of Linear and Nonlinear Viscoelastic Composite Materials", 17th Annual Meeting, Society of Engineering Science, Atlanta, Dec. 1980.

Technical Committee Membership:

National Materials Advisory Board, National Academy of Sciences, Committee on "High Temperature Metal and Ceramic Matrix Composites".

Awards:

Named Alumni Professor and Distinguished Professor of Aerospace and Civil Engineering.

Y. Weitsman

Conference Presentation:

"Stresses Due to Environmental Conditioning of Cross-Ply Graphite/ Epoxy Laminates", 3rd International Conference on Composite Materials, Paris, Aug. 1980. Also participated in panel discussion.

Technical Committee Membership:

AIAA Subcommittee on Design Allowables for Composite Materials.

In addition to the above activities, the faculty attended several conferences on composites, published papers on other projects, and worked as consultants to industry.

6. REFERENCES

1. Renton, W.J. and Ho, T., "The Effect of Environment on the Mechanical Response of AS/3501-6 Graphite/Epoxy Material", Vought Corp. Advanced Technology Center Final Report, Aug. 1978. Contract No. N00019-77-C-0369 with the Department of the Navy.

2. Williams, M.L., et al., "Mechanical Spectroscopy for Epoxy Resins", Interim Technical Report, Sept. 1977 - March 1979, Univ. of Pittsburgh, Contract No. F33615-77-C-5232 with AFML.

3. Struik, L.C.E., Physical Aging in Amorphous Polymers and Other Materials, Elsevier (1978).

4. Weitsman, Y., "Residual Thermal Stresses due to Cool-Down of Epoxy-Resin Composites". J. Applied Mechanics, ASME Vol. 46, No. 3, Sept. 1979, pp. 563-567.

5. Schapery, R.A., "A Theory of Crack Initiation and Growth in Visco-elastic Media: Part III, Analysis of Continuous Growth," Int. J. Fracture, Vol. 11, 1975, pp. 549-562.

6. Schapery, R.A., "A Method for Predicting Crack Growth in Non-homogeneous Viscoelastic Media", Int. J. Fracture, Vol. 14, 1978, pp. 293-309.

7. Yamini, S. and Young, R.J., "Stability of Crack Propagation in Epoxy Resins", Polymer, Vol. 18, 1977, pp. 1075-1080.

8. Ring, D.S., "Determination of the Relationship of Free Volume to Mechanical Behavior for an Epoxy System Subjected to Various Aging Histories", M.S. Thesis, Texas A&M University, Dec. 1979.

9. Schapery, R.A., "Correspondence Principles and a Generalized J Integral Theory for Deformation and Fracture Analysis of Nonlinear Viscoelastic Media", (Three-part report in preparation).

APPENDIX A

Recently Completed Reports and Publications

1. "Stresses Due To Environmental Conditioning of Cross-Ply Graphite/Epoxy Laminates" by D.A. Douglass and Y. Weitsman.

2. "Residual Thermal Stresses in an Unsymmetrical Cross-Ply Graphite/Epoxy Laminate" by B.D. Harper and Y. Weitsman.

3. "A Rapidly Convergent Scheme to Compute Moisture Profiles in Composite Materials Under Fluctuating Ambient Conditions" by Y. Weitsman.

4. "On Constitutive Equations for Viscoelastic Composite Materials with Damage" by R.A. Schapery.

5. "A Method for Determining the Mode I Delamination Fracture Toughness of Elastic and Viscoelastic Composite Materials" by D.F. Devitt, R.A. Schapery, and W.L. Bradley.

6. "Nonlinear Fracture Analysis of Viscoelastic Composite Materials Based on a Generalized J Integral Theory" by R.A. Schapery.

STRESSES DUE TO ENVIRONMENTAL CONDITIONING OF CROSS-PLY GRAPHITE/EPOXY LAMINATES

by David A. DOUGLASS

Sr. Structures Engineer, Bell Helicopter Textron
Fort Worth, Texas

and Yechiel WEITSMAN

Professor
Mechanics and Materials Center
Texas A&M University
College Station, Texas

This paper concerns the internal residual stresses due to the environmental conditioning of cross-ply graphite/epoxy laminates, where moisture is induced into the material by exposure to high relative humidity at elevated temperatures.

The stress fields resulting from conditioning at two temperature levels are evaluated for a balanced, symmetric cross-ply graphite/epoxy laminate by means of both elastic and viscoelastic analyses. The formulation considers temperature-dependent moisture diffusion and time, temperature and moisture dependent stress relaxation. The computations are based upon recent data and employ realistic values of material parameters.

The analysis shows that the viscoelastic stresses are much smaller than those predicted by elastic analysis, and that conditioning at 150°F results in residual stresses which are smaller than those reached during conditioning at 180°F.

Copied from:
ADVANCES ON COMPOSITE MATERIALS Volume I

Proceedings of the Third International Conference on Composite Materials, held in Paris, 26-29 August 1980

Edited by
A. R. Bunsell, et al. Ecole des Mines, Paris

INTRODUCTION

Increasing concern with the effects of temperature and moisture on the performance of composites demands the development of accelerated conditioning techniques. These conditioning schemes attempt to simulate extreme exposures to moisture and temperature which may be encountered in service life.

Since moisture diffuses extremely slow the conditioning process is accelerated by employing elevated temperatures which accelerate the moisture sorption and shorten the duration of the experiment.

It was observed that certain conditioning schemes induce damage in the composite. In order to develop time saving, yet non-damaging, laboratory experiments it is necessary to predict the stresses which arise due to moisture and temperature in composite laminates.

In this paper the moisture and temperature effects are incorporated into a viscoelastic constitutive relation, which is based upon creep data at various levels of temperatures and moisture contents. It is noted that both environmental factors act as swelling agents, which introduce stresses in the presence of geometric constraints. On the other hand, both moisture and temperature enhance the relaxation of stresses, thus compensating for their initial effects. While this "competition" is accounted for in the viscoelastic representation it cannot be considered within the context of an elastic response. Consequently, test articles which were conditioned in different manners will contain disparate residual stresses and perform differently under loads.

In this paper we consider a symmetric, balanced, cross-ply laminate. Results are presented for two conditioning schemes and comparison is provided with an elastic analysis. Additional results and further details are given in Ref. [1].

PRELIMINARY CONSIDERATIONS

For clarity we present individually the major factors present in moisture conditioning

Moisture Diffusion

The diffusion into thin composite laminates is found to follow Fick's second law [2], [3], which in one dimension reads

$$\frac{\partial m}{\partial t} = D \frac{\partial^2 m}{\partial z^2} \tag{1}$$

The solution to (1), under steady ambient conditions is given in two alternate forms [4]

$$m(z,t) = m_a - (m_a - m_0) \left\{1 - \sum_{n=1}^{\infty}(-1)^{n+1}\left[\operatorname{erfc}\left(\frac{2n-1-z/h}{2\sqrt{t^*}}\right) + \operatorname{erfc}\left(\frac{2n-1+z/h}{2\sqrt{t^*}}\right)\right]\right\} \tag{2}$$

and

$$m(z,t) = m_a - (m_a - m_0) \sum_{n=1}^{\infty} \frac{2}{\mu_n} (-1)^{n+1} \cos\left(\frac{\mu_n z}{h}\right) \exp(-\mu_n^2 t^*) \tag{3}$$

where the dimensionless time t^* is given by $t^* = \frac{Dt}{h^2}$, and in (3)

$$\mu_n = \frac{(2n-1)\pi}{2}$$

It can be shown that for $t^* < 0.29$ (2) converges rapidly while for $t^* > 0.29$ form (3) is more advantageous. In (1), (2) and (3) m is moisture, m_a is the constant ambient moisture, m_0 is a uniform initial moisture, z is the spatial

...ordinate across the thickness, t is time and D the moisture diffusivity.

It has been found [5] that the saturation level m_s depends on the relative ...midity RH. In graphite/epoxy systems a linear relationship $m_s = E(RH)$ is employ-...d. In addition, the diffusion coefficient D is temperature dependent [6]. This ...ependence is given by $D(T) = A_1 \exp(-B_1/T)$.

Swelling Due to Moisture

The transverse swelling of most graphite/epoxy systems due to moisture absorp-...on is sketched in Fig. 1 [7, 8]. The phenomenon is characterized by a moisture ...xpansion coefficient β_T.

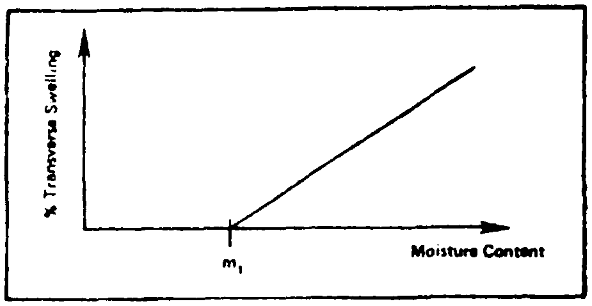

Fig. 1. Transverse Swelling Vs. Moisture Content

The transverse strain due to moisture swelling is expressed as follows

$$\begin{aligned} \epsilon_T &= \beta_T (m - m_1) \quad \text{for } m \geq m_1 \\ \epsilon_T &= 0 \qquad\qquad\qquad \text{for } m \leq m_1 \end{aligned} \tag{4}$$

In (4) m_1 is a threshold value below which moisture is not accompanied by any transverse swelling.

Measurements [8] indicate that the longitudinal swelling coefficient is ...gligibly small and we shall take $\beta_L = 0$.

Temperature Diffusion and Thermal Expansion

Data on temperature diffusion indicate that, for typical laminates, this pro-...ess preceeds much faster than all other time-dependent processes. Therefore we ...hall disregard temperature diffusion and consider spatially uniform, thermally ...quilibrated states.

In unidirectional laminae the thermal strains are completely characterized by ...e longitudinal and transverse coefficients of thermal expansion α_L and α_T.

Geometry and Notation

We shall consider symmetric, 0°/90° lay-ups and let the principal material ...es coincide with the x-y coordinates. The x axis is chosen parallel to the ...bers in the 0° plies. Whenever necessary we shall employ subscripts L and T to ...note longitudinal and transverse directions. See Fig. 2.

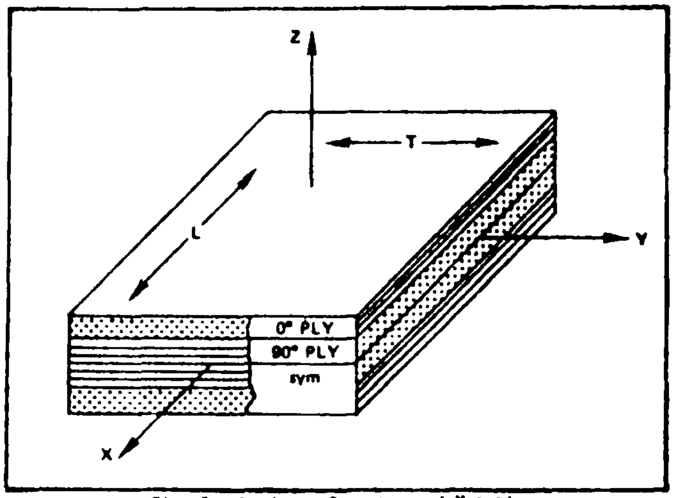

Fig. 2. Laminate Geometry and Notation.

Viscoelastic Behavior

The viscoelastic response of graphite/epoxy laminates in the transverse direction is of paramount significance during environmental conditioning. The time-dependent transverse compliance S_T can be expressed by a "power law" equation [9]

$$S_T = D_0(T,H) + D_1\left(\frac{t}{a(T,H)}\right)^q \qquad (5)$$

where D_0 is the initial compliance, t is time, $a(T,H)$ is the shift factor function which depends on humidity and temperature, and D_1 and q are material constants. The dependence of D_0 on T and H can be expressed by [9] $D_0(T,H) = aTH + bT + cH + d$.

However, in order to simplify computations we shall approximate $D_0(T,H)$ by its average value over the range of T and H in each conditioning scheme. This approximation entails errors of about 5%.

The data on the shift-factor function $a(T,H)$ can be expressed by

$$a(T,H) = a_1(T)a_2(H) \qquad \text{where}$$

$$\log a_1(T) = a_3 + a_4(1/T) + a_5(1/T)^2 \qquad \text{and} \qquad (6)$$

$$a_2(H) = a_6 m^{b_1}$$

The compliances S_L and S_{12} do not exhibit time, temperature and moisture dependence.

Elastic Compliances and Moduli

We shall take all elastic compliances and moduli as the initial viscoelatic values. Moduli are inverses of compliances, as follows

$$C_L = D_0/\Delta \ , \ C_T = S_L/\Delta \ , \ C_{12} = -S_{12}/\Delta \ , \text{ where } \Delta = S_L D_0 - S_{12}^2. \qquad (7)$$

Combined Stress - Strain Relations

Elastic

The combined elastic stress-strain relations for the plies considered herein, and for a state of plane stress, are

$$\begin{aligned}
\sigma_x^0 &= C_L\epsilon_x + C_{12}\epsilon_y - (C_L\alpha_L + C_{12}\alpha_T)\Delta T - C_{12}\beta_T(m - m_1) - C_L\beta_L m \\
\sigma_x^{90} &= C_T\epsilon_x + C_{12}\epsilon_y - (C_T\alpha_T + C_{12}\alpha_L)\Delta T - C_T\beta_T(m - m_1) - C_{12}\beta_L m \\
\sigma_y^0 &= C_{12}\epsilon_x + C_T\epsilon_y - (C_T\alpha_T + C_{12}\alpha_L)\Delta T - C_T\beta_T(m - m_1) - C_{12}\beta_L m \\
\sigma_y^{90} &= C_{12}\epsilon_x + C_L\epsilon_y - (C_L\alpha_L + C_{12}\alpha_T)\Delta T - C_{12}\beta_T(m - m_1) - C_L\beta_L m
\end{aligned} \tag{8}$$

where superscripts 0 and 90 denote ply orientations. It should be borne in mind that since $m = m(z,t)$, all stresses depend on z and t. However for the sake of notational brevity this dependence is suppressed.

Viscoelastic

In analogy with (8) the viscoelastic stress-strain relations for combined effects [10], expressed in terms of compliances, are

$$\begin{aligned}
&S_L\sigma_x^0 + S_{12}\sigma_y^0 = R_1^0 \\
&S_{12}\sigma_x^0 + D_0\sigma_y^0 + D_1\int_0^t (\xi - \xi')^q \frac{d\sigma_y^0}{d\tau}\, d\tau = R_2^0 \\
&D_0\sigma_x^{90} + D_1\int_0^t (\xi - \xi')^q \frac{d\sigma_x^{90}}{d\tau}\, d\tau + S_{12}\sigma_y^{90} = R_1^{90} \\
&S_{12}\sigma_x^{90} + S_L\sigma_y^{90} = R_2^{90}
\end{aligned} \tag{9}$$

where, in (9)

$$\xi = \xi(z,t) = \int_0^t \frac{ds}{a(T(S),m(z,s))} \quad , \quad \xi' = \xi'(z,\tau) = \int_0^\tau \frac{ds}{a(T(s),m(z,s))}$$

and

$$R_1^0 = \epsilon_x - \beta_L m - \alpha_L\Delta T \quad , \quad R_1^{90} = \epsilon_x - \beta_T(m - m_1) - \alpha_T\Delta T \quad ,$$

$$R_2^0 = \epsilon_y - \beta_T(m - m_1) - \alpha_T\Delta T \quad , \quad R_2^{90} = \epsilon_y - \beta_L m - \alpha_L\Delta T \; .$$

ELASTIC STRESS ANALYSIS

Consider a symmetric laminate composed of N_o 0° plies and N_{90} 90° plies. The laminate undergoes a total temperature change ΔT, which consists of cooling from cure to room temperature and then heating to the desired level of conditioning temperature at which moisture conditioning is enhanced. The laminate also absorbs moisture during storage prior to conditioning and due to conditioning at increased humidity. All this time the laminate is free of external loads.

The elastic stresses are obtained by superposing the solution for a geometrically constrained case, in which the moisture sorption and temperature variation are considered without any deformation, and the solution for strain fields $\epsilon_x(t)$ and $\epsilon_y(t)$ which are uniform throughout the thickness. The superposition is effected in such a manner that the net resultant forces F_x and F_y, in the x and y directions respectively, vanish. The requirements $\Sigma F_x = 0$, $\Sigma F_y = 0$, represent the absence of externally applied loads, but are insufficient to account for detailed edge effects, and provide the equations to determine the strains $\epsilon_x(t)$ and $\epsilon_y(t)$. Since the moisture profile at each time is known from the solution to the diffusion equation, denote the total contribution to swelling due to moisture in, say, the

i^{th} ply by

$$e_T(M_i^\phi) = \beta_T \int_{\substack{\text{Thickness of} \\ i^{th} \text{ ply}}} (m - m_i)\,dz \tag{10}$$

In (10), the superscript ϕ, which may be 0° or 90°, indicates the orientation of the i^{th} ply. Consequently, the cumulative transverse swelling due to moisture for all 0° plies is

$$e_T(M^0(t)) = \sum_{i=1}^{N_0} e_T(M_i^0)$$

and similarly for the 90° plies

$$e_T(M^{90}(t)) = \sum_{i=1}^{N_{90}} e_T(M_i^{90})$$

The total longitudinal swelling can be obtained in an analogous manner. However, since we take $\beta_L = 0$, these analogous terms will vanish in our case.

Denote h^0 and h^{90} as the total thickness of all of the 0^0 and 90^0 plies respectively, then employment of (8) together with the equilibrium requirements $\Sigma F_x = 0$, $\Sigma F_y = 0$ yield

$$\begin{aligned} (h^0 C_L + h^{90} C_T)\epsilon_x + (h^0 + h^{90}) C_{12} \epsilon_y &= R_1 \\ (h^0 + h^{90}) C_{12} \epsilon_x + (h^0 C_T + h^{90} C_L)\epsilon_y &= R_2 \end{aligned} \tag{11}$$

where

$$\begin{aligned} R_1 &= C_L e_L(M^0) + C_{12} e_T(M^0) + C_T e_T(M^{90}) + C_{12} e_L(M^{90}) \\ &\quad + h^0(C_L \alpha_L + C_{12} \alpha_T)\Delta T + h^{90}(C_T \alpha_T + C_{12} \alpha_L)\Delta T \\ R_2 &= C_{12} e_L(M^0) + C_T e_T(M^0) + C_{12} e_T(M^{90}) + C_L e_L(M^{90}) \\ &\quad + h^0(C_T \alpha_T + C_{12} \alpha_L)\Delta T + h^{90}(C_L \alpha_L + C_{12} \alpha_T)\Delta T \end{aligned} \tag{12}$$

The simultaneous solution of (11) yields the values of the time-dependent strains ϵ_x and ϵ_y. The stress profile due to temperature and moisture conditioning is obtained by substituting the strains from (11) into (8).

The time-dependent elastic stresses are thus determined for all times until moisture saturation is reached for each particular conditioning scheme. At this stage, the temperature is lowered down to room temperature, causing sudden increments in all stresses. These increments are obtained by solving a simplified version of (11), (12) and (8) in which R_1 and R_2 contain only suitable ΔT terms.

VISCOELASTIC STRESS ANALYSIS

Consider Eqs. (9). These equations contain four unknown stresses whose evaluation requires the solution of simultaneous integral equations.

To avoid this cumbersome task we invert the compliances and rewrite (9) to express stresses in terms of ε_x, ε_y, m and T.

As a first step toward this inversion consider the Laplace transform of (9).

Denoting $\bar{f}(p) = \int_0^\infty e^{-pt} f(t)dt$ and $p\bar{f}(p) = \hat{f}(p)$

we obtain from (9)

$$\hat{S}_L \bar{\sigma}_x{}^0 + \hat{S}_{12}\bar{\sigma}_y{}^0 = \bar{R}_1{}^0 \quad , \quad \hat{S}_{12}\bar{\sigma}_x{}^{90} + \hat{S}_L\bar{\sigma}_y{}^{90} = \bar{R}_2{}^{90} \quad ,$$

$$\hat{S}_T\bar{\sigma}_x{}^{90} + \hat{S}_{12}\bar{\sigma}_x{}^{90} = \bar{R}_1{}^{90} \quad , \quad \hat{S}_{12}\bar{\sigma}_x{}^0 + \hat{S}_T\bar{\sigma}_y{}^0 = \bar{R}_2{}^0 \tag{13}$$

Inverting (13) we obtain

$$\bar{\sigma}_x{}^0 = \hat{C}_L\bar{R}_1{}^0 + \hat{C}_{12}\bar{R}_2{}^0 \qquad \bar{\sigma}_x{}^{90} = \hat{C}_T\bar{R}_1{}^{90} + \hat{C}_{12}\bar{R}_2{}^{90}$$

$$\bar{\sigma}_y{}^0 = \hat{C}_{12}\bar{R}_1{}^0 + \hat{C}_T\bar{R}_2{}^0 \qquad \bar{\sigma}_y{}^{90} = \hat{C}_{12}\bar{R}_1{}^{90} + \hat{C}_L\bar{R}_2{}^{90} \tag{14}$$

where, in (14) $\hat{C}_L = \frac{\hat{S}_T}{\hat{\Delta}}$, $\hat{C}_T = \frac{\hat{S}_L}{\hat{\Delta}}$, $\hat{C}_{12} = -\frac{\hat{S}_{12}}{\hat{\Delta}}$

and $\Delta = \hat{S}_L\hat{S}_T - \hat{S}_{12}^2$.

In the present case, with S_L and S_{12} being constant, the only term which requires attention is S_T.

In view of (5)

$S_T = D_0 + D_1 t^q$

consequently

$$\hat{S}_T = D_0 + D_1 \frac{\Gamma(q+1)}{p^q} \tag{15}$$

We shall employ the approximate form [11], whereby F(t) can be expressed from (?) according to $F(t) = \hat{F}(p) |p = 1/2t$. Therefore (15) yields

$$S_T(t) = D_0(1 + At^q) \tag{16}$$

where

$$A = 2^q \frac{D_1\Gamma(q+1)}{D_0}$$

Similarly, instead of $\hat{\Delta}$ we shall write, upon inversion

$$\Delta(t) = S_L D_0(1 + At^q) - S_{12}^2 \tag{17}$$

Altogether, the Laplace transform inversion of (9) will give

$$\sigma_x^0(t) = \int_0^t \left\{ C_L[\xi(t) - \xi(\tau)] \frac{dR_1^0(\tau)}{d\tau} + C_{12}[\xi(t) - \xi(\tau)] \frac{dR_2^0(\tau)}{d\tau} \right\} d\tau$$

$$\sigma_y^0(t) = \int_0^t \left\{ C_{12}[\xi(t) - \xi(\tau)] \frac{dR_1^0(\tau)}{d\tau} + C_T[\xi(t) - \xi(\tau)] \frac{dR_2^0(\tau)}{d\tau} \right\} d\tau \qquad (18)$$

and similar expressions for $\sigma_x^{90}(t)$ and $\sigma_y^{90}(t)$.

Explicitly in (18), we have $C_L(t) = D_0(1+At^q)/\Delta(t)$, $C_T(t) = S_L/\Delta(t)$,

and $C_{12}(t) = -S_{12}/\Delta(t)$ where $\Delta(t) = S_L D_0(1+At^q) - S_{12}^2$

Just as in the elastic analysis we now have terms $R_1^0(t)$, $R_2^0(t)$, and also $R_1^{90}(t)$ and $R_2^{90}(t)$ which contain known values of moisture $m(z,t)$ and temperature $\Delta T(t)$ and yet unknown strains $\varepsilon_x(t)$ and $\varepsilon_y(t)$ which are spatially uniform. These unknown strains are present in order to reassure null resultant forces $\Sigma F_x(t) = 0$, $\Sigma F_y(t) = 0$. Note that the above requirement of null resultants which applies for all times, provides the conditions for the determination of $\varepsilon_x(t)$ and $\varepsilon_y(t)$ at all times.

In addition, we should note that the viscoelastic analysis considers the initial stresses and strains, $\varepsilon_x(0)$ and $\varepsilon_y(0)$, and accounts for their own relaxation as time progresses during the conditioning stage.

Finally, in order to clarify matters, we observe that during conditioning the moisture m varies but the temperature T remains constant, therefore $\Delta T = 0$ in R_1^0, R_2^0, etc. during that stage.

Altogether we have
$$\sigma_x^0(z,t) = -\left\{ \left[\alpha_L C_L(\xi) + \alpha_T C_{12}(\xi)\right](T_{cure} - T_{cond}) + \left[\beta_L C_L(\xi) + \beta_T C_{12}(\xi)\right]\left[m(z,0) - m_0\right] \right\} + C_L(\xi)\,\varepsilon_x(0) + C_{12}(\xi)\,\varepsilon_y(0)$$
$$+ \int_0^t \left\{ C_L[\xi(t) - \xi(\tau)] \frac{d\varepsilon_x(\tau)}{d\tau} + C_{12}[\xi(t) - \xi(\tau)] \frac{d\varepsilon_y(\tau)}{d\tau} \right.$$
$$\left. -\beta_L C_L[\xi(t) - \xi(\tau)] \frac{dm(z,\tau)}{d\tau} - \beta_T C_{12}[\xi(t) - \xi(\tau)] \frac{d[m(z,\tau) - m_1]}{d\tau} \right\} d\tau \qquad (19)$$

Similar expressions can be derived for $\sigma_x^{90}(z,t)$, $\sigma_y^0(z,t)$ and $\sigma_y^{90}(z,t)$. For details see Ref. [1].

In (19) $m(z,0)$ is the moisture level at the beginning of the conditioning stage. This moisture level, at $t = 0^+$, is taken to be the ambient conditioning moisture level at the outermost surface of the laminate ($z = \pm h$), while the remainder of the laminate remains at the initial moisture level due to storage.

Eq. (19), and its counterparts for σ_x^{90}, σ_y^0, and σ_y^{90}, express the time-dependent viscoelastic stresses until saturation time $t = t_f$. The value of t_f of course depends on the conditioning temperature T. At $t = t_f$ the temperature is lowered to the room temperature T_R, causing sudden stress increments.

These increments are computed elastically because of their rapid development, which rules out viscoelasticity.

Thus, at time $= t_f^+$ we get

$$\sigma_x^{0}(z,t_f^+) = \sigma_x^{0}(z,t_f^-) - [\alpha_L C_L(0) + \alpha_T C_{12}(0)](T_{cond} - T_g)$$

$$+ C_{12}(0)[\varepsilon_y(t_f^+) - \varepsilon_y(t_f^-)] + C_L(0)[\varepsilon_x(t_f^+) - \varepsilon_x(t_f^-)] \tag{20}$$

Analogous expressions can be derived for $\sigma_x^{90}(z,t_f^+)$, $\sigma_y^{0}(z,t_f^+)$, and $\sigma_y^{90}(z,t_f^+)$. For complete details see Ref. [1].

The time dependent strains $\varepsilon_x(t)$ and $\varepsilon_y(t)$ are determined from the requirement that $\int_{-h}^{h}\sigma_x(z,t)dz = 0$ and $\int_{-h}^{h}\sigma_y(z,t)dz = 0$ at all times t. The thus determined $\varepsilon_x(t)$ and $\varepsilon_y(t)$ are then reinserted into (19), (20), and the analogous expressions, to yield the actual stress distributions.

In order to perform the computations indicated in (19), we discretize the thickness of the laminate into portions Δz and the time interval into portions Δt. The thickness discretization is required in order to determine the moisture profile at each time and account for its effect on the "reduced time", $\xi = \xi(z,t)$. Furthermore, this discretization is required when performing the integration of stresses across the thickness to obtain $\Sigma F_x = 0$ and $\Sigma F_y = 0$. Satisfactory results were obtained by dividing each ply into five equal increments $\Delta z = 0.00025$ cm.

The discretization of the time domain t into portions Δt between $t_1 = 0$ and the current value t is required to evaluate the time integrals like, say,

$$\int_0^t C_L[\xi(t) - \xi(\tau)]\frac{d\varepsilon_x(\tau)}{d\tau}d\tau$$

For this purpose we employ a scheme similar to [12]. Denoting $t_1 = 0$, $t = t_{j+1}$ we get

$$\int_0^t C_L[\xi(t) - \xi(\tau)]\frac{d\varepsilon_x(\tau)}{d\tau}d\tau = \sum_{k=1}^{j}\int_{t_k}^{t_{k+1}} C_L[\xi(t) - \xi(\tau)]\frac{d\varepsilon_x(\tau)}{d\tau}d\tau$$

$$= \frac{1}{2}\sum_{k=1}^{j}\left\{C_L[\xi(t_{j+1}) - \xi(t_{k+1})] + C_L[\xi(t_{j+1}) - \xi(t_k)]\right\}[\varepsilon(t_{k+1}) - \varepsilon(t_k)] \tag{21}$$

Expression (21) contains all previously known strains $\varepsilon_x(t_1)$, $\varepsilon_x(t_2)$........, $\varepsilon_x(t_j)$ and the current, yet unknown, strain $\varepsilon_x(t_{j+1})$. In this manner the unknown strains $\varepsilon_x(t_{j+1})$ and, similarly, $\varepsilon_y(t_{j+1})$ are isolated and solved for in a time-marching sequence.

Satisfactory accuracy was obtained by taking six equal increments per decade along the logarithmic time scale.

MATERIAL PROPERTIES AND COMPUTATIONS

The material properties which entered the actual computations are summarized in Table 1 below. Due to the incompleteness of the experimental data it was necessary to employ data for two graphite/epoxy systems. Data marked with a star (*) refers to T300/5208 from Ref. [7], otherwise the data refers to AS/3501-6 from Ref. [9].

The actual computations aim at comparing the stresses for two conditioning environments. In both cases, the initial stresses are identical, and are attributed to the following causes:

Parameter	Symbol	Magnitude
Moisture diffusivity	A_1	$0.016715\ cm^2/sec.$*
$D = A_1 \exp(-B_1/T)$ (T in °K)	B_1	$4618.0°K$*
Coefficient of moisture expansion per 1% weight gain		
Longitudinal	β_L	0.*
Transverse	β_T	0.4899*
Moisture offset value	m_1	0.5450*
Coefficient of thermal expansion		
Longitudinal	α_L	$-.54 \times 10^{-6}$ cm/cm/°K*
Transverse	α_T	25.74×10^{-6} cm/cm/°K*
Initial transverse compliance D_0	a	$.12878 \times 10^{-11} \frac{kPa^{-1}}{°K \times R.H.}$
$D_0 = aTH + bT + CH + d$	b	$.14147 \times 10^{-9} \frac{kPa^{-1}}{°K}$
	c	$.29075 \times 10^{-9} \frac{kPa^{-1}}{R.H.}$
	d	$4.482 \times 10^{-7}\ kPa^{-1}$
Transverse compliance, creep	D_1	$.1631 \times 10^{-8}\ kPa^{-1}/sec.^q$
Power law exponent	q	0.18
Longitudinal compliance	S_L	$.7653 \times 10^{-8} kPa^{-1}$
"Cross effect" compliance	S_{12}	$-.2679 \times 10^{-8}\ kPa^{-1}$
Temperature shift factor function	a_3	-105.5
Eq. $(6)_1$	a_4	$6.183 \times 10^4\ °K$
	a_5	$-9.053 \times 10^6\ °K^2$
Moisture shift factor function	a_6	.06336
$a_2 = a_6 \times (\%m)^{b_1}$	b_1	-8.942
Moisture to R.H. conversion factor		
$m = E \times (\%R.H.)$	E	.01505*

Table 1. Material Properties

1. Cool-down from a cure temperature, $T_{cure} = 450°K$ (350°F) to room temperature, $T_{room} = 297°K$ (75°F).

2. Uniform moisture saturation during storage due to 50% relative humidity.

In actuality, the effect of the temperature rise from $T_{room} = 75°F$ to the conditioning temperature is incorporated into the initial conditions.

The two conditioning environments are:

1. 339°K (150°F) at 98% R.H.

2. 355°K (180°F) at 98% R.H.

The magnitudes of material parameters, which are dependent on the conditioning environment, are calculated for each environment and summarized in Table 2.

Results are shown for $[0_2/90_2]_s$ laminates. Further results, for other lay-ups are given in [1].

Parameter	Symbol	Conditioning Temperature 339°K	355°K	Units
Moisture diffusivity	D	$.2000 \times 10^{-8}$	$.3798 \times 10^{-8}$	cm^2/sec.
Initial transverse	D_0	$.1063 \times 10^{-6}$	$.1102 \times 10^{-6}$	kPa^{-1}
Temperature shift factor function	a_1	0.0137	0.00063	
Elastic moduli	C_L	131.1×10^6	131.8×10^6	kPa
	C_T	9.45×10^6	9.17×10^6	kPa
	C_{12}	3.303×10^6	3.203×10^6	kPa

Table 2. Conditioning Dependent Material Properties

RESULTS AND DISCUSSION

Figs. 3 and 4 exhibit the stresses $\sigma_x(z,t)$ and $\sigma_y(z,t)$ due to moisture sorption at 98% R.H. These figures provide comparisons between conditioning at 339°K (dashed lines) and at 355°K (solid lines) and demonstrate the "competition" between the effects of moisture and temperature as stress inducing agents on one hand and stress-relaxing parameters on the other hand.

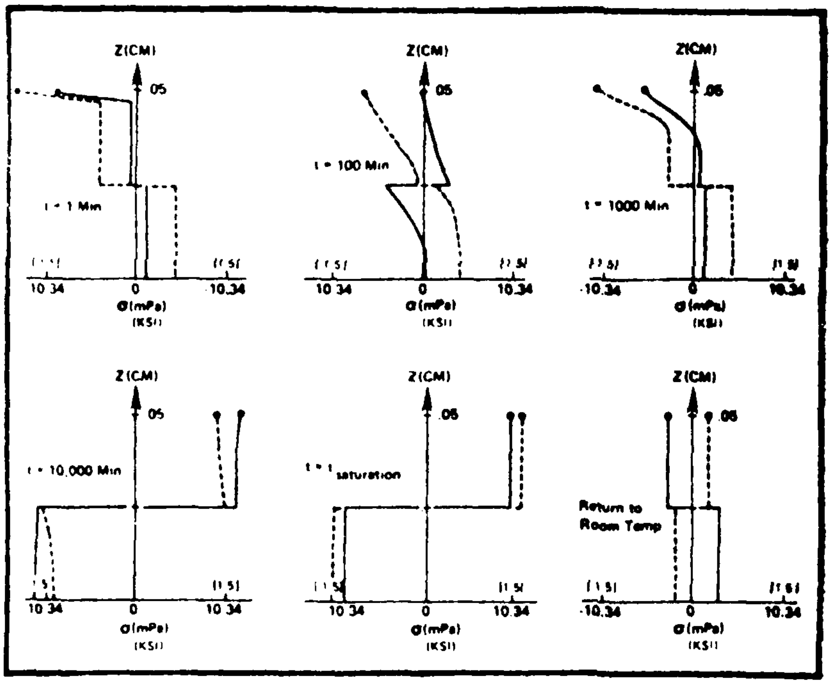

Fig. 3. The Viscoelastic Stresses σ_x Vs. The Spatial Coordinate z at Various Times t for $[0_2/90_2]_s$ laminate (z = 0 is Symmetry Plane) Due to Moisture Conditioning at 98% R.H. at 355°K (Solid Lines) and 339°K (Dashed Lines). σ in mPa (ksi in parentheses).

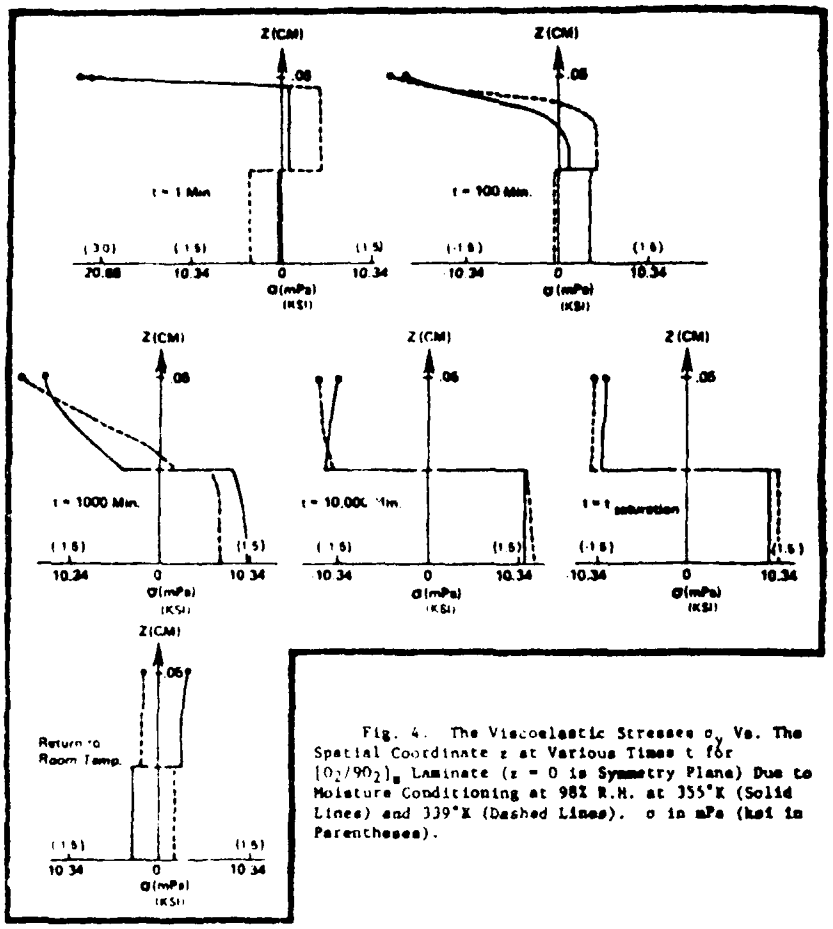

Fig. 4. The Viscoelastic Stresses σ_y Vs. The Spatial Coordinate z at Various Times t for $[0_2/90_2]_s$ Laminate (z = 0 is Symmetry Plane) Due to Moisture Conditioning at 98% R.H. at 355°K (Solid Lines) and 339°K (Dashed Lines). σ in mPa (ksi in Parentheses).

To appreciate the total effect of conditioning, consider the stresses σ_y at each conditioning temperature (Fig. 4). During the early stages of conditioning, t = 1 minute, for which there has been but minimal added moisture, the stress profiles reflect the difference between the two conditioning temperatures. However, as conditioning progresses, say up to 1000 minutes, the dependence of moisture sorption and the stress relaxation on the conditioning temperature becomes prominent. At this stage, there is noticeably more moisture sorption at 355°K that at 339°K as is evident by the larger compressive stresses in the transverse direction of the outer ply. Yet, at the outer surface of the laminate, where the boundaries were exposed to the ambient conditioning moisture level throughout the entire 1000 minutes of the conditioning stage, the compressive stresses are about 17 percent lower for the conditioning environment of 355°K. After 10,000 minutes we note that the slopes of the transverse stresses in the outer ply are of opposite signs. This contrast is attributed to the enhanced relaxation at 355°K. Finally, upon reaching moisture saturation (≈ 22 days at 355°K, and 43 days at 339°K), the stress profile in both the longitudinal and transverse directions is nearly uniform across the thickness; yet, the fact that the stress magnitudes are similar is purely

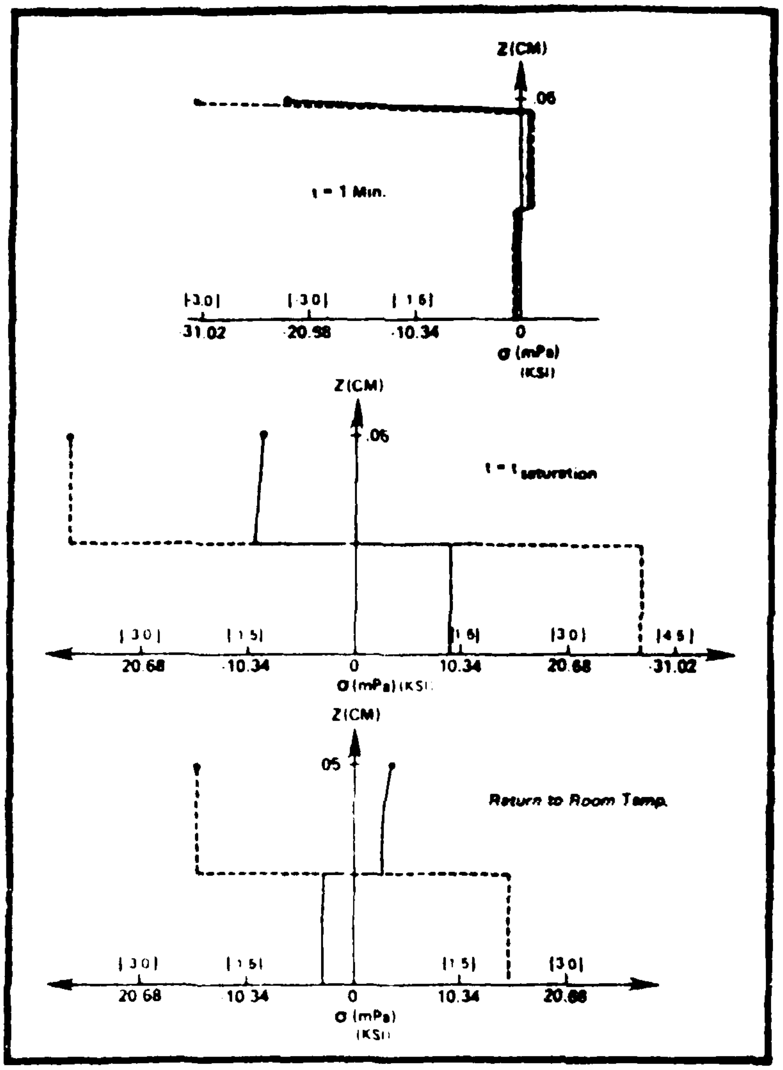

Fig. 5. The Stresses σ_y Vs. The Spatial Coordinate z at Various Times t Due to Conditioning at 98% R.H. at 355°K. Viscoelastic Results (Solid Lines) Vs. Linear Elastic Predictions (Dashed Lines). σ in mPa (ksi in parentheses).

coincidental.

The final cool-down to room temperature of 297°K superimposes additional stresses on the laminate. However, since conditioning at a lower temperature corresponds to a smaller stress increment, the stresses due to conditioning at 339°K are lower than those stresses resulting from conditioning at 355°K. Note also that the locations of tensile and compressive stresses are reversed.

For comparative purposes, the elastic and viscoelastic stresses are presented in Fig. 5 for conditioning at 355°K.

The figure shows that by discarding time-dependent response and overlooking stress relaxation the elastic analysis predicts stresses which differ from the viscoelastic results in sign and overestimates them by three to six fold.

REFERENCES

1 DOUGLASS, D.A., "Stresses Due to Environmental Conditioning of Cross-Ply Graphite/Epoxy Laminates," M.Sc. Thesis, Texas A&M University, August 1979.

2 SHIRREL, C.D., "Diffusion of Water Vapor in Graphite/Epoxy Laminates." In Advanced Composite Materials - Environmental Effects, STP 658 (ASTM) J.R. Vinson - Editor, 1978, pp. 21-42.

3 ALTHOF, W., "The Diffusion of Water Vapor in Humid Air into the Bondlines of Adhesive Bonded Metal Joints," Proc. of the 11th National SAMPE Technical Conference, Boston, Mass. Nov. 1979, pp. 309-315.

4 LUIKOV, A.V., "Analytical Heat Diffusion Theory," Academic Press, 1968, pp. 97-114.

5 DELASI, R. and WHITESIDE, J.B., "Effect of Moisture on Epoxy Resins and Composites." In Advanced Composite Materials - Environmental Effects, STP 658 (ASTM), J.R. Vinson - Editor, 1978, pp. 2-20.

6 WEITSMAN, Y., J. Composite Materials, Vol. 10, 1976, pp. 193-204.

7 MCKAGUE, E.L., and HALKIAS, J.E., Private Communication.

8 CROSSMAN, R.W., MAURI, R.E. and WARREN, R.J., "Hygrothermal Damage Mechanisms in Graphite/Epoxy Composites." Lockheel Palo Alto Research Laboratory. Final Report 1978.

9 RENTON, W.J. and HO, T., "The Effect of Environment on the Mechanical Behavior of AS/3501-6 Graphite-Epoxy Material," Vought Corp. Dallas, Texas. Report No. B-92100/80R-105, pp. 57-63.

10 SCHAPERY, R.A., J. Composite Materials, Vol. 1, 1967, pp. 228-266.

11 FUNG, Y.C., "Foundations of Solid Mechanics." Prentice-Hall, 1965, p. 417.

12 LEE, E.H., and ROGERS, T.G., J. Applied Mechanics, ASME Vol. 30, 1963, pp. 127-133.

RESIDUAL THERMAL STRESSES IN AN UNSYMMETRICAL CROSS-PLY GRAPHITE/EXPOXY LAMINATE

Brian Douglas Harper*
Y. Weitsman**
Texas A&M University
College Station, Texas

Abstract

This paper presents an exploratory investigation of the residual stresses in AS-3502 graphite/epoxy laminates due to cool-down from their cure temperature. Emphasis is placed on the significance of time-dependent material behavior and the potential utilization of this phenomenon to reduce residual stresses by a judicious choice of the cool down process. The analysis considers the time-dependent behavior of the material and all calculations employ recent data on the thermoviscoelastic response of the AS-3502 graphite/epoxy system. The viscoelastic analysis is verified through curvature measurements of unsymmetric cross-ply plates fabricated from the AS-3502 graphite-epoxy material.

Introduction

The curing of composite laminates at temperatures above their service temperature induces residual stresses upon cool down due to the difference in thermal expansion coefficients in the longitudinal and transverse directions of the laminae. It has long been recognized that the presence of residual stresses greatly affects the strength of composite laminates. For this reason there has been an increasing interest in development of improved methods to determine these stresses and to minimize their magnitudes.

Pagano and Hahn[1] utilized an approximate method for determining the residual stresses in an unsymmetrical cross-ply laminate. They considered [illegible] elastic behavior of the laminate at temperature T_0, while above that temperature T_0 they assumed a zero stress state.

It has been long noted that epoxies exhibit pronounced viscoelastic effects, consequently there exists both need and justification for an analysis which considers the time dependence of the material during the entire cool down process.

Douglass and Weitsman[2] used a viscoelastic analysis to predict the residual stresses in a symmetric cross-ply laminate due to both temperature and moisture effects; however no attempt was made to verify these results experimentally.

This paper presents a method for evaluating the residual stresses in unsymmetrical cross-ply laminates which employs linear viscoelasticity throughtout the cool down stage. Unsymmetric laminates are chosen because their deformation involves anti-clastic curvatures which are amenable to measurement, unlike the case of symmetric laminates. Several unsymmetric cross-ply AS-3502 graphite/epoxy laminates were fabricated and the curvatures measured to verify the viscoelastic analysis.

Due to the significant creep of epoxies, especially in the elevated-temperature range, there exists an optimal cool down path that will minimize the residual stresses. This optimal path is determined for the AS-3502 graphite/epoxy system using a method suggested by Weitsman[3].

Elastic Stress Analysis

The thermoelastic stress-strain relations for an orthotropic lamina under plane stress conditions are[4]

$$\sigma_i = C_{ij}(\varepsilon_j - \alpha_j \Delta T) \qquad i, j = 1, 2, 6 \quad (1)$$

In (1) and the sequel, σ is stress, ε is strain, C_{ij} are stiffnesses, α are coefficients of of thermal expansion, T is the temperature and ΔT the temperature difference.

Consider the cross-ply $0_n/90_n$ unsymmetrical laminate shown in figure 1.

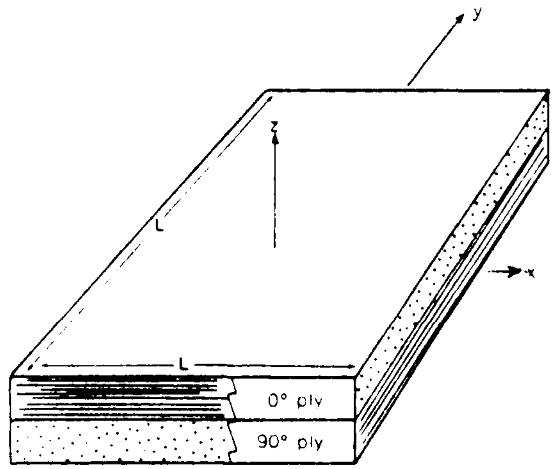

Fig. 1 Geometry of the Unsymmetric Cross-ply Laminated Plate.

Since in the principal directions σ_{12} vanishes and there exist no shear stress to normal strain coupling terms, we have

$$\gamma_{xy} = \varepsilon_{xy} = \tau_{xy} = 0$$

Referring to the individual laminae in Figure 1 we can express the stress-strain relations as follows:

*Graduate Student, Mechanical Engineering
**Professor, Mechanics & Materials Center, Civil Engineering Department

To appear in the proceedings of the 22nd SSD & Materials Conference, Altanta, Georgia, April 6-8, 1981.

$$\sigma_x^{0} = C_L\varepsilon_x + C_{12}\varepsilon_y - (C_L\alpha_L + C_{12}\alpha_T)\Delta T$$

$$\sigma_y^{0} = C_{12}\varepsilon_x + C_T\varepsilon_y - (C_{12}\alpha_L + C_T\alpha_T)\Delta T \qquad (2)$$

$$\sigma_x^{90} = C_T\varepsilon_x + C_{12}\varepsilon_y - (C_T\alpha_T + C_{12}\alpha_L)\Delta T$$

$$\sigma_y^{90} = C_{12}\varepsilon_x + C_L\varepsilon_y - (C_{12}\alpha_T + C_L\alpha_L)\Delta T$$

In equations (2) superscripts indicate ply orientation and subscripts L and T denote the properties in directions parallel and transverse to the fibers respectively.

Following the assumptions of classical plate theory[5] we can express the strains in terms of the midsurface displacements u_o, v_o, and w_o and get,

$$\varepsilon_x = \frac{\partial u_o}{\partial x} - z\frac{\partial^2 w_o}{\partial x^2}$$

$$\varepsilon_y = \frac{\partial v_o}{\partial y} - z\frac{\partial^2 w_o}{\partial y^2} \qquad (3)$$

Denoting midplane strains and curvatures in the usual manner

$$\varepsilon_x^{o} = \frac{\partial u_o}{\partial x},\quad \varepsilon_y^{o} = \frac{\partial v_o}{\partial y},\quad K_x = -\frac{\partial^2 w_o}{\partial x^2},\quad K_y = -\frac{\partial^2 w_o}{\partial y^2} \qquad (4)$$

equations (3) become

$$\varepsilon_x = \varepsilon_x^{o} + ZK_x,\quad \varepsilon_y = \varepsilon_y^{o} + ZK_y \qquad (5)$$

The midplane strains and curvatures in the 0/90 unsymmetrical laminate due to a uniform temperature change ΔT can be determined by requiring that the net resultant forces (N) and bending moments (M) which act on the plate must vanish. This results in the following expressions:

$$N_x = \int_{-h}^{0}\sigma_x^{90}\,dZ + \int_{0}^{h}\sigma_x^{0}\,dZ = 0$$

$$N_y = \int_{-h}^{0}\sigma_y^{90}\,dZ + \int_{0}^{h}\sigma_y^{0}\,dZ = 0$$

$$M_x = \int_{-h}^{0}Z\sigma_x^{90}\,dZ + \int_{0}^{h}Z\sigma_x^{0}\,dZ = 0 \qquad (6)$$

$$M_y = \int_{-h}^{0}Z\sigma_y^{90}\,dZ + \int_{0}^{h}Z\sigma_y^{0}\,dZ = 0$$

Combining equations (2), (5) and (6) we get

$$\varepsilon_x^{o} = \varepsilon_y^{o} = \frac{1}{D}\left[\frac{2}{3}(C_L+C_T-2C_{12})P - \frac{1}{2}(C_L-C_T)Q\right]\Delta T,\qquad hK_x = -hK_y$$

$$= \frac{1}{D}\left[(C_L+C_T+2C_{12})Q - (C_L-C_T)P\right]\Delta T \qquad (7)$$

where, in (7)

$$D = \frac{1}{3}\left[(C_L+C_T)^2 - 4C_{12}^2\right] - \frac{1}{2}(C_L-C_T)^2$$

$$P = (C_L+C_{12})\alpha_L + (C_T+C_{12})\alpha_T \qquad (8)$$

$$Q = (C_L-C_{12})\alpha_L - (C_T-C_{12})\alpha_T$$

Stresses may now be evaluated by incorporating the results from equations (7) into equations (2).

Viscoelastic Stress Analysis

It has been noted that graphite/epoxy composites exhibit a considerable amount of time dependent mechanical response, especially at elevated temperatures. This time dependence may be approximated by a viscoelastic constitutive relationship and employed to predict strains and curvatures due to cool down from the cure temperature.

Although the behaviour of polymeric resins immediately after cure exhibits dependence on such complicated factors as aging time, quenching rates and perhaps on a variety of non-linear effects we shall assume herein a linear and thermorheologically simple (TRS) viscoelastic behaviour.

Data on graphite/epoxy[6] indicate that the assumption of TRS behavior involves only small errors.

Accordingly, the transient thermal response can be related by means of a single temperature-dependent function $A_T(T)$ which is called the "shift-factor".

The time-dependent portion of the viscoelastic behavior involves reduced-times, which are denoted in the sequel by $\xi(t)$ and $\xi(\tau)$, where

$$\xi(t) = \int_0^t \frac{ds}{A_T[T(s)]},\quad \xi(\tau) = \int_0^\tau \frac{ds}{A_T[T(s)]} \qquad (9)$$

The viscoelastic counterparts of the elastic expressions (2) are:

$$\sigma_x^{o}(t) = \int_0^t \Big\{ C_L[\xi(t)-\xi(\tau)]\frac{d\varepsilon_x(\tau)}{d\tau} + C_{12}[\xi(t)-\xi(\tau)]\frac{d\varepsilon_y(\tau)}{d\tau} - \Big[\alpha_L C_L[\xi(t)-\xi(\tau)] + \alpha_T C_{12}[\xi(t)-\xi(\tau)]\Big]\frac{d\Delta T(\tau)}{d\tau}\Big\}\,d\tau \qquad (10a)$$

$$\sigma_y^o(t) = \int_0^t \Big\{ C_{12}[\xi(t) - \xi(\tau)] \frac{d\varepsilon_x(\tau)}{d\tau} + C_T[\xi(t) - \xi(\tau)] \frac{d\varepsilon_y(\tau)}{d\tau} - \Big[\alpha_L C_{12}[\xi(t) - \xi(\tau)] + \alpha_T C_T[\xi(t) - \xi(\tau)] \Big] \frac{d\Delta T(\tau)}{d\tau} \Big\} d\tau \qquad (10b)$$

Also, $\sigma_x^{1o}(t)$ and $\sigma_y^{1o}(t)$ can be obtained from $\sigma_x^o(t)$ and $\sigma_y^o(t)$, respectively, by interchanging the roles of ε_x and ε_y in (10).

In the case of thermorheologically simple behavior we can obtain viscoelastic solutions from the results to analogous elasticity problems by means of the so-called correspondence principle. The principle remains valid if at any give time the temperature is spatially uniform. In our case this condition is satisfied to a sufficient degree of accuracy due to the high thermal conductivity of graphite/epoxy laminates.

In this paper we shall employ the correspondence principle in conjunction with an approximate technique for the inversion of the Laplace-transformed elasticity solution. Applied together those principle and technique combine to yield the "quasi-elastic" method.[7] Accordingly, the viscoelastic response function to a unit input is approximated by an elasticity solution in which all elastic constants are replaced by the corresponding reduced-time dependent properties. Once this unit response function is obtained, the response to any general input may be obtained by means of the convolution integral.

Consequently, we obtain the following expressions for the time dependent midplane strains and curvatures in view of [illegible]

$$\varepsilon_y^o(t) = \int_0^t \frac{1}{D[\xi(t) - \xi(\tau)]} \Big\{ \frac{h}{3} \Big[C_L[\xi(t) - \xi(\tau)] + C_T[\xi(t) - \xi(\tau)] - [illegible]\, C_{12}[\xi(t) - \xi(\tau)] \Big] P[\xi(t) - \xi(\tau)] - \frac{h}{2} \Big[C_L[\xi(t) - \xi(\tau)] - C_T[\xi(t) - \xi(\tau)] \Big] Q[\xi(t) - \xi(\tau)] \Big\} \frac{d\Delta T(\tau)}{d\tau} d\tau \qquad (11)$$

$$\kappa_y(t) = [illegible]\, h\kappa_x(t) + \int_0^t \frac{1}{D[\xi(t) - \xi(\tau)]} \Big\{ \Big[C_L[\xi(t) - \xi(\tau)] + C_T[\xi(t) - \xi(\tau)] + 2C_{12}[\xi(t) - \xi(\tau)] \Big] Q\Big[\xi(t) - \xi(\tau)\Big] - \Big[C_L[\xi(t) - \xi(\tau)] - C_T[\xi(t) - \xi(\tau)] \Big] P[\xi(t) - \xi(\tau)] \Big\} \frac{d\Delta T(\tau)}{d\tau} d\tau \qquad (12)$$

where, in (12), $D[\xi(t) - \xi(\tau)]$, $P[\xi(t) - \xi(\tau)]$, and $Q[\xi(t) - \xi(\tau)]$ are obtained from D, P and Q in (8) with moduli C_{ij} replaced by $C_{ij}[\xi(t) - \xi(\tau)]$.

In the AS-3502 graphite/epoxy system used in this work, the only compliance which exhibits significant time dependent behaviour is the transverse compliance S_T[6]. The time dependent transverse compliance S_T, can be expressed by a "power law" equation of the form

$$S_T(t) = D_1 \left[\frac{t}{A_T(T)} + \tau_o \right]^q \qquad (13)$$

where t is time, and D_1, q and τ_o are material constants. Furthermore, the shift-factor is given by[6]

$$A_T(T) = \exp(-T/A + B) \qquad (14)$$

where T is the temperature in degrees Kelvin and A and B are material constants.

Since equations (10) - (12) contain stiffnesses rather than compliances it is necessary to invert the compliance matrix to obtain the time dependent stiffnesses. Performing this inversion we get

$$C_L(t) = \frac{S_T(t)}{\Delta(t)}, \; C_T(t) = \frac{S_L}{\Delta(t)}, \; C_{12}(t) = \frac{-S_{12}}{\Delta(t)} \qquad (15)$$

where $\quad \Delta(t) = S_L S_T(t) - S_{12}^2$

In order to perform the computations indicated in (12) we discretize the time domain into portions Δt between $t_1 = 0$ and the current value t. Consider for example the convolution integral,

$$\int_0^t F[\xi(t) - \xi(\tau)] \frac{d\Delta T(\tau)}{d\tau} d\tau. \qquad (16)$$

Denoting $t_1 = 0$ and $t = t_{j+1}$ (16) reduces to

$$\int_0^t F[\xi(t) - \xi(\tau)] \frac{d\Delta T(\tau)}{d\tau} d\tau = \sum_{k=1}^{j} \int_{t_k}^{t_{k+1}} F[\xi(t) - \xi(\tau)] \frac{d\Delta T(\tau)}{d\tau} d\tau = \frac{1}{2} \sum_{K=1}^{j} \Big\{ F[\xi(t_{j+1}) - \xi(t_{k+1})] + F[\xi(t_{j+1}) - \xi(t_k)] \Big\} \Big[\Delta T(t_{k+1}) - \Delta T(t_K) \Big] \qquad (17)$$

Optimal Time-Temperature Path

Reverting to compliances in place of stiffnesses in (7) and employing the quasi-elastic approximate method we obtain the following expression

$$hK_x(t) = \int_0^t F[\xi(t) - \xi(\tau)] \frac{d\Delta T(\tau)}{d\tau} d\tau \quad (18)$$

in (18)

$$F(t) = \frac{6[2S_L(\alpha_L - \alpha_T)S_T(t) - 2S_{12}^2(\alpha_L - \alpha_T)]}{S_T^2(t) + 14S_L S_T(t) + S_L^2 - 16S_{12}^2} \quad (19)$$

Also $\quad \Delta T(\tau) = T(\tau) - T_I$,

where T_I is the stress free reference temperature.

The residual stresses in an elastic material depend strictly on the temperature difference ΔT, and not the time-temperature path employed to achieve that temperature difference. A viscoelastic material, however, has time dependent material properties which are strongly affected by temperature. Since the relaxation of residual stresses are enhanced at elevated temperatures, there exists an optimal cool down path $T(t)$ which minimizes the residual stress.

With prescribed initial (elevated) temperature T_I, final temperature T_F and cooling time t_f a solution for the optimal path $T(t)$ can be obtained for a wide class of functions $F(t)$ in (18). We take T_I to be cure temperature, at which the laminate is assumed stress free, and T_F as the room temperature.

The optimal path $T(t)$ which minimizes the curvature K can be derived by a method developed by Weitsman[3].

Accordingly, it can be shown that this optimal path contains discontinuities at $t = 0$ and $t = t_f$. The first temperature drop, from T_I to T_o, is determined from the transcendental equation

$$T_o - T_I = \frac{A_T'(T_o)}{A_T''(T_o)} \quad (20)$$

For an exponential temperature shift factor function as in equation (14), equation (20) reduces to $T_o - T_I = A$.

In the time interval between the initial and final discontinuities it was shown that the optimal path $T(t)$ is governed by the equation

$$\frac{dT}{dt} = \frac{F''[\xi(t_f) - \xi(t)]}{F'[\xi(t_f) - \xi(t)]} \frac{A_T'[T(t)]}{A_T[T(t)]A_T''[T(t)]} \quad (21)$$

In (20) and (21), primes indicate derivatives with respect to the argument.

The optimal time-temperature path is constructed by iteration through the employment of (21). Dividing the time period t_f into n equal subintervals Δt the iteration on (21) may be carried out by selecting a guess value $T(t_f^-)$ denoted by T_f. Then at $t = t_f^-$ equation (21) gives

$$\left.\frac{dT}{dt}\right|_{t = t_f} = \frac{F''(0)}{F'(0)} \frac{A_T'(T_f)}{A_T(T_f)A_T''(T_f)} \quad (22)$$

and the discretization of t_f into increments Δt yields

$$T(t_f - \Delta t) = T_f + \frac{A_T'(T_f)}{A_T(T_f)A_T''(T_f)} \frac{F''(0)}{F'(0)}$$

With both T_f and $T(t_f - \Delta t)$ known we extrapolate (21) back to $t = t_f - 2\Delta t$ to determine $T(t_f - 2\Delta t)$. Continued exprapolation of (21) back to $t = 0$ yields a value of $T(0)$ that will generally be different from T_o determined by (20). If $T(0) > T_o$ a new guess value of T_f is selected less than the original T_f and vice versa.

This iteration is continued until a value of T_f is found which gives $T(0) = T_o$ to some desired accuracy.

The value of T_f thus determined will generally be different from the room temperature, which thereby determines the discontinuity in the optimal time-temperature path at time $t = t_f$.

Summary of Material Parameters*

The properties of the AS-35-2 graphite/epoxy system used in this study are presented in Table 1.

Table 1. Material Properties[6].

Parameter	Symbol	Magnitude
COMPLIANCE		
Longitudinal	S_L	.552
"Cross Effect"	S_{12}	-.160
Transverse	S_T	6.12
COEFFICIENT OF THERMAL EXPANSION		
Longitudinal	α_L	-.27
Transverse	α_T	21.8
TEMPERATURE SHIFT FACTOR FUNCTION		
Equation (14)	A	6.0
	B	49.7
TIME DEPENDENT TRANSV. COMPLIANCE		
Equation (13)	τ_0	.222
For $0 \leq \log t \leq 5.8$	D_1^0	.618
	q	.00667
For $0 \leq \log t \leq 8.4$	D_1	.506
	q	.0217
$\log t \leq 8.4$	D_1	.305
	q	.048

In Table 1, all compliances are in 10^{-7} psi^{-1}. A is in °K, D_1 is in 10^{-6} psi^{-1} $min.^{-q}$ and τ_0,t in minutes.

* To check the fabrication process of our specimens we determined experimentally the values of E_L, E_T as well as σ^{ult}. Our moduli were slightly higher than those recorded in literature. We also found $\sigma_L^{ult} = 233.5$ ksi $\sigma_T^{ult} = 5.89$ ksi as compared to 218.4 ksi and 6.31 ksi, respectively.

Experimental Determination of Curvatures

Unsymmetric $0^\circ_{12}/90^\circ_{12}$ 6" square plates were made from AS-3502 graphite/epoxy material. These specific dimensions were selected in order to obtain thermal strains and consequent out-of-plane deflections which were sufficiently large for ease of measurement, and yet small enough relative to the plate thickness to maintain the validity of the kinematic assumptions of classical plate theory.

Twenty such panels were manufactured and measured. These panels were divided among five groups, each group undergoing its own cool down history from cure temperature to room temperature. These time-temperature histories are shown in Figures 2 and 3. (Note that in Fig. 3 the time is given in hours, while in Fig. 2, which shows the fast cooling-path "A", the time is in minutes.)

Upon cool down the curvatures of the plates were determined by securing the plate-specimens to three fixed supports which defined a reference plane. The deflections of the plates relative to this reference plane were then measured using dial gauges.

In view of the last two of equations (4) we have

$$w = \frac{1}{2}\kappa_x x^2 + \frac{1}{2}\kappa_y y^2 \qquad (24)$$

The measured values of w thus enable use to calculate κ_x and κ_y. The curvatures were calculated both with and without the assumption that $\kappa_x = -\kappa_y$.

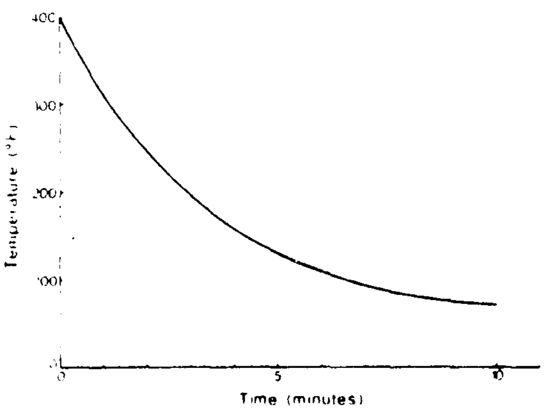

Figure 2. Cool Down Path "A"

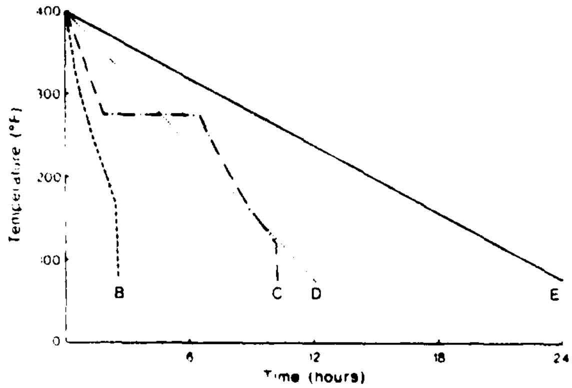

Figure 3. Cool-Down Paths "B" thru "E"

The locations of the points where w was measured on the surface of the plate are shown in Fig. 4, where all distances are in inches.

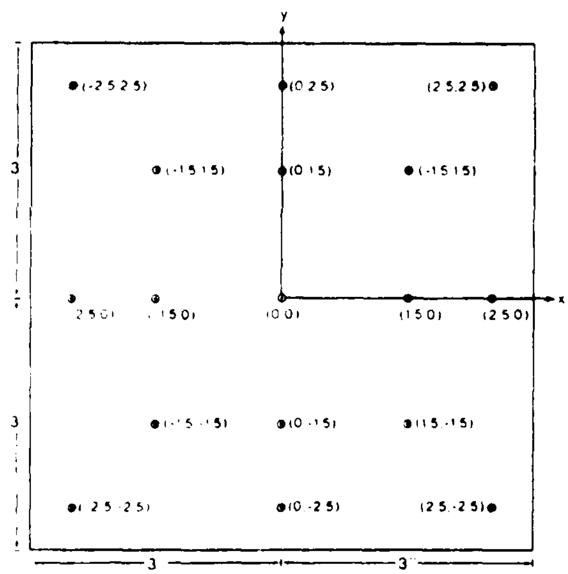

Figure 4. Location of Points where Deflections were Measured

Computations

The computations performed in this study were aimed at two purposes:

1. To compare experimentally determined curvatures to those predicted by (12) employing the paths A-E shown in Figs. 2 and 3.

2. To determine the optimal time-temperature paths that will minimize the curvatures for cooling times of 50, 100, and 200 minutes.

All calculations employed the material properties for the AS-3502 graphite/epoxy system.

Results

In order to assess reproducibility and data scatter several plates were cooled down along the same time-temperature path. We therefore had 9 samples cooled along path "B", 2 samples along path "C" and 3 samples in each of the remaining cool-down paths "A", "D", and "E", for a total of 20 samples.

Unfortunately, the relatively thick 24 ply, 6" square plate presented an unforseen problem. It appears that the thermal excursion from cure to room temperature gives rise to stresses that are close to the transverse strength of the laminas, thus making them highly susceptible to fracture. In fact all of the samples except those cooled according to path C contained cracks.

Table 2 contains the measured curvatures as well as a list of the number of cracks detected in each sample. The table contains also the theoretical curvature computed according to equation (12). In all cases the cracks occurred along directions paralled to the fibers. The difference in the magnitude of K_x and K_y can be attributed to the uneven number of cracks in the 0° and 90° plies. Due to this uneveness it was found worthwhile to employ the average of K_x and K_y (K_A in Table 2) when making comparisons to the theoretical curvature.

It may be noted from Table 2 that the effect of the cracks is to diminish the magnitudes of the observed curvature to values lower than those predicted by equation (12). With increasing number of cracks, the discrepancy between observed and theoretical curvature is found to increase. The samples containing few or no cracks (i.e., samples 4, 10, 13 and 14) had average curvatures which were very close to those predicted by (12).

In Table 2 there seems to be no obvious relation between the cool down time and the number of cracks obtained. This is most apparent by observing that the samples in the 12 hour cool down path D contain, on the average, more cracks than the samples in the 4 hour cool down path B.

It is quite possible that the cracks were caused by the fabrication procedure. When a sample is layed up, a cork dam is placed around it to keep the resin from flowing when it is in a nearly liquid state immediately prior to cure. It was noticed that the samples in cool down profiles A, B, D and E cracked when this cork was removed from the edge of the samples. Apparently the samples were so close to failure that even the small amount of pressure applied in removing the cork sufficed to propagate the cracks. To circumvent this factor we placed a teflon sheet between the cork and the sample when employing cool down profile C, which allowed these plates to be effectively separated from the cork dam without the formation of any cracks.

To get a better understanding of the effect of the cracks on the observed curvature, cracks were purposely induced into one of the uncracked samples (sample 14) and the subsequent change in curvature was recorded. Table 3 contains the number of cracks in sample 14 with the resulting average curvature. Also included is the fraction of the uncracked curvature measured orginally.

The number of cracks in sample 14 versus the fraction of the uncracked curvature resulting from those cracks is shown in Fig. 5.

In order to salvage as much information as possible from the flawed specimens we employed the results depicted in Fig. 5 to retrace the uncracked curvature of the specimens in cool-down profiles A, B, D and E. These retraced uncracked curvatures are presented in Table 4, where the theoretical values predicted by equation (12) are listed for purpose of comparison.

Table 2. Experimental and Theoretical Curvatures.

Sample	Cool Path	No. Cracks	K_x (in^{-1})	K_y (in^{-1})	K_A (in^{-1})	K (Theory) (in^{-1})
1	A	17	.0218	-.0158	.0188	.0249
2	A	13	.0186	-.0178	.0182	.0252
3	A	13	.0190	-.0218	.0204	.0253
4	B	5	.0211	-.0271	.0241	.0250
5	B	10	.0194	-.0236	.0215	.0241
6	B	10	.0209	-.0213	.0211	.0243
7	B	8	.0200	-.0178	.0189	.0241
8	B	7	.0247	-.0164	.0206	.0234
9	B	16	.0221	-.0138	.0179	.0243
10	B	3	.0278	-.0207	.0243	.0247
11	B	12	.0204	-.0218	.0211	.0240
12	B	12	.0151	-.0247	.0199	.0246
13	C	0	.0274	-.0226	.0250	.0252
14	C	0	.0272	-.0226	.0249	.0256
15	D	13	.0175	-.0208	.0191	.0247
16	D	16	.0183	-.0215	.0199	.0247
17	D	30	.0147	-.0173	.0160	.0241
18	E	8	.0233	-.0202	.0217	.0243
19	E	7	.0237	-.0210	.0223	.0252
20	E	9	.0220	-.0223	.0221	.0249

Table 3. The Effect of Cracks on the Curvature of Specimen 14.

Number of Cracks	K_A (in^{-1})	Fraction of Uncracked K
0	.0249	1.
3	.0239	.960
5	.0240	.964
7	.0227	.912
9	.0225	.904
10	.0203	.815
12	.0206	.827
14	.0194	.779
16	.0176	.707
18	.0175	.703
22	.0165	.663
27	.0156	.627

Table 4. Retraced-Experimental Curvatures and Theoretical Values

Specimen	Predicted K (in^{-1})	Theoretical K (in^{-1})
1	.0252	.0249
2	.0249	.0252
3	.0244	.0253
4	.0209	.0250
5	.0223	.0241
6	.0243	.0243
7	.0248	.0241
8	.0257	.0234
9	.0242	.0243
10	.0261	.0247
11	.0228	.0240
12	.0255	.0246
15	.0239	.0247
16	.0270	.0247
17	.0255	.0241
18	.0240	.0243
19	.0242	.0252
20	.0249	.0249

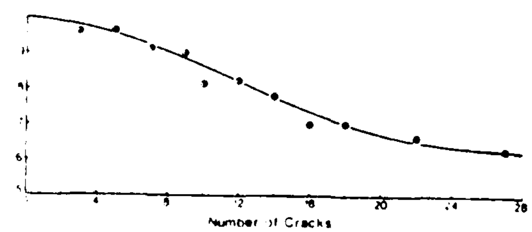

Figure 5. Fraction of Uncracked Curvature Versus Number of Cracks for Sample 14.

To exclude the effects of variation of plate thickness which occur from sample to sample we consider the dimensionless quantity hK_x.*

* Equation (12) shows that hK_x remains constant for each specified cooling history.

The average of the quantity hK_A for each cool down path is listed in Table 5 together with the corresponding theoretical value of hK.

Very good agreement exists between this average observed hK_A and the theoretically predicted value. Discrepancies range between 4% for cool down path D and less than 1% for path B. Note the general agreement with viscoelastic predictions, as compared with up to 12% departure from the linear-elastic result.

The optimal time-temperature path was calculated for cooling times t_f = 50, 100 and 200 min. using equations (20) and (21) and the iterative scheme outlined in (23).

The three optimal time-temperature paths calculated are presented in Fig. 6 along with the resulting time-dependent curvature predicted by (12). Discontinuities occurred at t = 0 and t = t_f, with a nearly linear path during $t_f > t > 0$.

Figure 7 presents the optimal curvature versus the logarithm of the cool-down time t_f (t_f in minutes). The elastic curvature calculated using

Table 5. Comparison between Averaged hK_A and Theory.

Path	Measured and Adjusted hK (in/in)	Theoretical hK_x (in/in)	
		Viscoelastic	Elastic
A	.00167 ± .00004	.00169	.00186
B	.00162 ± .00013	.00163	.00186
C	.00160 ± .00002	.00162	.00186
D	.00167 ± .00011	.00160	.00186
E	.00156 ± .00004	.00159	.00186

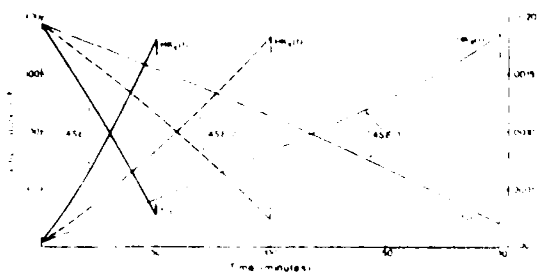

Figure 6. Optimal Time-Temperature Paths with Resulting Time Dependent Curvature.

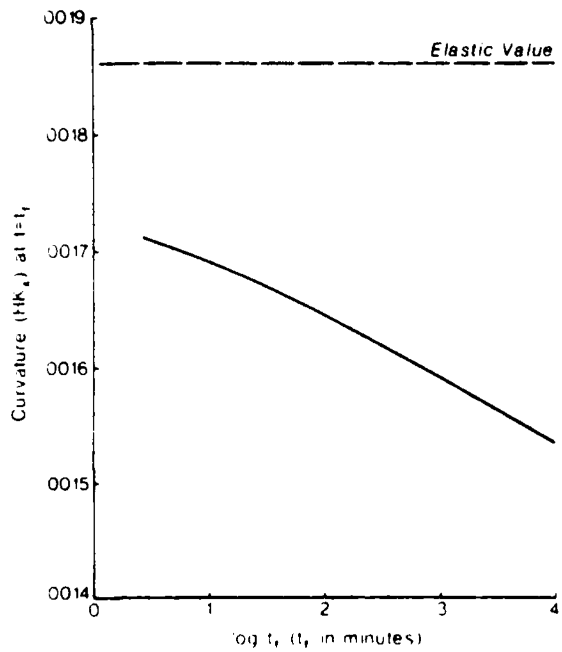

Figure 7. Optimal Curvature Versus Log t_f

(7), is shown in dashed line. As expected from viscoelasticity, longer cool-down times yield greater stress relaxation with a subsequent reduction of the optimal curvature.

Concluding Remarks

This paper presented an analysis and experimental results of the effects of viscoelastic response of composite laminates during the thermal cool-down stage. Although we must view the present data as preliminary, it provides encouraging evidence that the above-mentioned effects are detectable by direct measurements. Somewhat inadvertently, the fracture and failure which persistently occurred in the experiments, indicate that the residual thermal stresses are of severe magnitudes and must not be ignored in laminate designs.

Further studies, based upon this paper are currently in progress.

References

1. N. J. Pagano, H. T. Hahn, "Evaluation of Composite Curing Stresses," Composite Materials: Testing and Design (Fourth Conference), ASTM STP 617, American Society for Testing and Materials, 1977, pp. 317-329.

2. D. A. Douglass, Y. Weitsman, "Stresses Due to Environmental Conditioning of Cross-Ply Graphite/Epoxy Laminates," 3rd International Conference on Composite Materials, Paris, France. A. R. Bunsell et. al., Editors, Vol. 1, pp. 529-542, Pergamon Press (1980).

3. Y. Weitsman, "Optimal Cool Down in Linear Viscoelasticity," Journal of Applied Mechanics, Vol. 47, (1980), pp. 35-39.

4. R. M. Jones, Mechanics of Composite Materials, Scripta (1975).

5. S. Timoshenko, S. Woinowsky-Krieger, Theory of Plates and Shells, McGraw Hill (1959).

6. K. G. Kibler, "Time Dependent Environmental Behavior of Graphite/Epoxy Composites." Technical Report AFWAL-TR-80-4052 (Final Report for period 1 August 1977-31 January 1980), May 1980. General Dynamics Corp. Fort Worth, Texas.

Acknowledgement

This investigation was supported by the Air Force Office of Scientific Research (AFOSR) under contract No. F 49620-78-C-0034.

This support is gratefully acknowledged.

MM 3724-81-6

A RAPIDLY CONVERGENT SCHEME TO COMPUTE MOISTURE PROFILES IN COMPOSITE MATERIALS UNDER FLUCTUATING AMBIENT CONDITIONS

by

Y. Weitsman*

Abstract

This paper presents a highly efficient numerical scheme to compute the moisture distribution in composite materials and adhesive joints under time varying ambient relative humidities and temperatures. The moisture diffusion is assumed to follow Fick's laws. It is shown that by appropriate switching among the various forms of the analytic solutions, all involving infinite series, it is possible to attain extremely high accuracy by means of a meagre number of terms.

An example is provided to illustrate the method.

*Professor, Mechanics and Material Center
Civil Engineering Department
Texas A&M University
College Station, Texas 77843

BASIC CONSIDERATIONS

Consider a moisture sorption process that is described by the classical diffusion laws. In the one dimensional case we have

$$\frac{\partial m}{\partial t} = D \frac{\partial^2 m}{\partial x^2} \qquad (1)$$

to which we must attach initial and boundary conditions.

In (1) $m = m(x,t)$ is moisture content, x is the spatial coordinate, t is time and D is the coefficient of moisture diffusion.

It has been observed [1] [2] that the equilibrium moisture content depends on the ambient relative humidity, and we shall also assume that the boundary conditions are determined by the same quantity. Furthermore, the moisture diffusivity was found to be most sensitive to temperature [3] [4]. Several empirical relationships were proposed, and we shall employ

$$M = Cr^{\alpha} \qquad (2)$$

$$D(T) = D_R \exp(A/T_R - A/T) \qquad (3)$$

In (2) and (3) M is the equilibrium moisture content, r the ambient relative humidity, T the temperature, T_R the reference temperature and A, C, α the material constants.

In accordance with previous analyses [5] [6] we can uncouple the process of heat diffusion from all other time-dependent material processes, e.g. moisture-diffusion or stress-relaxation. This simplification is justified because for all practical temperature fluctuations and geometrical dimensions the time required to reach thermal equilibrium is several orders of magnitude shorter than the time-scales for moisture diffusion or for relaxation response. Consequently, we consider spatially uniform temperature profiles, namely $T = T(t)$ as prescribed by the fluctuations in ambient temperature, when analyzing transient moisture diffusion.

SYMMETRIC EXPOSURE

Consider an infinite plate of thickness 2L. Let $-L \le x \le L$ and assume an initial uniform moisture distribution m_0. When the plate is exposed to an elevated ambient relative humidity the boundary moisture is given by μ, namely $m(x = \pm L, t) = \mu$. Due to the symmetry of the present problem it suffices to analyze only the region $0 \le x \le L$.

For constant μ the moisture content $m(x,t)$ is given by well known expressions [7] [8]. Since we aim at extending those expressions to the case of fluctuating $\mu(t)$ and temperature $T(t)$ we choose to represent them in the following form

$$m(x,t) - m_0 I_0(x,t) = \mu\, I(x,t) \tag{4}$$

The functions $I_0(x,t)$ and $I(x,t)$ take two alternate forms

$$I_0(x,t) = \begin{cases} C(x,t) \\ \text{or} \\ 1 - E(x,t) \end{cases}, \quad I(x,t) = \begin{cases} 1 - C(x,t) \\ \text{or} \\ E(x,t) \end{cases} \tag{5}$$

In (5)

$$C(x,t) = -2\sum_{n=1}^{\infty} (-1)^{n+1} \cos(p_n x/L) \exp(-p_n^2 t^*) \tag{6}$$

and

$$E(x,t) = \sum_{n=1}^{\infty} (-1)^{n+1} \left[\operatorname{erfc}\left(\frac{2n - 1 - x/L}{2\sqrt{t^*}}\right) + \operatorname{erfc}\left(\frac{2n - 1 + x/L}{2\sqrt{t^*}}\right)\right] \tag{7}$$

$$\text{with } p_n = (2n - 1)\pi/2 \quad \text{and } t^* = Dt/L^2. \tag{8}$$

The complementary error function erfc(z) decays rapidly with z. Its asymptotic value is given by [9] erfc $z \sim (\sqrt{\pi}\, z)^{-1} \exp(-z^2)$ consequently, for computational precision of $O(10^{-16})$ - as obtains in "double precision" routines in digital computers - we can set erfc $z = 0$ for $z > 5.877$. In the sequal we shall designate this number by λ.

The rapid decay of erfc z implies that series (7) converges rapidly for short times. On the other hand it is obvious that series (6) converges rapidly for long times. To achieve computational efficiency we should therefore switch among the two forms of equations (5).

Straightforward arithmetics yields that accuracy of $O(10^{-16})$ is maintained by the following set of rules

for $\left(\frac{i-1}{2\lambda}\right)^2 < t^* < \left(\frac{i}{2\lambda}\right)^2$ use i terms in series (7) (9a)

for $\left(\frac{5}{2\lambda}\right)^2 < t^* < \frac{Q}{9^2}$ use five terms in series (6) (9b)

for $\frac{Q}{(2i+1)^2} < t^* < \frac{Q}{(2i-1)^2}$ use i terms in series (6) (9c)

In (9a) and (9c) $i = 1, 2, 3, 4$. Also $Q = 14.93$ and $\lambda = 5.877$.

For $t^* > Q$ the moisture distribution is uniform to within $O(10^{-16})$.

It follows from (9a) that we never need more than the four following terms in series (7):

$$\mathrm{erfc}\left(\frac{1 - x/L}{2\sqrt{t^*}}\right) + \mathrm{erfc}\left(\frac{1 + x/L}{2\sqrt{t^*}}\right) - \mathrm{erfc}\left(\frac{3 - x/L}{2\sqrt{t^*}}\right) - \mathrm{erfc}\left(\frac{3 + x/L}{2\sqrt{t^*}}\right)$$

It can be noted that the form of expressions (9) remains valid for <u>any</u> desired accuracy ε, except that λ and Q depend on ε. Obviously for a smaller accuracy we require even fewer terms in (6) and (7).

Consider now the case of fluctuating temperatures, $T = T(t)$. In view of (3) the diffusivity D is now time dependent and the non-dimensional time t^* in (8) becomes a complicated function of real-time t. However, if we consider $t^* = D_R t/L^2$ at the reference temperature $T = T_R$ then in analogy with thermoviscoelasticity [10] we can replace t^* with the reduced non-dimensional time ξ^* whenever $T = T(t)$ as follows

$$\xi^* = \frac{D_R}{L^2} \int_0^t \exp[A/T_R - A/T(s)]ds \tag{10}$$

The moisture distribution under fluctuating temperatures is given by (4) with t^* replaced by ξ^*. In view of the single-valuedness of $\xi^* = \xi^*(t)$ it is always possible to convert the results back to real time t.

Consider next the case of fluctuating ambient relative humidity $r = r(t)$. By equation (2) this implies $\mu = \mu(t)$. When $\mu = \mu(t)$ and $T = T(t)$ equation (4) yields, upon employment of the superposition integral

$$m(x,t) = m_0 I_0(x,\xi^*) = \int_0^t I[x,\xi^*(t) - \xi^*(\tau)]\, m'(\tau)d\tau \tag{11}$$

Equation (11) must of course be evaluated numerically.

NON-SYMMETRIC EXPOSURE

Consider now an infinite plate of thickness L whose faces $x=0$ and $x=L$ are exposed to different relative humidities which fluctuate independently of each other. We still assume that all temperature fluctuations are spatially uniform within the entire plate.

The solution to differing, but constant boundary conditions $m(o,t) = \mu^{o}$ and $m(L,t) = \mu^{L}$ with null initial moisture $m(x,o) = o$ can be expressed as follows

$$m(x,t) = \mu^{o} H_{o}(x,t^{*}) + \mu^{L} H_{L}(x,t^{*}) \tag{12}$$

with

$$H_{o}(x,t^{*}) = \begin{cases} S_{o}(x,t^{*}) \\ \text{or} \\ U_{o}(x,t^{*}) \end{cases} \qquad H_{L}(x,t^{*}) = \begin{cases} S_{L}(x,t^{*}) \\ \text{or} \\ U_{L}(x,t^{*}) \end{cases} \tag{13}$$

In (13)

$$\begin{aligned} S_{o}(x,t^{*}) &= 1 - \frac{x}{L} - \frac{2}{\pi} \sum_{n=1}^{\infty} \frac{1}{n} \sin\frac{q_n x}{L} \exp(-n^2\pi^2 t^{*}) \\ S_{L}(x,t^{*}) &= \frac{x}{L} + \frac{2}{\pi} \sum_{n=1}^{\infty} \frac{\cos n\pi}{n} \sin\frac{q_n x}{L} \exp(-n^2\pi^2 t^{*}) \end{aligned} \tag{14}$$

$$\begin{aligned} U_{o}(x,t^{*}) &= \operatorname{erfc}\left(\frac{x/L}{2\sqrt{t^{*}}}\right) + V_{o}(x,t^{*}) - W_{o}(x,t^{*}) \\ U_{L}(x,t^{*}) &= \operatorname{erfc}\left(\frac{1-x/L}{2\sqrt{t^{*}}}\right) + V_{L}(x,t^{*}) - W_{L}(x,t^{*}) \end{aligned} \tag{15}$$

The functions V and W in (15) represent the following infinite series

$$\begin{aligned} V_{o}(x,t^{*}) &= \sum_{n=1}^{\infty} \operatorname{erfc}\left(\frac{2n+x/L}{2\sqrt{t^{*}}}\right) \\ W_{o}(x,t^{*}) &= \sum_{n=o}^{\infty} \operatorname{erfc}\left(\frac{2(n+1)-x/L}{2\sqrt{t^{*}}}\right) \\ V_{L}(x,t^{*}) &= \sum_{n=1}^{\infty} \operatorname{erfc}\left(\frac{2n+1-x/L}{2\sqrt{t^{*}}}\right) \\ W_{L}(x,t^{*}) &= \sum_{n=o}^{\infty} \operatorname{erfc}\left(\frac{2n+1+x/L}{2\sqrt{t^{*}}}\right) \end{aligned} \tag{16}$$

In (12) - (16) $t^* = Dt/L^2$ and $q_n = n\pi$.

Expressions (14) are available in the literature [8], while (15) is obtained by means of a straightforward Laplace transform and inversion method.

Maximal efficiency in evaluating H_o and H_L is again obtained by switching between their alternate forms given in (13) and detailed in (14) - (16), because (14) is efficient for long times and (15) is advantageous for short times. For instance, for an accuracy of $O(10^{-16})$ we never need more than four terms in each of U_o, U_L, S_o and S_L as listed in Table I below. For a lesser accuracy the number of terms is of course smaller.

Range	Largest Number of Terms in Each Series						Total Number Terms in (12)
	V_o	V_L	W_o	W_L	S_o	S_L	
$0<t^\star<(\frac{1}{\lambda})^2$	0	0	0	0	0	0	2
$(\frac{1}{\lambda})^2<t^\star<(\frac{3}{2\lambda})^2$	1	1	0	0	0	0	4
$(\frac{3}{2\lambda})^2<t^\star<(\frac{2}{\lambda})^2$	1	1	1	1	0	0	6
$(\frac{2}{\lambda})^2<t^\star<\frac{R}{5}$	2	2	1	1	0	0	8
$\frac{R}{(i+1)}<t^\star<\frac{R}{i}$ (i=4,3,2,1,0)	0	0	0	0	i	i	2i

Table 1: Number of Terms Required in Various Truncated Series to Attain Accuracy of $O(10^{-16})$ in Moisture Profile ($\lambda=5{,}877$, $R = 16/\pi^2 \log e$)

For fluctuating boundary conditions $\mu^o(t)$ and $\mu^L(t)$, and with varying temperature $T(t)$ we employ the reduced time $\xi^\star$ given in (10) and a superposition integral analogous to (11) to get

$$m(x,t) = \int_0^t \left\{ H_o[x, \xi(t) - \xi(\tau)] \frac{d\mu^o(\tau)}{d\tau} + H_L[x, \xi(t) - \xi(\tau)] \frac{d\mu^L(\tau)}{d\tau} \right\} d\tau$$

THE NUMERICAL SCHEME

To compute the moisture $m(x,t)$ we divide the time-span of interest t_f into n, not necessarily equal, sub-intervals. These intervals $\Delta_i = t_i - t_{i-1}$ $(i = 1, 2, \ldots n)$ with $t_0 = 0$ and $t_n = t_f$ should be selected in a manner that both the ambient moistures $\mu^o(t)$ and $\mu^L(t)$ as well as the temperature $T(t)$ are represented to within a satisfactory approximation by the "staircase" functions*

$$\mu^o(t) = \mu_i^o, \quad \mu^L(t) = \mu_i^L, \quad T(t) = T_i$$

$$\text{for} \quad t_{i-1} < t < t_i \quad (i = 1, 2, \ldots n) \tag{18}$$

Note that in the symmetric case $\mu_o = m_o$.

Denote $g_i = \exp(A/T_R - A/T_i)$

then (10) yields

$$\xi_i^* = \frac{D_R}{L^2} \sum_{k=1}^{i} (t_k - t_{k-1})\, g_K \quad (i = 1, 2, \ldots n) \tag{19}$$

Thereby

$$\xi_{ij}^* = \xi_i^* - \xi_j^* = \frac{D_R}{L^2} \sum_{k=j+1}^{i} (t_k - t_{k-1})\, g_k \tag{20}$$

$$(j = 0, 1, \ldots i-1, \quad i = 1, 2, \ldots n)$$

* Obviously, only one ambient moisture $\mu(t)$ is involved in the symmetric case.

The integrals (11) and (17) are now represented respectively by the sums

$$m(x,t_i) = m_o I_o(x,\xi_i^*) + \sum_{j=1}^{i} (\mu_j - \mu_{j-1})\, I(x,\zeta_{ij}^*) \tag{21}$$

and

$$m(x,t_i) = \sum_{j=1}^{i} \Big[(\mu_j^o - \mu_{j-1}^o)\, H_o\, (x,\zeta_{ij}^*) + (\mu_j^L - \mu_{j-1}^L)\; H_L(x,\zeta_{ij}^*) \Big] \tag{22}$$

Expressions (21) and (22) remain valid for any intermediate time $\hat{t}_i$ where $t_{i-1} < \hat{t}_i < t_i$, provided we substitute the value of $\hat{t}_i$ in place of t_i in (19) and (20) as well as in (21) and (22).

Computational efficiency is achieved by switching between the two alternate forms given in (5) and (13) which is accomplished by testing the ranges of ξ_i^* and ζ_{ij}^* according to rules (9a) - (9c) or in Table 1, respectively. Obviously ξ_i^* and ζ_{ij}^* must replace t^* in equations (9) and in Table 1.

A NUMERICAL EXAMPLE FOR THE SYMMETRIC CASE

To illustrate the method we consider the case of a sixteen ply 5208/T300 graphite/epoxy laminate with L = 0.04". For this material $D_R = 1.5019 \times 10^{-8}$ in^2/min and A = 6340.

The composite laminate was considered to be exposed to fluctuating ambient relative humidity, which is reflected as a fluctuating boundary moisture μ, and to fluctuating temperatures.

Two cases were considered. In the first case both the ambient RH and temperature fluctuated in phase while in the second situation the fluctuation was out of phase. Specifically, in both cases the ambient moisture content fluctuated between 1% weight-gain and 1/2% weight-gain every 5000 minutes. In case 1 the temperature varied from 350°K to 297°K every 5000 minutes while in case 2 the temperature fluctuated between 297°K and 350°K with the same frequency of 5000 minutes (but out of phase with the moisture). Case 1 is shown by solid lines and case 2 is marked by dashed lines in Fig. 1.

The results, exhibited in Fig. 1., show the variation of moisture level with time at a station located at x = 0.035".

Note that sharp slopes in $m(x,t)$ vs. t occur during the high-temperature time intervals. Consequently the in-phase case approaches the saturation level of $m(x,t) = 1\%$. Conversely, for the case that peak levels of $T(t)$ and $\mu(t)$ are out of phase the moisture level at x = 0.035" approaches 0.5%. The details are shown by the heavy lines in Fig. 1.

Figure Title:

Moisture Levels at x = 0.035" vs. Time in a 0.08" Thick 5208/T300 Graphite/Epoxy Laminate That is Exposed Symmetrically to Two Cases of Fluctuating Ambient Relative-Humidity and Temperature.

Case 1: R.H. In-Phase With Temperature

Case 2: R.H. Out-of-Phase With Temperature

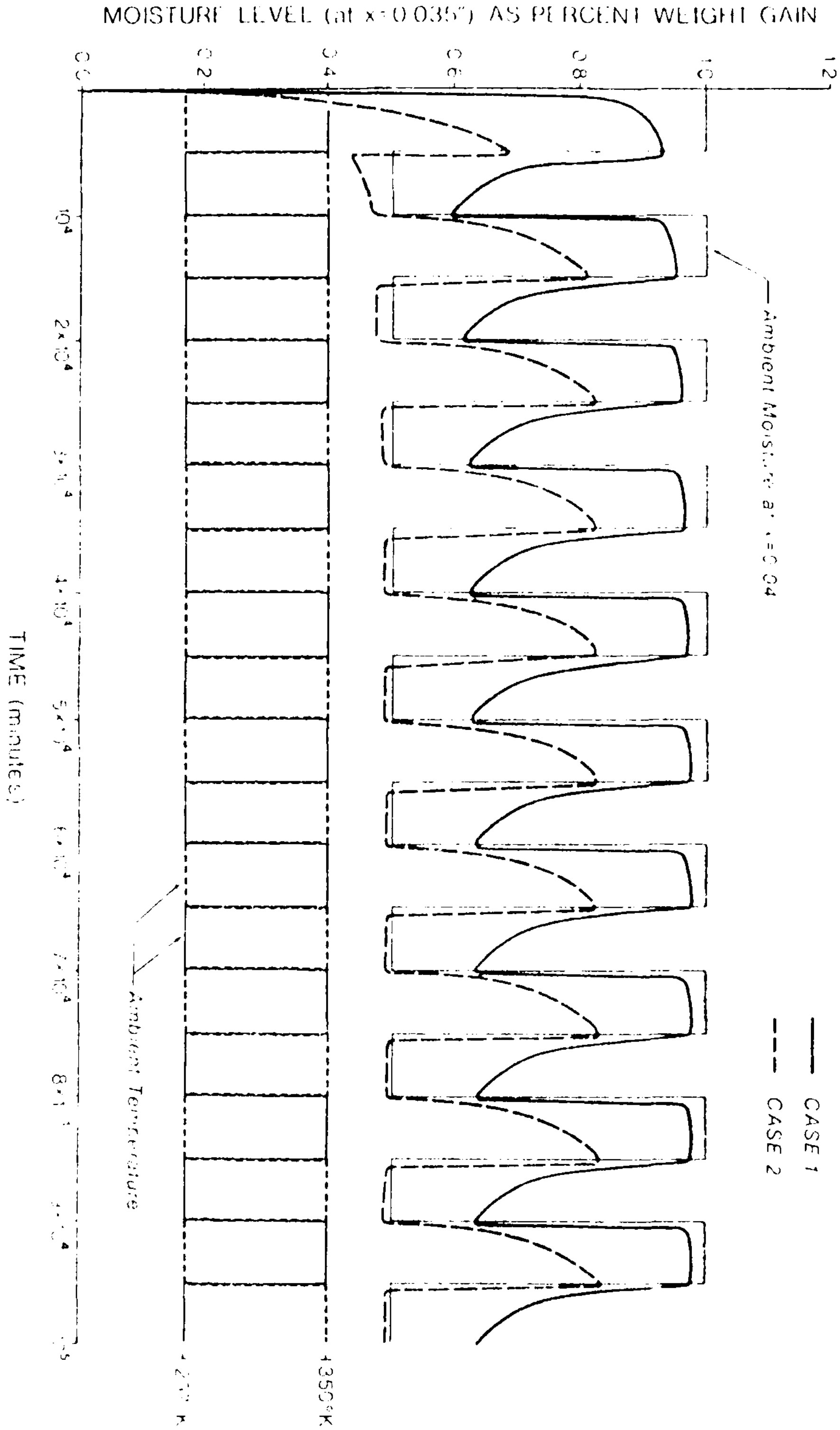
MOISTURE LEVEL (at x=0.035") AS PERCENT WEIGHT GAIN
TIME (minutes)
CASE 1
CASE 2
1355°K

REFERENCES

[1] Shen, C. H. and Springer, G. S., "Moisture Adsorption and Desorption of Composite Materials", Journal Comp. Mat., Vol. 10, Jan. 1976, pp. 36-54.

[2] DeIasi, R. and Whiteside, J. B., "Effect of Moisture on Epoxy Resins and Composites." In Advanced Composite Materials - Environmental Effects, STP 658 (ASTM), J. R. Vinson - Editor, 1978, pp. 2-20

[3] Shirrel, C. D., "Diffusion of Water Vapor in Graphite/Epoxy Laminates." In Advanced Composite Materials - Environmental Effects, STP 658 (ASTM) J. R. Vinson - Editor, 1978, pp. 21-42.

[4] McKague, E. L. and Halkias, J. E., Private Communication.

[5] Weitsman, Y., "Diffusion With Time-Varying Diffusivity, With Application to Moisture-Sorption in Composites", Journal Comp. Mat., Vol 10, July 1976, pp. 193-204.

[6] Douglass, D. A. and Weitsman, Y., "Stresses Due to Environmental Conditioning of Cross-Ply Graphite/Epoxy Laminates", Proc. Third International Conference on Composite Materials (ICCM3), Paris, France. A. R. Bunsell et. al., Editors, Vol. 1, pp. 529-542, Pergamon Press (1980).

[7] Luikov, A. V., "Analytical Heat Diffusion Theory", Academic Press, 1968, pp. 97-114.

[8] Crank, J., "The Mathematical Theory of Diffusion", Oxford University Press, 2nd ed., 1975, pp. 47, 104-105.

[9] Abramowitz, M. and Stegun, L. A., "Handbook of Mathematical Functions", National Bureau of Standards, June 1964, p. 298.

[10] Morland, L. W. and Lee, E. H., "Stress Analysis for Linear Visco-elastic Materials With Temperature Variation", Transactions Society of Rheology, Vol. IV, 1960, pp. 233-263.

ACKNOWLEDGEMENTS

This work was conducted, in part, under Contract F33615-79-C-5517 from the Air Force Material Laboratory (AFML/AFWAL) and in part under Contract F 49620-78-C-003 from the Air Force Office of Scientific Research (AFOSR). This support is gratefully acknowledged.

April 1980

ON CONSTITUTIVE EQUATIONS FOR VISCOELASTIC COMPOSITE MATERIALS WITH DAMAGE*

R. A. Schapery

Mechanics and Materials Center

Civil Engineering Department

Texas A&M University

College Station, TX. 77843

Abstract

Three-dimensional constitutive equations are derived for viscoelastic composite materials with time-dependent damage. Starting with the assumption that the material is linearly viscoelastic when the damage is constant and that the damage consists of flaws as characterized by internal displacement discontinuities, we investigate the effect of time-dependent growth and healing of these flaws on the global stress-strain equations for materials under transient stresses and temperature. Prediction of flaw growth itself is then discussed. Some concluding remarks pertain to the characterization of nonlinear viscoelastic materials including the effect of damage.

Introduction

The thermomechanical response of many materials is significantly effected by the development of micro-flaws. With viscoelastic materials the current state depends on the history of this damage, and therefore the overall material response may be much more complex than for elastic materials or for viscoelastic materials without damage. Another complication results when the previously developed flaw surfaces rejoin and thereby produce an increase in material stiffness; the interface contact depends on the history of flaw development and global thermomechanical inputs.

Particles, fibers, and lamina interfaces usually serve as both micro-flaw sources (partly as a result of local stress concentrations) and as arrest points after local stable or unstable growth. Therefore, composite materials having a brittle or weak matrix may undergo a considerable amount of global softening prior to overall fracture. Considering the complex microstructure of these materials, one may expect that any realistic global constitutive equation which accounts for damage will be extremely involved. However, as shown in this paper, it is possible to rigorously develop explicit, realistic equations by accounting for certain simplifying features of many composites, such as a matrix that is relatively soft compared to the reinforcing material. The approach followed here is much more general than used previously for a particulate composite under uniaxial stress (Schapery, 1974a); but for uniaxial stress and without rejoining of flaw surfaces the present equations take the same form as the earlier ones.

Inasmuch as the purpose of this paper is to help provide a basis for discussion at the Workshop by describing the writer's approach, we shall not attempt here to review relevant work of other investigators. Instead, it is hoped that the Workshop will serve this purpose.

*Prepared for presentation at the National Science Foundation Damage Workshop, Cincinnati, May 4 - 7, 1980

Linear Viscoelastic Constitutive Equations with Damage

Consider an isotropic or anisotropic composite material element. We assume that it is globally homogeneous with or without damage; i.e. the scale of stress/strain nonuniformities due to any physical source (cracks, voids, particles, fibers, etc.) is assumed small compared to the size of the material element. We further assume that the material is linearly viscoelastic except for damage.

Using single index notation for the global or average stresses, σ_i, and strains, ε_i, (Sokolnikoff, 1956), general linear relations between these variables and a uniform temperature change, ΔT, may be written in the form of nereditary integrals,

$$\varepsilon_i = \left\{ S_{ij}\dot{\sigma}_j \right\} + \left\{ \alpha_i \Delta\dot{T} \right\} \qquad i, j = 1, \ldots 6 \tag{1}$$

where the braces are abreviated notation for a hereditary integral; viz.,

$$\left\{ S\dot{\sigma} \right\} \equiv \int_{0^-}^{t} S(t,\tau) \frac{\partial \sigma}{\partial \tau} d\tau \tag{2}$$

and a repeated index is to be summed over its range. We suppose that $\varepsilon_i = \sigma_i = \Delta T = 0$ for $t<0$; the lower limit in Eq. (2) is 0^- rather than 0 in order to allow for step-function inputs at $t = 0$. Each quantity $S_{ij} = S_{ij}(t,\tau)$ is a "creep compliance," which is equal to the strain ε_i at time t due to a unit value of stress σ_j applied at time τ. Similarly, the thermal coefficient $\alpha_i = \alpha_i(t,\tau)$ is also a creep compliance since it is the strain ε_i at t due to a unit value of ΔT applied at τ. If all of these compliances are functions of the time difference $t - \tau$, instead of t and τ separately, the material is said to be "nonaging;" otherwise "aging" exists. This aging may be the result of one or more processes, including chemical reactions. However, we assume the compliances do not depend on stress, and therefore damage is not yet included.

The damage to be considered here consists of surfaces of internal displacement discontinuities as defined by a set of discrete parameters $u_m (m = 7, 8, \ldots, N)$. These quantities represent the three components of relative displacement (opening and sliding) at as many points on adjacent internal surfaces as needed to accurately represent the relative movement between all material points which were together before the damage occurred. All surfaces which develop during the time period of interest are to be included. The resultant force acting between a pair of these points prior to complete separation is denoted by three components f_m.

This procedure of modeling the traction and relative displacement distributions along current and future surfaces of displacement discontinuity by displacements and forces at discrete material points is, of course, what one would follow in a finite element representation of the entire material element. However, we do not require that the continuum itself be represented in this fashion. Rather, it is assumed only that the continuum is a linear viscoelastic (aging or nonaging) material.

There is assumed to be a thin layer along the surfaces of flaw prolongation in which all large strains and nonlinear material behavior exists. This is the same assumption used by Schapery (1975) in deriving equations for predicting speed of individual cracks in linear viscoelastic media. The mechanical and failure behavior of this thin layer is defined by the N-6 functionals,

$$f_m = F(u_n, t); \quad m,n = 7, \ldots N \tag{3}$$

expressing the forces between adjacent material points at the continuum boundary on each side of the thin layer of nonlinear, failing material as functions of displacement history and possibly time (to account for chemical aging, diffusion of liquid at crack faces, etc.). In predicting global mechanical behavior we shall neglect flaw-edge details and simply specify that either a force is zero (e.g. a free crack surface) or else the conjugate relative displacement is zero (e.g. a point in the continuum ahead of a crack tip). Other, more general cases could be considered, including friction between crack faces, pressure of fluid in cracks, etc.; but for now this simplification will be used. Later we shall briefly consider the effect of subsequent contact between the faces and healing. It is proposed to use more detailed behavior at each flaw-edge as given by Eq. (3), in order to predict their initiation and speed.

It should be emphasized that crack growth is contained in the following analysis as only a special case, and not the only case. Local failure at isolated individual or groups of points is taken into account. In principle, therefore, phenomena such as failure of individual fibers in a fibrous composite, groups of extended polymer chains, and rubber matrix material between near-contact points of hard particles in a highly-filled rubber can be treated. For example, in the latter case some of the forces f_m would represent forces acting between particles at the points of near-contact, and the rubber between any pair of these points would be characterized by one of the functionals in Eq. (3).

Let us now write out different forms of the linear viscoelastic constitutive equations for the continuum by starting with the generalized form of Eq. (1) in which global strains ε_i and internal forces f_m are expressed as linear functionals of global stresses σ_i, relative displacements u_m, and temperature change:

$$\varepsilon_i = \left\{S_{ij}\dot{\sigma}_j\right\} + \left\{S_{in}\dot{u}_n\right\} + \left\{\alpha_i \Delta\dot{T}\right\} \tag{4a}$$

$$f_m = \left\{S_{mj}\dot{\sigma}_j\right\} + \left\{S_{mn}\dot{u}_n\right\} + \left\{\alpha_m \Delta\dot{T}\right\} \tag{4b}$$

When all u_n are zero the material is by definition undamaged and Eq. (1) is recovered from Eq. (4a); the compliances S_{ij} and α_i in Eq. (4a) are the same as those in Eq. (1). Another useful form of these relations is

$$\sigma_i = \left\{C_{ij}\dot{\varepsilon}_j\right\} + \left\{C_{in}\dot{u}_n\right\} - \left\{\beta_i \Delta\dot{T}\right\} \tag{5a}$$

$$f_m = \left\{C_{mj}\dot{\varepsilon}_j\right\} + \left\{C_{mn}\dot{u}_n\right\} - \left\{\beta_m \Delta\dot{T}\right\} \tag{5b}$$

where C_{ij} defines the functionals which are the inverses of those associated with S_{ij}; viz.,

$$\varepsilon_i = \left\{S_{ij}\left\{\dot{C}_{jh}\dot{\varepsilon}_h\right\}\right\} \qquad h = 1,\ldots 6 \tag{6}$$

which reduce to relations of the type in Eq. (26). The remaining kernels C_{in}, β_i, etc., obey similar relations; e.g.

$$-\left\{S_{in}\dot{u}_n\right\} = \left\{S_{ij}\left\{\dot{C}_{jn}\dot{u}_n\right\}\right\} \tag{7}$$

The functions C_{ij} define mechanical behavior in the undamaged state ($u_n \equiv 0$). They are called relaxation moduli as they are the stresses due to unit strains applied at $t = \tau$. In general, we shall refer to all kernels or material functions in Eq. (5) as relaxation functions.

Next, we shall order the forces f_m such that m increases with increasing time of local failure, where the time of local failure is defined to be the time at which f_m first vanishes when $u_m \neq 0$. Inasmuch as both normal and shearing forces are included in the set f_m and failure may occur at more than one point at a given time, the number of discrete failure times will be less than the number of nodal points.

With this in mind, suppose that $t_K (K = 1, 2, \ldots)$ is the Kth distinct failure time, where $f_7 = f_8 = \ldots f_k = 0$, and all material points corresponding to $k + 1$, $k + 2$, ... N have not yet failed. As discussed previously, we shall predict global response by neglecting the effect of a partial local failure (f_m, $u_m \neq 0$).

Write out Eq. (4) for this state at $t = t_K$:

$$\epsilon_i = \left\{S_{ij}\dot{\sigma}_j\right\} + \left\{S_{ip}\dot{u}_p\right\} + \left\{\alpha_i \Delta\dot{T}\right\} \tag{8}$$

$$0 = \left\{S_{qj}\dot{\sigma}_j\right\} + \left\{S_{qp}\dot{u}_p\right\} + \left\{\alpha_q \Delta\dot{T}\right\} \tag{9}$$

$$f_r = \left\{S_{rj}\dot{\sigma}_j\right\} + \left\{S_{rp}\dot{u}_p\right\} + \left\{\alpha_r \Delta\dot{T}\right\} \tag{10}$$

where

$$\begin{aligned} p, q &= 7, 8, \ldots k \\ r &= k + 1, k + 2, \ldots N \end{aligned} \tag{11}$$

Equation (9) provides a set of $k - 6$ equations from which the $k - 6$ values of u_p may be found. Substitution of these displacements into Eq. (8) then yields the desired global constitutive equations for the damaged material.

In order to obtain some explicit results we shall introduce a certain simplification which is applicable to many composite and monolithic materials; this point will be argued following the analysis. Referring to Eq. (5), we assume that all relaxation functions are proportional to a single relaxation modulus, $E = E(t,\tau)$, for uniaxial loading (say),

$$C_{ab} = C^\circ_{ab} \frac{E}{E_R} \quad , \quad \beta_a = \beta^\circ_a \frac{E}{E_R} \tag{12}$$

where $a, b = 1, 2, \ldots N$, and $E_R \equiv E_R(t_R, \tau_R)$; the modulus E_R is a constant (the modulus at reference times t_R, τ_R) which is introduced so that the dimensions of the constants C°_{ab} and β°_a will be the same as the original relaxation functions. Substitute Eq. (12) into Eq. (5) and obtain a set of equations for an "equivalent" elastic material,

$$\sigma_i = C^\circ_{ij}\epsilon^e_j + C^\circ_{in}u^e_n - \beta^\circ_i \Delta T^e \tag{13a}$$

$$f_m = C^\circ_{mj}\epsilon^e_j + C^\circ_{mn}u^e_n - \beta^\circ_m \Delta T^e \tag{13b}$$

where

$$\epsilon^e_j \equiv \frac{1}{E_R}\left\{E\dot{\epsilon}_j\right\} , \; u^e_n \equiv \frac{1}{E_R}\left\{E\dot{u}_n\right\} , \; \Delta T^e \equiv \frac{1}{E_R}\left\{E\Delta\dot{T}\right\} \tag{14}$$

After replacing all strains, displacements, and temperature change in Eqs. (4) and (8-10) by the corresponding quantities in Eq. (14) only constant compliances remain (because Eqs. (4) and (8)-(10) characterize the same material element as Eq. (13)). Obviously, Eqs. (8)-(10) become

$$\varepsilon_i^e = S^\circ_{ij}\sigma_j + S^\circ_{ip}u_p^e + \alpha_i^\circ \Delta T^e \tag{15a}$$

$$0 = S^\circ_{qj}\sigma_j + S^\circ_{qp}u_p^e + \alpha_q^\circ \Delta T^e \tag{15b}$$

$$f_r = S^\circ_{rj}\sigma_j + S^\circ_{rp}u_p^e + \alpha_r^\circ \Delta T^e \tag{15c}$$

where

$$\begin{gathered}\left[S^\circ_{ij}\right] = \left[C^\circ_{ij}\right]^{-1}, -S^\circ_{in} = S^\circ_{ij}C^\circ_{jn}, \ \alpha_i^\circ = S^\circ_{ij}\beta_j^\circ \\ S^\circ_{mj} = C^\circ_{mi}S^\circ_{ij}, \ S^\circ_{mn} = C^\circ_{mi}S^\circ_{in} + C^\circ_{mn}, \ \alpha_m^\circ = C^\circ_{mi}\alpha_i^\circ - \beta_m^\circ\end{gathered} \tag{16}$$

and recall that

$$i,j = 1, \ldots, 6; \quad m,n = 7, \ldots, N; \quad p,q = 7, \ldots, k; \quad r = k+1, \ldots, N.$$

The relative displacements follow from Eq. (15b) and the definition $\left[T^\circ_{pq}\right] = \left[S^\circ_{pq}\right]^{-1}$,

$$u_p^e = - T^\circ_{pq}S^\circ_{qj}\sigma_j - T^\circ_{pq}\alpha_q^\circ \Delta T^e \tag{17}$$

and substitution into Eq. (15a) yields the desired constitutive equations at the time $t = t_K$:

$$\varepsilon_i^e = \left(S^\circ_{ij} + \Delta S_{ij}\right)\sigma_j + \left(\alpha_i^\circ + \Delta\alpha_i\right)\Delta T^e \tag{18}$$

where
$$\Delta S_{ij} \equiv - S^\circ_{ip}T^\circ_{pq}S^\circ_{qj}, \quad \Delta\alpha_i \equiv - S^\circ_{ip}T^\circ_{pq}\alpha_q^\circ \tag{19}$$

As there normally will be a large number of points of local failure, it is desirable to express Eq. (18) in terms of distribution functions for ΔS_{ij}. Thus, let

$$n_{ij}(S, t_f)\, dSdt_f \text{ and } n_i(S, t_f)\, dSdt_f$$

be the number of material points which contribute to ΔS_{ij} and $\Delta\alpha_i$ (respectively) an amount between S and S + dS when the local failure time is between t_f and $t_f + dt_f$. Hence, at the current time t,

$$\Delta S_{ij} = \int_{-\infty}^{\infty}\int_0^t n_{ij}(S, t_f)SdSdt_f \tag{20a}$$

$$\Delta\alpha_i = \int_{-\infty}^{\infty}\int_0^t n_i(S, t_f)SdSdt_f \tag{20b}$$

Equation (18) can now be written as

$$\epsilon_i^e = \left(S_{ij}^\circ + \int_o^t F_{ij}(t_f)dt_f\right)\sigma_j + \left(\alpha_i^\circ + \int_o^t F_i(t_f)dt_f\right)\Delta T^e \tag{21}$$

where new distribution functions have been introduced,

$$F_{ij}(t_f) \equiv \int_{-\infty}^{\infty} n_{ij}(S, t_f)SdS \tag{22a}$$

$$F_i(t_f) \equiv \int_{-\infty}^{\infty} n_i(S, t_f)SdS \tag{22b}$$

Recall that ϵ_i^e and ΔT^e have been defined in Eq. (14); explicitly,

$$\epsilon_i^e = \frac{1}{E_R}\int_{o^-}^t E(t, \tau)\frac{\partial \epsilon_i}{\partial \tau}d\tau \tag{23a}$$

$$\Delta T^e = \frac{1}{E_R}\int_{o^-}^t E(t, \tau)\frac{\partial \Delta T}{\partial \tau}d\tau \tag{23b}$$

where E_R is the modulus at arbitrarily selected reference times t_R and τ_R. It is very interesting to observe that the constitutive equations (4) and (5) for a viscoelastic material with damage have, as a direct result of Eq. (12), reduced to those for a linear elastic material with time-dependent properties; but the strain and temperature histories are in general different from the actual ones.

Effect of Flaw Closing and Healing. Equation (21) is based on the assumption that the forces f_m are zero up to the current time after local failure at the associated material point occurs. However, in many cases this will not be true, as with load reversal and/or the application of a large external pressure. For the latter case, interfacial normal and shear stresses may exist. If the forces f_q where this occurs are known, we can readily correct Eq. (18) for them. Referring to Eq. (15b), we see that they will be accounted for if the associated α_q° in Eq. (19) are replaced by $\alpha_q^\circ - (f_q/\Delta T^e)$. On the other hand, the flaw closure upon unloading will produce contact forces which depend on loading and temperature history. Also, the flaws may again be capable of supporting tensile forces if rebonding occurs. In this latter case the time at which contact is established may be appreciably affected by the intermolecular forces of attraction if they are sufficiently large; indeed, the closing rate is governed by an equation that is analogous to that for crack growth (Schapery, 1976).

In order to deal with this problem involving interfacial contact and possible healing let us start with the linear constitutive equations in the form,

$$\epsilon_i = \left\{\hat{S}_{ij}\dot{\sigma}_j\right\} + \left\{\hat{S}_{in}\dot{f}_n\right\} + \left\{\hat{\alpha}_i\Delta\dot{T}\right\} \tag{24a}$$

$$u_m = \left\{\hat{S}_{mj}\dot{\sigma}_j\right\} + \left\{\hat{S}_{mn}\dot{f}_n\right\} + \left\{\hat{\alpha}_m\Delta\dot{T}\right\} \tag{24b}$$

The material functions are different from those in Eq. (4); of course, they can be expressed in terms of the latter ones. Note that $\hat{S}_{ij}$ and $\hat{\alpha}_i$ define global mechanical response for the maximum amount of damage (all $f_m = 0$), whereas S_{ij} and α_i define response without damage (all $u_m = 0$). Let us again introduce the simplification given in Eq. (12). However, rather than using modified strains and temperature, we shall apply an equivalent modification to the stresses and forces. First, define the mechanical creep compliance $D = D(t, \tau)$ for uniaxial loading by

$$\varepsilon = \{D\{E\dot{\varepsilon}\}\} \tag{25}$$

Inasmuch as D and E are independent of strain history, we can use in Eq. (25) the unit-step strain history $\varepsilon = H(t - \tau_o)$, where $H(t - \tau_o)$ vanishes when $t < \tau_o$ and is unity when $t > \tau_o$. Equation (25) reduces to the integral equation,

$$H(t - \tau_o) = \int_{\tau_o^-}^{t} D(t, \tau) \frac{\partial}{\partial \tau} E(\tau, \tau_o)\, d\tau \tag{26}$$

The lower limit is τ_o^-, rather than τ_o; the relaxation modulus $E(\tau, \tau_o)$ is discontinuous at $\tau = \tau_o$, and therefore the contribution from the singularity in $\partial E/\partial\tau$ must be included. For a nonaging material $E = E(t - \tau)$, and Eq. (26) may be easily Laplace transformed,

$$1 = s^2 \bar{D} \bar{E} \tag{27}$$

where the overbar denotes a Laplace transform and s is the transform parameter.

Next, define

$$\sigma_j^e = \frac{1}{D_R}\left\{D\dot{\sigma}_j\right\}, \quad f_n^e = \frac{1}{D_R}\left\{D\dot{f}_n\right\}, \quad D_R \equiv E_R^{-1} \tag{28}$$

Equations (5), (12), and (28) imply Eq. (24) reduces to the equations for an equivalent elastic material,

$$\varepsilon_i = \hat{S}^{\circ}_{ij}\sigma_j^e + \hat{S}^{\circ}_{in} f_n^e + \hat{\alpha}^{\circ}_i \Delta T \tag{29a}$$

$$u_m = \hat{S}^{\circ}_{mj}\sigma_j^e + \hat{S}^{\circ}_{mn} f_n^e + \hat{\alpha}^{\circ}_m \Delta T \tag{29b}$$

where $\hat{S}^{\circ}_{ab}$ and $\hat{\alpha}^{\circ}_a$ (with a, b = 1, ..., N) are constants,

$$\hat{S}^{\circ}_{ab} = \hat{S}_{ab}\frac{D_R}{D}, \quad \hat{\alpha}^{\circ}_a = \hat{\alpha}_a \frac{D_R}{D} \tag{30}$$

This choice of variables will simplify the subsequent contact analysis. However, it is first of interest to consider an implication of Eq. (29a) when rewritten in terms of ε_i^e, ΔT^e, σ_j, and f_n. For a state of constant damage (as defined by the particular set of f_n which vanish) Eqs. (29a) and (21) must be in agreement, regardless of whether or not the mechanical variables are constant in time. Thus,

$$\hat{S}^{\circ}_{ij} = S^{\circ}_{ij} + \int_0^{t_d} F_{ij}(t_f)\,dt_f, \quad \hat{\alpha}^{\circ}_i = \alpha^{\circ}_i + \int_0^{t_d} F_i(t_f)\,dt_f \tag{31}$$

where t_d is the time at which the constant damage state is first reached.

Now, suppose that a constant damage state is maintained for a period of time which is long enough for the values of f_n^e in Eq. (28) to essentially vanish; the stress history need not be constant during this time.

The quantity $\{D\dot{f}\}$ can be interpreted as the mechanical strain due to a uniaxial stress history $\sigma = f\ (t)$ for an undamaged specimen; therefore, the behavior of $\{Df_n\}$ when $f_n = 0$ is the same as the time-dependence of strain in a so-called recovery period. Consequently, it is necessary to assume that the material element under consideration is such that the strain due to stress eventually approaches zero after stress is removed; a crosslinked polymer under constant or increasing temperature exhibits such behavior. If this condition is not met, then the long-time value of f_n^e (assuming it exists) should be subtracted from f_n^e and the difference used in a modified version of the subsequent analysis.

Let us further assume that $u_m = 0$ at all points where contact occurs; i.e., material points on adjacent surfaces are assumed to rejoin with the same points as before local failure. In this case, the problem is completely analogous to the problem of damage growth, in which the roles of f_n^e and u_n^e are interchanged (cf. Eqs. (15) and (29). Of course the order in which local failure occurs is not necessarily the same as that for local contact; it is not necessary to reorder f_n and u_n to reflect this behavior. Equation (29b) can be solved for all f_n^e where contact occurs since the u_n are zero. If desired, one could then solve the integral equation in Eq. (28) for the contact force history, $f_n = f_n(t)$, using the previously derived f_n^e.

In view of the above considerations, the resulting constitutive equations will have the same form as those in Eqs. (21)-(23):

$$\epsilon_i = \left(\hat{S}_{ij} + \int_{t_d}^{t} \hat{F}_{ij}(t_c)dt_c\right)\sigma_j + \left(\hat{\alpha}_i^{\circ} + \int_{t_d}^{t} \hat{F}_i(t_c)dt_c\right)\Delta T \tag{32}$$

with the distribution functions

$$\hat{F}_{ij}(t_c) = \int_{-\infty}^{\infty} \hat{n}_{ij}(S,\ t_c)SdS \tag{33a}$$

$$\hat{F}_i(t_c) = \int_{-\infty}^{\infty} \hat{n}_i(S,\ t_c)SdS \tag{33b}$$

Also,

$$\hat{n}_{ij}(S,\ t_c)dSdt_c \text{ and } \hat{n}_i(S,\ t_c)dSdt_c \tag{34}$$

are the number of material points which contribute to $\Delta\hat{S}_{ij}$ and $\Delta\hat{\alpha}_i$ (respectively) an amount between S and S + dS when the local contact time is between t_c and $t_c + dt_c$.

Constitutive Equations with Combined Damage Growth and Flaw Contact/Healing. Both sets of equations for damage growth, Eq. (21), and subsequent rejoining of flaw surfaces, Eq. (32), are contained in the following set:

$$\varepsilon_i = \frac{1}{D_R} \int_{0^-}^{t} D(t, \tau) \frac{\partial}{\partial \tau} \left[S_{ij}^{T}(t, \tau) \sigma_j(\tau) \right] d\tau$$

$$+ \frac{1}{D_R} \int_{0^-}^{t} D(t, \tau) \frac{\partial}{\partial \tau} \left[\alpha_i^{T}(t, \tau) \Delta T^{e}(\tau) \right] d\tau \tag{35}$$

where

$$S_{ij}^{T}(t, \tau) = S_{ij}^{\circ} + \int_{0}^{\tau} F_{ij}(t_f) dt_f + \int_{0}^{t} \hat{F}_{ij}(t_c) dt_c \tag{36a}$$

$$\alpha_i^{T}(t, \tau) = \alpha_i^{\circ} + \int_{0}^{\tau} F_i(t_f) dt_f + \int_{0}^{t} \hat{F}_i(t_c) dt_c \tag{36b}$$

In the development of the theory, the distribution functions in Eq. (36) were assumed to vanish at certain times, depending on whether or not there was flaw surface contact or the damage was constant. However, Eq. (35) may have more general applicability. If internal failures and contact occur simultaneously at different points, and there is not significant interaction between these processes, one can show that Eq. (35) will be applicable.

We have not yet discussed the mathematical properties of the various relaxation and compliance functions which appear throughout the analysis. Although they will not be listed here, it is of interest to observe that since the material is linearly viscoelastic for a fixed amount of damage, equilibrium and nonequilibrium thermodynamics provide considerable explicit information (e.g. Fung, 1965; Schapery, 1964). For example, S_{ij}^{T} is symmetric and positive definite. Moreover, the form of Eq. (35) is such that material symmetry requirements may be easily introduced. Indeed, restrictions on S_{ij}^{T} and α_i^{T} carry over directly from linear elasticity theory. Also, through the integrals for damage and contact effects in Eq. (36), a material's symmetry can change. For example, without damage the material may be isotropic (as characterized by S_{ij}° and α_i°). If flaws develop into a regular pattern (e.g., an array of parallel cracks), so as to produce an orthotropic material, say, the distribution functions in Eq. (36) will possess the same transformation properties as linear elastic moduli of orthotropic materials.

The effect of temperature on mechanical properties is included in the present theory. For example, with constant or transient temperatures the aging form of the various material functions (e.g. $D(t, \tau)$), permits us to introduce thermorheologically simple behavior, as well as other more involved behavior (e.g. Schapery, 1974b); this is accomplished through an appropriate choice of $D(t, \tau)$.

As the final matter in this section, let us consider the basis for Eq. (12). Assume the composite material consists of only one viscoelastic phase. Furthermore, suppose that this phase is isotropic and has a timewise constant Poisson's ratio and thermal expansion coefficient, which is a good assumption for many materials (Schapery, 1974b). The other phases are assumed to be either relatively very rigid or soft (holes and cracks). Then, Eq. (12) can be established directly from dimensional analysis. If the composite contains continuous and straight, stiff fibers, it is not necessary to introduce the severe assumption that their axial modulus is infinite. Rather, the stress σ_i in Eq. (13) can be redefined (ε_i and C_{ij} modified accordingly) so that it does not include the axial force in the fibers; the effect of broken fibers is easily predicted by means of this redefined stress.

AD-A097 297 TEXAS A AND M UNIV COLLEGE STATION MECHANICS AND MAT--ETC F/G 11/4
COMPOSITE MATERIALS FOR STRUCTURAL DESIGN.(U)
FEB 81 R A SCHAPERY, W L BRADLEY, W E HAISLER F49620-78-C-0034
UNCLASSIFIED MM-3724-81-5 AFOSR-TR-81-0326 NL

2 of 2
AD
A097297

END
DATE
FILMED
5 81
DTIC

Stochastic Models of Microcracking and Failure

The constitutive relations, Eq. (35), are expressed in terms of distribution functions for the time-dependent number of local failure and interfacial contact sites. These functions in turn depend on the stress and temperature histories, and in this section we shall briefly review the writer's approach to the prediction of this dependence as well as the prediction of global failure.

Analysis of Microcracking. First, it is noted that in principle the failure and contact processes can be predicted from Eqs. (13) for the continuum (or the more general set, Eq. (5)), together with local constitutive equations for the material at the failure sites. However, considerable simplification is needed for real materials considering their highly complex microstructure. We treated this problem for local failure in past work (Schapery, 1974 a, c) by applying viscoelastic crack growth theory to isolated preexisting flaws; based on experimental data, crack speed was assumed to obey a power law in the local stress intensity factor for the opening mode of growth. Typically, these initial flaws are predicted to become unstable with very little growth. Therefore, their influence on global response was neglected until the time of instability (local failure). The global softening effect was taken into account after an assumed period of rapid growth and arrest. The analysis, including consideration of the statistical distribution of initial flaw sizes, microstructure geometry, etc., results in the prediction that global softening functions (such as F_{ij} and F_i) depend on only the current Lebesgue norm of stress. With later consideration of mixed-mode growth and growth-retardation effects due to large strains, a generalized damage parameter was proposed for isotropic media under global proportional loading (Schapery, 1978),

$$L_f(t) \equiv \int_0^t W(t')\left|\sigma\right|^q \left|\varepsilon\right|^p dt' \tag{37}$$

where q and p are positive (and typically >>1). W(t) is a positive function of time through dependence on local fracture energy, temperature-dependent material parameters, chemical aging, etc. The stress σ and strain ε are global variables. The use of total strain was based on solid propellant data, although other integrand variables (e.g. strain due to damage) may be more appropriate for different materials; but use of a function of L_f itself as a factor in the integrand has no essential effect on Eq. (21) because Eq. (37) can then be solved explicitly for L_f, and the resulting effect is identical to that without the factor.

Considerable simplification results if the distribution functions in Eq. (36) depend on time through a single parameter, such as L_f; of course, for general loading conditions one would have to use at least suitably defined stress and strain invariants instead of σ and ε. In this event, and assuming contact effects can be characterized using an analogous parameter L_c (but with values of p and q different from those in Eq. (37)) Eq. (36) becomes

$$\begin{aligned} S_{ij}^T(t,\tau) &\equiv T_{ij}\left[L_c(t),\ L_f(\tau)\right] \\ \alpha_i^T(t,\tau) &\equiv T_i\left[L_c(t),\ L_f(\tau)\right] \end{aligned} \tag{38}$$

where T_{ij} and T_i are to be interpreted as material functions of L_f and L_c. These functions may be found using experimental results from mechanical tests; Beckwith (1974) demonstrates this in which a one-dimensional, isothermal version of Eq. (35)

with damage only (Schapery 1974a) is employed using results from multiple-step creep and recovery tests.

A similar one-dimensional case of Eq. (35), together with a damage parameter similar to Eq. (37), was recently used by Schapery (1979) to characterize and predict the behavior of solid propellant with non-decreasing strain input under isothermal and nonisothermal conditions. Specifically, the stress is

$$\sigma = \sigma_o / T_d \tag{39}$$

where σ_o is the linear viscoelastic stress $\sigma_o = \{E(\dot{\varepsilon} - \alpha\Delta\dot{T})\}$ (without damage), W is a function of temperature, and T_d is a function of the damage parameter Eq. (37); the strain factor was not restricted to a power law, but this form with $p \approx q \approx 10$ fits the data quite well. Note that by solving Eq. (39) for strain, the result has the same form as Eq. (35). A softening function T_d consistent with experimental data is

$$T_d = e^{CL_f/q} \tag{40}$$

where C is a positive constant. Equations (39) and (40) may be used to obtain stress as an explicit function of strain,

$$\sigma = \sigma_o \left[1 + CL_o\right]^{-1/q} \tag{41}$$

where

$$L_o \equiv \int_o^t W(t')(\sigma_o/f)^q \, dt' \tag{42}$$

in which $\sigma_o \geq 0$, and $f = f(\varepsilon)$ replaces $\varepsilon^{p/q}$. Equation (41) predicts some very interesting types of behavior which have been reported for solid propellant. For example, with $q >> 1$, $\dot{L}_o > 0$, and $CL_o >> 1$, the stress is practically independent of strain history. Also, given the strain history in the form $\varepsilon = \varepsilon_A g(t)$ and $p = q$, we find σ/ε_A is independent of ε_A, but the material is nonlinear; this type of behavior has been reported by Farris (1971) for solid propellant at small strains.

<u>Stochastic Model for Global Fracture</u>. If one approximates the global failure of a composite or monolithic material as being due to the growth of one dominant flaw, then a relatively simple probabilistic fracture theory results by using the same type of power law flaw growth model used to develop Eq. (37). The principal result is expressed by the equation (Schapery, 1974c)

$$P_f(0 \leq t \leq t_T) = P_L \tag{43}$$

where P_f is the probability of failure, P_L is the master cumulative distribution function for creep-rupture tests or constant amplitude fatigue tests and t_T is the final time of interest. Now, with the condition that one must set $L = L_{max}$ ($\equiv$ largest value of L up to the current time) whenever the following equation predicts $L < L_{max}$, we use in Eq. (43) the expression

$$L(t) = \log \left[\frac{B_1 \sigma^{2/m}}{k^2} + \int_0^t c k^q \sigma^q dt' \right] \tag{44}$$

with $L_T \equiv L(t_T)$; also, B_1 is a function of material properties and m and k are constants.

This result can be viewed as an extension of the analysis of Halpin et al. (1973) to time-dependent stresses and temperatures. The coefficient c is not necessarily constant; for example, it may depend on strain, damage, temperature, and complex frequency effects. Special cases of Eq. (43) have met with some success with solid propellant and fibrous composites; but more study is needed before its range of validity can be established.

Except for the first term in Eq. (44), which is often negligible, the parameters for global fracture, L, and for local damage, L_f, are essentially the same. This is a direct result of having used for both predictions a crack speed equation of the form $da/dt \sim K_I^q$, where K_I is the opening-mode stress intensity factor. Global fracture is assumed to result from unstable growth of a dominant crack in the opening mode of deformation. Therefore, one can imagine many situations in which this model would not apply. Nevertheless, it does provide a convenient reference case against which more involved behavior can be compared.

Concluding Remarks

So far in this paper we have considered material behavior which is linearly viscoelastic except for damage. The problem of developing explicit nonlinear viscoelastic constitutive equations (with constant or varying damage) which are both realistic and useful is of course much more difficult. However, a study of actual behavior does reveal certain simplicity which, if introduced in a damage theory, results in equations which are not much more complicated than Eq. (21) or (35). Consider, for example, the behavior of carbon-black filled rubber. As a summary of the findings of several investigators on large strain, uniaxial stress-strain behavior of rubber, we may write (Mullins, 1969):

$$\varepsilon = F(\sigma_{max})\, g(\sigma) \tag{45}$$

where ε and σ are "engineering" strain and stress, respectively, F reflects the effect of damage in that it is a function of the maximum value of stress, σ_{max}, (considering the entire history of loading) and $g(\sigma)$ is a nonlinear function of stress; viscoelastic and healing effects are not included in this expression. The coefficient F is also a function of the volume fraction of particles, but their effect on $g(\sigma)$ is very small.

A generalization of Eq. (45) that contains Eq. (39) for viscoelastic behavior as a special case may be obtained by replacing σ in Eq. (39) by $g(\sigma)$. On the basis of this finding, one is lead to generalize Eq. (35) by proposing the following three-dimensional constitutive equation for anisotropic or isotropic materials,

$$\varepsilon_{ij} = \frac{1}{D_R} \left\{ D \frac{\partial \dot{W}}{\partial \sigma_{ij}} \right\} \tag{46}$$

where ε_{ij} and σ_{ij} are suitably defined strain and stress tensors for finite strain, and $W = W(\sigma_{ij}, T, \text{damage})$ is the Gibbs free energy function for an elastic material with damage. Similar, slightly more involved equations have been developed in part from nonequilibrium thermodynamics and applied to solid propellant (Schapery, 1973). However, their range of validity is essentially unknown as experimental data are still very limited. It would certainly be helpful to have a good physical model which both predicts the type of simplicity exemplified by Eq. (45) and is valid for multiaxial stress states. In this regard, it is of interest to observe that we can derive Eq. (45) for nonlinear elastic materials by assuming the flaws do not interact and the maximum stress affects their growth but not the specific process involved in local failure. Assumption of a distribution of local strengths or initial flaw sizes would result in the dependence on maximum stress, as would the assumption that the coefficient F is a function of $L_f^{1/q}$ with $q \rightarrow \infty$, where p and W(t') are finite (cf. Eq. (37)).

Finally, we note that the form of the parameters L_f in Eq. (37) and L in Eq. (44), and their dependence on stress, are predicted from linear viscoelastic fracture mechanics theory. Dependence of the integrand on global strain (and/or parameters defining the global damage state) would be predicted from the linear theory if the local fracture energy for the material at a crack tip depends on these quantities. For example, with solid propellant there is a broad distribution of particle sizes, and the material at one crack tip may contain many much smaller flaws; thus, the damage state of the composite material could be expected to effect the fracture energy for any single crack. Consistent with this observation is the fact that crack speed in solid propellant becomes independent of strain when the strain exceeds the value at which new vacoules form (Schapery, 1979); the speed, however, continues to increase rapidly with the stress intensity factor. The strain may affect not only the local fracture properties, but also the nonlinear form of the energy available for driving cracks. This latter case for large applied strains is illustrated by Andrews (1968) with globally elastic materials and by Brockway and Schapery (1978) with viscoelastic materials.

Acknowledgment

This work was sponsored by the Air Force Office of Scientific Research under Contract No. F49620-78-C-0034 with Texas A&M University.

References

Andrews, E. H., (1968), Fracture in Polymers, Oliver & Boyd, London.

Beckwith, S. W., (1974), "Viscoelastic Characterization of a Nonlinear, Glass/Epoxy Composite Including the Effects of Damage", Texas A&M University Report No. MM 2895-74-8.

Brockway, G. S., and Schapery, R. A., (1978), "Some Viscoelastic Crack Growth Relations for Orthotropic and Prestrained Viscoelastic Media", Eng. Fracture Mechanics, Vol. 10, p. 453.

Farris, R. J., (1971), "The Stress-Strain Behavior of Mechanically Degradable Polymers", Polymer Networks: Structural and Mechanical Properties, A. J. Chompff and S. Newman, Eds., Plenum.

Fung, Y. C., (1965), Foundations of Solid Mechanics, Prentice-Hall, Englewood Cliffs, N. J.

Halpin, J. C., Jerina, K. L., and Johnson, T. A., (1973), "Characterization of Composites for the Purpose of Reliability Evaluation", Analysis of Test Methods for High Modulus Fibers and Composites, ASTM STP 521, American Society for Testing and Materials, p. 5.

Mullins, L., (1969), "Softening of Rubber by Deformation", Rubber Chemistry and Technology, Vol. 42, p. 339.

Schapery, R. A., (1964), "Application of Thermodynamics to Thermomechanical, Fracture and Birefringent Phenomena in Viscoelastic Media", J. Appl. Phys., p. 1451.

Schapery, R. A., (1973), "Studies on the Nonlinear Viscoelastic Behavior of Solid Propellant", Texas A&M University Report No. MM 2803-73-2 (Air Force Report No. AFRPL-TR-73-50).

Schapery, R. A., (1974a), "A Nonlinear Constitutive Theory for Particulate Composites based on Viscoelastic Fracture Mechanics", Proc. of the 11th Meeting of the Joint Army-Navy-NASA Air Force Structures & Mechanical Behavior Working Group, Chemical Propulsion Information Agency, Pub. No. 253.

Schapery, R. A., (1974b), "Viscoelastic Behavior and Analysis of Composite Materials", Chapter 4 in Composite Materials, Vol. 2, G. P. Sendeckyj, Ed., Academic Press, p. 85.

Schapery, R. A., (1974c), "Application of Viscoelastic Fracture Mechanics to Nonlinear Behavior and Fracture of Solid Propellant", Texas A&M University Report No. MM 2995-74-5.

Schapery, R. A., (1975), "A Theory of Crack Initiation and Growth in Viscoelastic Media", Int. J. Fracture, Vol. II:Part I, "Theoretical Development". p. 141; Part II,"Approximate Methods of Analysis", p. 369; Part III, "Analysis of Continuous Growth", p. 549.

Schapery, R. A., (1976), "A Theory of Time-Dependent Bonding for Viscoelastic Media", Texas A&M University Report No. MM 3064-76-4 (AFOSR Scientific Report).

Schapery, R. A., (1978), "Fracture Mechanics of Solid Propellants", Fracture Mechanics, Ed. by N. Perrone, H. Liebowitz, D. Mulville, W. Pilkey; Univ. Press of Virginia, Charlottesville, p. 387.

Schapery, R. A., (1979), "Mechanical and Fracture Analysis of Solid Propellant under Slow Cooling", in "Predictive Techniques for Failure Mechanisms in Solid Rocket Motors", Chemical Systems Division Report No. CSD2540-FR (Air Force Report No. AFRPL-TR-79-87), Vol. VI., p. 1335.

Sokolnikoff, I. S., (1956), Mathematical Theory of Elasticity, McGraw-Hill, New York.

A Method for Determining the Mode I Delamination Fracture Toughness of Elastic and Viscoelastic Composite Materials

D.F. Devitt

Vought Corporation
Dallas, Texas 75265

R.A. Schapery

Civil and Aerospace Engineering
Texas A&M University
College Station, Texas 77843

and

W.L. Bradley

Mechanical Engineering
Texas A&M University
College Station, Texas 77843

(Received July 1, 1980)

ABSTRACT

A method using a longitudinally split, laminated beam specimen is developed to obtain delamination fracture toughness as a function of the rate of crack propagation. First, the relation between energy release rate, applied displacement, and various laminate parameters is derived using a large displacement, small strain theory. Experiments employing glass/epoxy composites with axially oriented fibers and of three different thicknesses and a wide range of loading rates are then described. Although the beam deflections and rotations are very large, good agreement between measured and predicted beam compliance is demonstrated. The energy release rate G and crack speed $\dot{a}$ are shown to obey the power law $G \sim \dot{a}^{0.1}$; essentially the same result is obtained for all three laminate thicknesses.

INTRODUCTION

Predictions of the useful life for composite material components require a comprehensive understanding of the material's response to complex load

J. COMPOSITE MATERIALS, Vol. 14 (October 1980), p. 270
0021-9983/80/04 0270—15 $04.50/0

histories in anticipated service environments with the presence of defects such as microcracks, voids, and delaminations. Such defects can occur during manufacturing or may develop in service, causing structural degradation or failures at stresses well below the strength levels expected for defect free material. Linear elastic fracture mechanics (LEFM) has been developed to deal with crack-like defects by relating defect geometry and design stress to a material response, normally called the fracture toughness. The fracture toughness of a material is usually characterized by critical energy release rate G_c or the critical stress intensity factor K_c.

In an ideal, monolithic, isotropic material the fracture toughness is independent of the orientation of the crack plane for a given mode of deformation at the crack tip, such as the opening mode (Mode I). However, in an anisotropic composite material, the material response may vary considerably depending on the plane of fracture and the energy dissipative processes involved. Work to date for Mode I has indicated K_{Ic} values of 15-30 MPa$\sqrt{m}$ for center notched tensile specimens of fiber-reinforced plastic laminates [1]; these compare favorably with aluminum alloys often used in the aircraft industry which have K_{Ic} values of 23-44 MPa$\sqrt{m}$ [2].

Growth of interlaminar flaws (delamination) is an important part of the failure process in many laminates [3,4]. Compressive fatigue appears to be an especially severe type of loading in producing delaminations [5,6]; out-of-plane stresses developed through compressive loading and local buckling are thought to be the primary cause of such delamination type fractures. These observations indicate that the delamination fracture toughness may be the critical toughness parameter for fatigue stressing where in-plane stresses are compressive.

While considerable effort has been expended to define fracture toughness for tensile loading of laminates with flaws normal to lamina planes, very little has been done to better define and understand the delamination fracture behavior. Apparently, the few studies that have been conducted to characterize delamination have utilized surface notched specimens (cf. Figure 1a) that give a mixed tensile and shear stress state at the delamination crack tip [3, 7, 8]; precluded, therefore, is determination of K_{Ic} or G_{Ic} for the opening mode of delamination in which only tensile stresses across the crack plane exist near the crack tip. In order to fully characterize delamination fracture toughness we believe it is necessary to study the effect of various proportions of tensile and shearing stresses at the crack tip, including pure tension.

The objective of the investigation described herein has been to develop an experimental approach with the associated analysis to obtain the fracture toughness for the opening mode of delamination. An axially-split beam geometry, Figure 1b, was chosen to give essentially pure opening mode fracture. To support the study of thin laminates, nonlinear beam theory was used

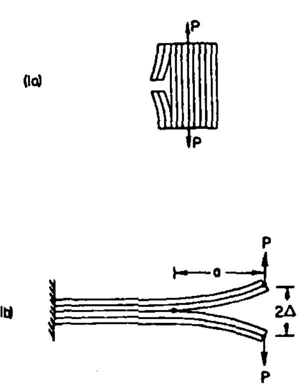

Figure 1. Specimens used in delamination fracture toughness studies: (a) Wang/Mandell Specimen; (b) Split laminate specimen used in our tests.

in the analysis. Experimental measurements were made on a unidirectional glass/epoxy composite (Scotchply) with axially oriented fibers to verify the analysis and allow determination of the delamination fracture toughness of this material. The analytical approach for elastic behavior is presented in the next section, followed by a generalization for limited viscoelastic behavior and a description of the experimental program. The experimental results are then used with the theory to characterize analytically the fracture behavior and check for internal consistency of the results.

The thin, split beam geometry gives rise to stable crack growth, and therefore is particularly suited to determine the relation between slow crack speed and energy release rate. A portion of our study therefore has been devoted to characterizing the fracture toughness of a viscoelastic laminate.

ANALYTICAL PROCEDURES FOR ELASTIC BEHAVIOR

Consider the beam specimen in Figure 1b, in which the delamination crack tip is at the point $x = a$. The energy release rate associated with a virtual crack growth of an amount da is, by definition, the mechanical energy that becomes available at the crack tip per unit area of new surface. In terms of the total strain energy in an elastic beam, W, this release rate is [9],

$$G = -\frac{1}{B}\frac{\partial W}{\partial a} \tag{1}$$

where the derivative is evaluated for constant beam tip displacement Δ. Also, B is specimen width normal to the page. The value of G at which the crack actually starts to propogate is the critical energy release rate or fracture toughness, G_c.

Evaluation of Equation (1) for our specimen geometry is based on an approximate analysis in which strain energy is determined for the cantilevered beam in Figure 2; the relevant parameters are tip displacement, Δ, beam length, L, area moment of inertia, I, and the axial modulus of elasticity, E. The analysis for a nonlinear beam in terms of these parameters is presented next. Primary results of the theory are given in dimensionless form in a table for general use in reducing data.

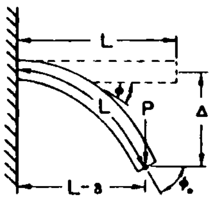

Figure 2. Nomenclature used in nonlinear analysis of cantilevered beam.

Strain Energy in a Nonlinear Beam

The strain energy due to bending of a beam of length L is, according to elementary beam theory,

$$W_1 = \tfrac{1}{2} \int_0^L \frac{M^2}{EI}\, ds \tag{2}$$

where M is the local bending moment.

As a result of the low flexural rigidity of thin composite specimens, large deflections and rotations may be present during the test and need to be accounted for in the analysis. Such a correction to linear beam theory has been made by Bisshopp and Drucker [10], in which they allowed for arbitrarily large rotations and bending deflections. A linear stress-strain equation and small strains were assumed.

The beam nomenclature and geometric relationships are shown in Figure 2, and the principal results are [10]:

$$\left[\frac{PL^2}{EI}\right]^{1/2} = \frac{1}{\sqrt{2}} \int_0^{\phi_0} (\sin\phi_0 - \sin\phi)^{-1/2}\, d\phi \tag{3a}$$

and

$$\frac{\Delta}{L} = \frac{1}{\sqrt{2}} \left[\frac{EI}{PL^2}\right]^{1/2} \int_0^{\phi_0} \frac{\sin\phi\, d\phi}{(\sin\phi_0 - \sin\phi)^{1/2}} \tag{3b}$$

where ϕ_0 is the angle of the tangent at the loaded end (cf. Figure 2), ϕ is the angle at intermediate points, P is the load, and the remaining terms were defined previously. After determining the appropriate change of variables and transformations, Bisshopp and Drucker were able to rearrange Equation (3) into the form

$$\left[\frac{PL^2}{EI}\right]^{1/2} = F(k) - F(k,\ \theta_1) \tag{4a}$$

and

$$\frac{\Delta}{L} = 1 - 2\left[\frac{E(k) - E(k,\ \theta_1)}{F(k) - F(k,\ \theta_1)}\right] \tag{4b}$$

where $F(k)$ and $E(k)$ are the complete elliptic integrals of the first and second kind, respectively; also, $F(k, \theta_1)$ and $E(k,\ \theta_1)$ are the corresponding incomplete elliptic integrals. The elliptic parameters k and θ_1 are related to ϕ_0:

$$k \equiv \frac{1}{\sqrt{2}}(1 + \sin\phi_0)^{1/2},\ \theta_1 \equiv \sin^{-1}(\sqrt{2}\ k)^{-1} \tag{5}$$

Notice that Equation (5) implies the results in Equation (4) are functions of only one parameter, say ϕ_0; hence, they are implicitly related with the correspondence presented in the second and third columns in Table 1 and in Figure 3.

Table 1. Nonlinear Beam Variables.

ϕ_0 (deg)		$\frac{PL^2}{EI}$	$\frac{\Delta}{L}$	$\frac{WL}{2EI}$	$\frac{GBL^2}{2EI}$	$\frac{GB}{2P}$
	Linear Theory	$3\frac{\Delta}{L}$	$\frac{\Delta}{L}$	$\frac{3}{2}(\frac{\Delta}{L})^2$	$\frac{9}{2}(\frac{\Delta}{L})^2$	$\frac{3}{2}(\frac{\Delta}{L})$
10		.3530	.1160	.0203	.0613	.1737
20		.7306	.2302	.0817	.2499	.3421
30		1.1626	.3406	.1854	.5814	.5000
40		1.6923	.4455	.3338	1.0880	.6429
50		2.3922	.5437	.5320	1.8330	.7662
60		3.4054	.6340	.7901	2.9502	.8663
70		5.0812	.7167	1.1331	4.7758	.9399
80		8.6787	.7948	1.6486	8.5558	.9858
86		14.9058	.8472	2.2411	14.9293	1.0002
88		20.7282	.8711	2.2600	20.9704	1.0117
90		-	1.0000	-		

Next, the strain energy stored in both cantilevers comprising the split beam is calculated. Combining the general definition for strain energy W_1 in a beam, Equation (2), with the specific results from nonlinear beam analysis given in [10], one may express the total strain energy $W = 2W_1$ in terms of elliptic integrals as follows:

$$\frac{WL}{2EI} = 2[F(k) - F(k,\theta_1)]^2 \qquad (6)$$

$$\left[\frac{E(k) - E(k,\theta_1)}{F(k) - F(k,\theta_1)} + (k^2 - 1)\right] \qquad (6)$$

This nondimensional result is presented in Figure 4 and the fourth column in Table 1. For comparison, we record also the linear solutions,

$$\frac{PL^2}{EI} = 3\frac{\Delta}{L}, \quad \frac{WL}{2EI} = \frac{3}{2}\left(\frac{\Delta}{L}\right)^2 \qquad (7)$$

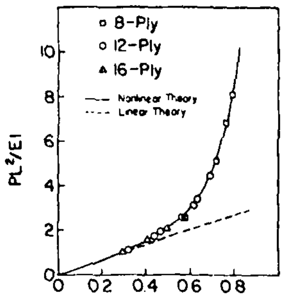

Figure 3. Nondimensional load-deflection curve for cantilevered beam. Symbols indicate experimental data from split laminate.

Energy Release Rate G for a Nonlinear Beam

The energy release rate as defined in Equation (1) can now be evaluated using Equation (6). However, in keeping with beam notation, the length L is used instead of the symbol "a" to denote crack length; hence

$$G \equiv -\frac{1}{B}\frac{\partial W}{\partial L} \qquad (8)$$

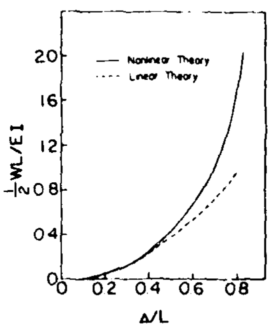

Figure 4. Nondimensional strain energy for cantilevered beam.

Prediction of G may be easily accomplished by first writing,

$$\frac{WL}{2EI} = f(\Delta/L) \qquad (9)$$

where $f = f(\Delta/L)$ is the solid curve in Figure 4. Thus,

$$\frac{1}{2}\frac{\partial W}{\partial L}\bigg|_{\Delta} = -\frac{EI}{L^2}\left[f\left(\frac{\Delta}{L}\right) + \frac{\Delta}{L}\frac{\partial f(\Delta/L)}{\partial(\Delta/L)}\right] \qquad (10)$$

Next, define S,

$$S \equiv d\,(\log f)/d\,(\log\,(\Delta/L)) \tag{11}$$

Therefore, from Equations (8) — (11),

$$G = \frac{EI}{BL^2}\,\frac{WL}{EI}\,(1 + S) = \frac{W}{BL}\,(1 + S) \tag{12}$$

A rearrangement of Equation (12) yields a nondimensional form of the energy release rate,

$$\frac{GBL^2}{2EI} = \frac{WL}{2EI}\;(1 + S) \tag{13}$$

Since both WL/EI and S in Equation (13) are functions of Δ/L, GBL^2/EI is an implicit function of Δ/L; it has been evaluated and is presented in Table 1 and in Figure 5. Linear theory yields $S = 2$, and therefore from Equations (7) and (13),

$$\frac{GBL^2}{2EI} = \frac{9}{2}\,\left(\frac{\Delta}{L}\right)^2 \tag{14}$$

which is shown in Figure 5. The last column in Table 1 is the ratio of the fifth to the second column; this ratio, $GB/2P$, enables the calculation of G without using the flexural rigidity, EI.

Suppose that during quasi-static crack growth, one determines Δ and L at any given time in a delamination fracture test. One may then use Figure 5 or Table 1 to determine G_c directly because $G_c = G$ for a slowly growing crack. That slow, controlled crack growth can indeed be achieved with this test is discussed next.

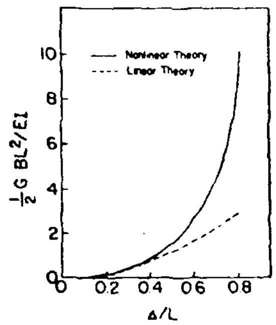

Figure 5. Nondimensional energy release rate for cantilevered beam.

Stability of the Crack Growth

It is clear that increasing the load or grip displacement for a fixed crack length will increase the strain energy stored in the specimen. From Figure 4 it is also apparent that crack extension (increasing L) which occurs at constant grip displacement results in a decrease in the strain energy stored in the specimen, as shown schematically in Figure 6. As the specimen with fixed crack size L_1 is deformed from Δ_1 to Δ_2, the strain energy obviously increases. The strain energy release rate also increases as the test goes from a to b (cf. Table 1).

Suppose at b the critical energy release rate is exceeded slightly and crack extension for constant Δ occurs, changing the crack length from L_1 to L_2. At point c the energy release rate is again insufficient to give crack extension, so that further loading to point d is necessary, which again corresponds to G being slightly larger than the critical energy release rate, G_c. Crack extension occurs from L_2 to L_3 as one moves along d-e. We may conclude from these considerations that crack growth is stable in a controlled displacement test if G_c does not change with L (or, at least, if it does not decrease rapidly with L).

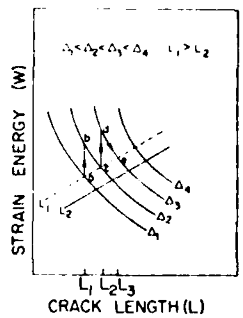

Figure 6. Schematic of strain energy versus crack length for constant grip displacement.

In an actual test the loading and crack extension occur more or less continuously, instead of in steps. Indeed, with negligible kinetic energy (quasi-static loading and slow crack growth) the energy release rate is essentially equal to G_c at all times. The path a-c-e for $G = G_c$ represented by the dotted line (not necessarily straight) in Figure 6 would be followed in an actual experiment.

In summary, the relationships between Δ/L and P, W and G have been determined in terms of elliptic integrals using nonlinear beam analysis. These results are summarized in Figures 3, 4 and 5 and Table 1; they will be used to analyze the experimental results following the next section, which is concerned with extension of these results to include rate effects at the crack tip.

EFFECT OF LOCAL VISCOELASTIC BEHAVIOR

The above theoretical prediction of energy release rate, G, can be used for viscoelastic materials if the axial stress-strain relation is essentially elastic and viscoelastic effects are limited to a small zone around the crack tip. In many cases, these conditions will be met for thin laminates consisting of a polymeric matrix and a large volume fraction of continuous glass, graphite, or boron fibers oriented in the axial direction. If the matrix is very soft, large inelastic shear deformations and possibly significant microcracking may occur away from the crack plane. Assuming these complications do not exist, the material in the neighborhood of the crack tip must absorb essentially all of the available energy during slow crack growth, and we may write

$$G = 2\,\Gamma_b \tag{15}$$

The quantity Γ_b is the fracture energy; it is the energy *required* to produce a unit of new surface at the crack speed $\dot{L}$. This energy may include energy of polymer chain failure, energy absorbed in local (near-crack tip) viscoelastic deformation processes, fiber fracture, and fiber-matrix debonding. In analogy with the discussion in [12] for monolithic materials, we conclude if the speed does not change appreciably in the time required for the crack to propagate a distance equal to the scale of the local deformation and failure processes, Γ_b will depend on the instantaneous crack speed but not on the history of loading and not on the rate of change of $\dot{L}$. If the speed dependence of Γ_b is due primarily to viscoelastic behavior of the intact matrix near the tip, we further expect it to obey a power law, $\Phi_b \sim \dot{L}^n$, where n is constant [12]. Thus, in view of Equation (15), the energy release rate will obey the same power law, $G \sim \dot{L}^n$.

Whether or not the result for the split beam (viz., $G = G(\dot{L})$) can be used with other geometries, such as growth of a through-crack in a tensile sample with fibers at 90° to the load, depends at least on the scale of the zone of fracture at the crack tip and the extent of viscoelastic behavior. It is expected that it will apply as long as viscoelastic and failure processes are highly localized to the crack tip. With large scale viscoelastic effects, the value of Γ_b may not change, but one cannot use Equation (15) as it relates Γ_b to an elastic energy release rate.

The effect of crack speed is illustrated schematically in Figure 6, where different paths are followed for different crack speeds. For the usual case in which $d\Gamma_b/d\dot{L}>0$, the path will move upward, as shown in the figure.

Finally, it is to be noted that if Γ_b is constant, Equation (15) may be replaced by the equivalent statement $G = G_c$, which is the critical energy release rate. We prefer to *not* use the symbol G_c instead of $2\Gamma_b$ for materials in which Γ_b depends on crack speed because the term "critical energy release rate" normally refers to a quantity that defines the boundary between no-growth and growth.

EXPERIMENTAL PROCEDURES AND RESULTS

The experimental program to be described in this section had two objectives: (1) to experimentally verify the nonlinear beam analysis; and (2) to obtain the relation between energy release rate and crack growth rate. First, specimen preparation and testing will be described and typical raw data presented. Reduction of the data to energy release rate values using the previously described nonlinear beam analysis is then accomplished, and the results are presented in tabular and graphical form.

Specimen Preparation

Scotchply, which is an E-glass reinforced type 1003 epoxy, was selected for this study because it is translucent, which makes the visual measurement of the moving crack front during testing quite easy. Eight, twelve, and sixteen ply

30.5 cm × 30.5 cm panels were laid up using prepreg tape containing continuous fiberglass filaments. Teflon was inserted along one edge of each panel to provide the initial midplane delamination crack. All lamina had the same fiber orientation in the laminates. After curing in accordance with the suppliers specifications, the 30.5 cm square laminates were cut parallel to the fiber direction into 2.54 cm wide unidirectional test strips. The cured lamina thickness was about 0.021 cm, giving laminate thicknesses of 0.170, 0.259 and 0.338 cm, respectively, for the 8, 12 and 16 ply specimens.

Test Procedure

The specimens were tested in an ambient environment (approximately 75 °F and 50% RH) using an Instron tensile test machine with a one thousand pound load cell; a twenty pound full scale range was used. Special grips were designed to allow the load to be applied along a fixed line of action while permitting a virtually free rotation of the loaded ends of the split beam (cf. Figure 7), as was assumed in the analysis. Load was monitored as a function of time using a strip chart recorder. The displacement versus time was calculated from the crosshead speed. The crack position as a function of time was noted visually as the crack front passed reference marks on the specimens. Typical experimental results are presented in Table 2 for a twelve ply specimen tested at a crosshead speed of 2.5 cm/minute. Five each of the eight, twelve and sixteen ply specimens were tested at a crosshead speed of 2.5 cm/minute. Two specimens were tested with increasing crosshead speed.

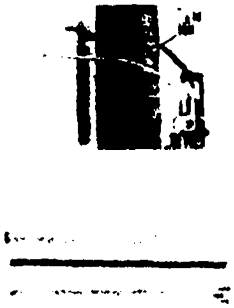

Figure 7. Split laminate specimen showing (a) hinge attachment used for loading and (b) deformation in crack growth test.

Data Reduction

The measured data included load, P, grip displacement, 2Δ, and crack length, L; they can be easily used to give instantaneous energy release rate, G, using the analysis described in an earlier section, especially the results in the last column in Table 1. After determining Δ/L, Lagrangian interpolation was used to calculate both PL^3/EI and $GB/2P$. The results of these interpolations, along with the subsequent calculation of the energy release rate, G, are summarized in Table 2. The crack growth rate was calculated from the measured values of grip displacement versus crack extension, L, knowing the rate of grip displacement. From each set of measured values of P, 2Δ, and L, the fifth column in Table 2 was used to derive individual values of EI; they were averaged with respect to length for each laminate for later use.

Table 2. Experimentally Measured Values of Crack Length, L, Load, P, and Grip Displacement, 2Δ, for Twelve-Ply Specimen. Also Tabulated are Various Dimensionless Terms Used in Determining G and Checking Theory.

L (cm)	2Δ (cm)	P (N)	Δ/L	$\frac{PL^2}{EI}$ (Theory)	$\frac{GB}{2P}$ (Theory)	G N/m
8.9	5.6	27.0	.32	1.07	.470	991
10.2	7.2	24.4	.36	1.26	.530	1010
11.4	9.2	22.1	.40	1.47	.583	1020
12.7	11.1	20.6	.44	1.66	.636	1020
14.0	13.1	18.9	.47	1.83	.676	993
15.2	15.1	17.8	.50	2.04	.713	987
16.5	17.6	17.0	.53	2.29	.750	1010
17.8	19.8	16.3	.56	2.54	.786	1010
19.1	22.4	15.8	.59	2.85	.819	1020
20.3	24.7	14.8	.61	3.10	.843	978
21.6	26.9	14.1	.62	3.22	.853	949
22.9	28.9	12.9	.63	3.34	.862	878
24.1	32.1	13.2	.66	3.81	.899	930
25.4	35.1	13.4	.69	4.46	.921	970

DISCUSSION

Load-Deflection Relationship

Results taken from 8, 12, and 16 ply specimens have been plotted in Figure 3. While PL^2/EI can be predicted by the analysis, as shown by the solid line, the values may also be determined directly from measured quantities. The accuracy of the analysis is clearly demonstrated by the fact that the experimental data points for all three thicknesses fall nicely on the curve predicted from the analysis when a constant, average value of EI for each laminate is used. Another way of demonstrating the accuracy of the analysis is to predict the crack length L at various times in a test using the measured values of P and 2Δ and the average EI. The predicted values of L are compared with the experimental results in Table 3 for a twelve-ply specimen. The agreement is seen to be excellent, due in large part to the insensitivity of L to the experimentally determined parameters.

This method of determining the instantaneous crack length should be very

Table 3. Comparison of Measured Values of Crack Length, L, To Value Calculated Using Nonlinear Beam Analysis and Measured Values of Grip Displacement, 2Δ, and Load, P.

Measured Crack Length (cm)	Calculated Crack Length (cm)
8.89	8.91
10.16	10.13
11.43	11.48
12.70	12.70
13.97	13.97
15.24	15.21
16.51	16.54
17.78	17.70
19.05	19.05
20.32	20.35
21.59	21.56
22.86	22.91
24.13	24.26
25.40	25.55

useful in tests of opaque materials, such as graphite/epoxy laminates. However, for high accuracy the value of *EI* employed in the prediction of crack length should be obtained directly from the laminate using one or more pre-determined lengths and theory (i.e. second and third columns of Table 1). This is necessitated by the fact that predicted values of *EI* differ somewhat from the measurements, possibly due to nonuniformity in the fiber distribution. Further, the photomicrographs of the twelve ply laminate in Figure 8 show that the local distribution is quite heterogeneous. In many cases the fibers appear to be in contact, which could be a significant factor in producing the scatter in the delamination fracture energy discussed next.

Energy Release Rate-Crack Speed Relationship

The energy release rate is plotted against crack speed in Figure 9. The data can be approximated by a power law $G \sim \dot{L}^{0.1}$ Schapery [12] has predicted that crack growth rates in viscoelastic material may be described by an equation of the form $\dot{L} \sim K_I^q$ where $q = 2(1 + 1/m)$ if the intrinsic fracture energy and strength at the crack tip are independent of crack speed and the creep compliance, D, obeys the power law $D \sim t^m$. For many glassy polymers, including

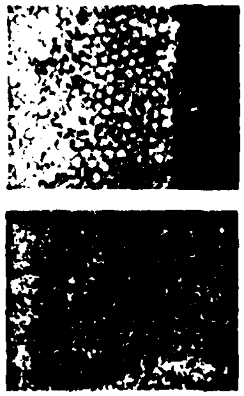

Figure 8. Photomicrographs of Scotchply showing distribution of glass fibers in epoxy matrix: (l) 12 plies, 500x.; (b) 12 plies, 100x.

the epoxy resin in Scotchply, the creep compliance is of the form $D = D_o + D_1 t^n$ [13]. The value of D_1 increases with increased molecular mobility, such as may result from the increase in volume due to the high triaxial stresses near a crack tip. If D_1 is sufficiently large then $m \simeq n$. Inasmuch as $K_I \sim G^{1/2}$ (cf. Equation (16)) and $G \sim \dot{L}^{0.1}$, we obtain $q \simeq 20$ and $n \simeq 0.1$ if $m \simeq n$. In order to check this value for n, creep/recovery tests were run on unidirectional tensile specimens of Scotchply with a 90° fiber angle to determine the time dependence of the matrix. An exponent of $n \simeq 0.05 - 0.10$ was determined for these tests, which is consistent with the fracture results for delamination fracture toughness. However, the data are so limited that one should consider the relationship $q \simeq 2(1 + 1/n)$ as very tentative.

Fracture toughness of unidirectional Scotchply has been measured by *Wu* [14] using a center-notched specimen with 90° fibers. Averaging out rate effects in order to obtain a single critical stress intensity factor, he obtained for K_{IC} a value of 1.9 $MPa\sqrt{m}$. These results may be compared to our results if G values are expressed in terms of K_I using the relationship

$$K_I = (\hat{E}G)^{1/2} \tag{16}$$

where $\hat{E}$ is the effective modulus and can be shown to be approximately equal to one half the transverse modulus E_{22} for an orthotropic material [15]. Utilizing the manufacturer's predicted value for E_{22} of $9.7 \times 10^3 MPa$ and our observed range of G values of 525 — 1000 N/m gives a predicted range of values for K_I of 1.6 — 2.2 $MPa\sqrt{m}$ which brackets Wu's result for K_{IC}. These values may also be compared with values measured for metals and various plastics, as summarized in Table 4.

Several simplifying assumptions were made implicitly in the analysis that appear to be justified by the good agreement between the measurements and predictions from the nonlinear beam analysis, as seen in Figure 3. These assumptions include plane stress and "rigid wall" behavior at the beam end point, which in our specimen is the crack front. The actual behavior in this crack tip region may only be described by a more complex three dimensional analysis using finite elements; however, the departure from these idealizations appears to have a negligible effect on the overall load-deformation relation (cf. Figure 3), and consequently a small effect on strain energy stored, in that it

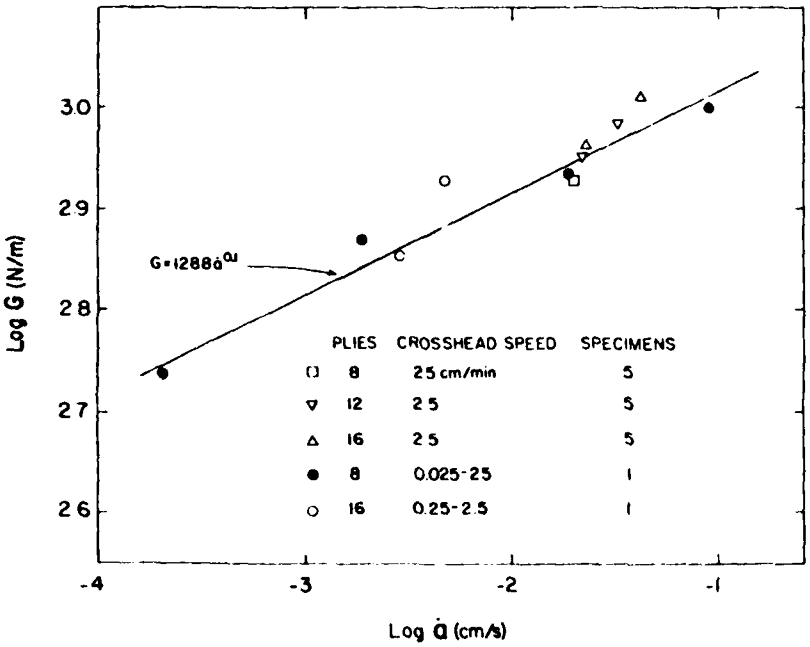

Figure 9. Energy release rate versus crack speed for three different thicknesses of Scotchply.

Table 4. Typical Fracture Toughness Parameters (K_{IC} and G_C)

Material	K_{IC} MPa$\sqrt{m}$	G_c KN/m
Metals [5, 10]		
Ti-6Al-4V	115	121
7075-T651	24	8
4340	60 - 99	18 - 49
2024 T3	44	27
Thermoplastic Materials [11, 12]		
Polymethyl Methacrylate	1.6 - 1.9	1.1
Polystyrene	0.98 - 1.1	0.35
Polyvinyl Chloride	1.6 - 2.3	1.2
Nylon - 6, 6	0.51 - 0.83	0.25
Polyethylene	0.83 - 1.2	5.0

may effectively be neglected. Significant breakage of glass fibers away from the crack plane could also have introduced an error into the bending rigidity and energy release rate. Sample calculations indicate that the axial stress in the beam never approached the failure value; furthermore, almost no fiber fracture was noted in the tests other than along the crack plane. Finally, as a result of transverse strains (normal to the loading direction), the beam has a compound curvature which would tend to stiffen the beam and depend on beam length. Again, in view of the agreement in Figure 3, this effect was apparently negligible for the specimens used.

CONCLUSIONS

A simple approach to the determination of delamination fracture toughness in the opening mode has been developed using a split beam and a nonlinear analysis. The analysis has been confirmed with experimental measurements on Scotchply using specimens of three thicknesses, tested over a wide range of crack growth rates. The measured range of energy release rates of 525—1000 *N/m* for the range of crack growth rates studied is shown to be consistent with predictions from an idealized viscoelastic crack growth theory and viscoelastic behavior of the resin as determined from creep/recovery tests.

ACKNOWLEDGEMENT

This research was sponsored by the Air Force Office of Scientific Research under contract No. F49620-78-C-0034 with Texas A&M University.

The authors are indebted to Professor K.L. Jerina for his valuable guidance in the experimental phase of the study and to Mr. R.C. Hulsey for his very able assistance in conducting tests during the latter stages of the work and for making the photomicrographs in Figure 8. This paper is based, in part, on the M.S. Thesis of the first author submitted to Texas A&M University.

Important related work on interlaminar fracture was brought to the authors' attention by W.D. Bascom after completing this paper; see Letters, *Composites,* July 1980, pp. 131-132 for reference to several studies. Apparently, the nonlinear beam theory and characterization of delamination speed energy release rate behavior have not been previously addressed.

REFERENCES

1. Kausch, H.H., *Polymer Fracture,* Springer-Verlag, Berlin, 1978, p. 256
2. Hertzberg, R.W., *Deformation and Fracture Mechanics of Engineering Materials,* Wiley, New York, 1976, p. 285.
3. Kulkarni, S.V., Pipes, R.B., Ramkumar, R.L., Scott, W.R., "The Analytical, Experimental, and Nondestructive Evaluation of the Criticality of an Interlaminar Defect in a Composite Laminate", Proceedings of the 1978 International Conference on Composite Materials, Toronto, 1978, pp. 1057-1071.
4. Reifsnider, K.L. "Mechanics of Failure of Composite Materials," In *Fracture Mechanics,* Proc. 10th Symposium on Naval Structural Mechanics, Univ. Press of Virginia, 1978, pp. 317-331

5. Grimes, G.C., and Adams, D.F., "Investigation of Compression Fatigue Properties of Advanced Composites", Northrop Technical Report, NOR 79-17, Dept. of the Navy, NASC Contracts N00019-77-C-0518 and N00019-77-C-0519 with Northrop and the University of Wyoming, October 1979.
6. Wilkins, Dick, General Dynamics, Fort Worth, Texas, private communication.
7. Wang, S.S. and Mandell, J.F., "Analysis of Delamination in Unidirectional and Crossplied Fiber-Composites Containing Surface Cracks", NASA Technical Report NASA-CR-135248, May 1977.
8. Wang, S.S., "Delamination Crack Growth in Unidirectional Fiber-Reinforced Composites Under Static and Cyclic Loading", ASTM Symposium on Composite Materials-Testing and Design, March 20, 1978, New Orleans, Louisiana.
9. Hertzberg, R.W., *Deformation and Fracture Mechanics of Engineering Materials*, Wiley, New York, 1976, p. 260.
10. Bisshopp, K.E., and Drucker, D.C., "Large Deflection of Cantilever Beams," *Quarterly of Applied Math*, Vo III, 1945, p. 272.
11. Selby, Samuel M. (Editor in Chief), *Standard Mathematical Tables*, 19th Edition, The Chemical Rubber Co., Cleveland, Ohio, July 1971.
12. Schapery, R.A. "A Theory of Crack Initiation and Growth in Viscoelastic Media. III Analysis of Continuous Growth," *Int. J. Fracture*, Vol. 11, 1975, p. 549.
13. Schapery, R.A., "Viscoelastic Behavior and Analysis of Composite Materials", in *Composite Materials*, Vol. 2, G.P. Sendeckyj Ed., Academic Press, 1974, p. 85.
14. Wu, E.M., "Fracture Mechanics of Anisotropic Plates", *Progress in Materials Science*, Vol. I, 1968, Technomics, Stanford, Connecticut, p. 20.
15. Brockway, G.S., and Schapery, R.A., "Some Viscoelastic Crack Growth Relations for Orthotropic and Prestrained Media", *Eng'g Fracture Mechanics*, Vol. 10, 1978, p. 453.

NONLINEAR FRACTURE ANALYSIS OF VISCOELASTIC COMPOSITE MATERIALS BASED ON A GENERALIZED J INTEGRAL THEORY

R. A. Schapery
Civil Engineering Department
Texas A&M University
College Station, TX 77843

ABSTRACT

Pertinent results from a generalized J integral theory for nonlinear viscoelastic media are first reviewed, and then some special cases for power-law materials are given to illustrate their application in crack growth and failure analysis. This theory was recently developed by the author; it is a generalization of the familiar J integral theory which is customarily restricted to nonlinear elastic and viscous materials and to materials obeying the classical deformation theory of plasticity. Some experimental results from cyclic and transient loading of fibrous and particulate composites are then given and, together with the theory, are used in a tentative interpretation of the viscoelastic fracture process.

NOMENCLATURE

a	notch or crack size
$\dot{a}$	crack speed
a_T, a_{TM}	time-scale shift factor for temperature and moisture effects
$C_1 - C_5$	unspecified constants
D	creep compliance for uniaxial loading
e	superscript denoting pseudo-elastic variables
E_R	reference modulus
i, j	indices corresponding to coordinate directions (1,2,3)
J, J', J_v	J integrals for elastic, viscous, and viscoelastic media, respectively
K_I	stress intensity factor for opening mode
k	exponent relating crack speed and J_v
n_i	vector normal to J integral path
n, N	exponents defining time-dependence and nonlinearity, respectively
P	potential energy of body and applied loads

Published in Proceedings of the Japan - U.S. Conference on Composite Materials, Tokyo, January, 1981.

P_T	designates location of mathematical crack tip
q	exponent relating crack speed and applied stress
T_i	surface tractions
u_i	displacements
W, W'	energy density
x_i	Cartesian coordinates
α	length of failure zone
Γ'	path used to evaluate J integral
Γ	intrinsic fracture energy
ϵ_{ij}, $\dot{\epsilon}_{ij}$	strains and strain rates, respectively
σ_{ij}	stresses
σ_m	magnitude of normal stress at crack tip
σ_o	constant (yield stress if $N<<1$)
τ	time variable of integration
Φ	pseudo strain energy density
Φ_c	pseudo complementary energy density

INTRODUCTION

Time-dependent deformation behavior of the matrix constituent in many composites is often very pronounced, especially in elevated temperature environments; exposure of polymer-matrix composites to high relative humidity leads to similar behavior and aggravates the effect of temperature if sufficient time is provided for absorption of the water vapor. This time-dependence, or viscoelasticity, is an important factor in determining the rate of growth of micro- and macrocracks (including delamination cracks). Complicating the composite response characteristics is nonlinearity on the macroscale (although often due in part to matrix microcracking) and on the microscales of the reinforcing fibers or particles and the crack tip structure. Development of realistic theoretical models of damage growth and failure therefore requires in many cases that one account for both time-dependence and nonlinearity in the deformation behavior. In spite of the complexity of the problem, it is believed possible to develop at this time practical models which will be useful in aiding our understanding of structural response of composites so that improved materials, structural design methods, and reliability can be realized.

In this paper we briefly describe and then apply a new fracture theory (1), based on the so-called J integral (2), for analyzing micro- and macrocracking in nonlinear viscoelastic composites.

Following (2), the J integral is defined for two-dimensional problems by

$$J = \int_{\Gamma'} (W dx_2 - T_i \frac{\partial u_i}{\partial x_1} ds) \tag{1}$$

where, as shown in Fig.1, Γ' is a curve surrounding the notch tip, and repeated indices imply summation over their range. The quantity $W=W(\epsilon_{ij})$ is defined such that

$$\sigma_{ij} = \partial W/\partial \epsilon_{ij} \tag{2}$$

where σ_{ij} and ϵ_{ij} are the stress and strain tensors, respectively. Thus, W is the strain energy density or an analogous potential function in the deformation plasticity theory. Also, T_i is the traction vector, in which $T_i=\sigma_{ij}n_j$. The displacement vector is denoted by u_i. A very useful feature of J is that its value is independent of path Γ' if W does not depend on the coordinate x_1 (cf. Fig.1) other than through the dependence of ε_{ij} on x_1; the material may be anisotropic and have properties that vary with x_2. A second important characteristic, especially for experimental characterization of fracture, is that if the notch tip is advanced an amount da without change in tip structure,

$$J = -\partial P/\partial a, \tag{3}$$

which is the rate of decrease of potential energy (of the body and applied loads) with respect to notch length per unit thickness normal to the page.

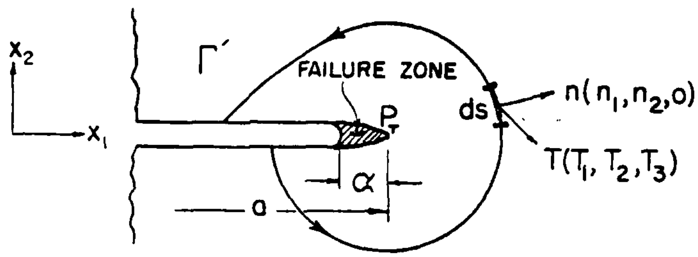

Fig.1 Crack or notch in elastic material, with tip at P; highly damaged material is shaded.

Over ten years ago, Rice (2) developed and applied the J integral for two-dimensional deformation fields (plane strain, generalized plane stress, and antiplane strain) in nonlinear elastic media with notches or cracks. This work, which was theoretically limited to small strains, lead the way to major developments during the past decade in the engineering characterization and analysis of fracture initiation in metals with both small scale and large scale plastic deformations (e.g., 3, 4). (Although the J integral was seemingly developed for elastic materials, the constitutive equation for the deformation theory of plasticity without unloading is anlogous to that for elastic materials in the sense that it may be written as in Eq.(2); consequently, application to fracture initiation in ductile metals has been successful.)

The J integral can be interpreted as a conservation law for mechanical energy. As such, one would expect to be able to deduce a three-dimensional generalization with large strains if suitable measures of stress and strain are used. Indeed, such a version does exist; as noted by Knowles and Sternberg (5), in their study of finite elastic deformations near a crack tip, this conservation law is implicit in an early result due to Eshelby (6) in the theory of continuous dislocations. The J integral with large plastic deformations was used by McMeeking (7) in a study of phenomena at crack tips, including void growth. Rice (8) has reviewed applications to stable crack growth in rate-independent media.

An integral, say J', with properties analogous to those for J may be defined for nonlinear viscous media when the constitutive equation can be expressed in the form

$$\sigma_{ij} = \partial W'/\partial \dot{\varepsilon}_{ij} \tag{4}$$

where $W'=W'(\dot{\varepsilon}_{ij})$ and $\dot{\varepsilon}_{ij}$ is strain rate. The same definition as in Eq.(1) is used for J', except strain rates and velocities replace strains and displacements. Landes and Begley (9) showed that crack speed $\dot{a}$ in two different specimen geometries of superalloy at high temperature may be correlated in terms of J'; viz., $\dot{a}=\dot{a}(J')$. Sakata and Finnie (10) and Ohji, et al. (11) independently studied stress intensity factor K_I and J', respectively, as fracture parameters for nonlinear viscous materials. Many papers have now appeared which provide strong experimental support for the hypothesis that

$\dot{a}=\dot{a}(J')$ for creeping metals at high temperatures under constant and variable loading, and the reader is referred to (12-14) for recent work and citations of other studies.

In order to provide a rigorous theoretical argument that J' is the appropriate basic parameter for correlating fracture data, and to relate observed behavior to basic material properties, it is believed necessary to investigate crack-tip behavior under locally finite stresses in which a finite scale for damage and material separation exists (e.g., the length α in Fig.1.). To the author's knowledge, previous theoretical studies involving nonlinear viscous or viscoelastic behavior outside of the failure zone have introduced strain rates which are infinite at the crack tip for mathematically sharp cracks. The basic shortcoming of such singular fields can be illustrated by analysis of linear viscoelastic media, as reviewed by Rice (8). For example, starting with a solution for finite stresses, Schapery (15) proved that if the magnitude of the crack-tip stress is mathematically increased without limit, the scale α vanishes and crack growth becomes independent of the linear viscoelastic properties; only the initial value of compliance or modulus remains. Associated infinite strain rates produce the physically unacceptable prediction. Numerous publications on the analysis of crack growth in linear viscoelastic media, based on a finite crack-tip stress, now exist (e.g., see (8) and (15-20)).

Very recently, Schapery (1) extended the J integral concept to nonlinear viscoelastic media for both initiation and growth of cracks. This work is based on finite crack tip stresses, so that one may derive basic failure behavior related to the physical characteristics which define the zone of intensive damage at the crack tip. This region is called the "failure zone" (whose length is α in Fig.1) rather than damage zone; the theory in (1) allows for certain kinds of damage in the nonlinear material surrounding the crack tip, such as the type of stable microcracking and void growth that develops in many composites if the stress level is not too high. For propagating cracks, a layer of the highly damaged material that was once in the failure zone will be left on the crack faces. It was assumed in (1) that this layer is thin enough to be neglected in predicting stresses and strains in the neighborhood of the crack tip; thus, α is the only scale parameter that reflects the local failure process for propagating cracks (as well as that for cracks which just start to grow, corresponding to the fracture initiation condition).

In the present paper we first give the constitutive equation used in developing the generalized J integral theory. Discussed next is the relation of crack speed to the generalized J integral, designated by J_v for a viscoelastic material. An explicit relation between crack speed and applied stress is then stated for a single crack in a power law material; both time-dependence and stress-dependent nonlinearity are assumed to obey power laws. The two independent exponents combine to yield one exponent defining the crack speed as a power law in stress; for fatigue loading of monolithic materials and certain types of composites, the same exponent relates number of cycles to failure and applied stress. When used with theory, the values of experimentally determined exponents are very helpful in identifying primary physical mechanisms affecting crack growth and failure. This point is illustrated by using data on fatigue failure of graphite fiber-reinforced epoxy laminates and macrocrack propagation in composite solid propellant (which is rubber with a high volume fraction of hard particles).

NONLINEAR CONSTITUTIVE EQUATION

The relation between stress and strain tensors is assumed in the form

$$\epsilon_{ij} = E_R \int_{0-}^{t} D(t-\tau,\ t)\frac{\partial \epsilon^{e}_{ij}}{\partial \tau}d\tau \tag{5}$$

where the ϵ^{e}_{ij} are termed pseudo-strains, and are functions of stresses (as well as temperature and moisture, depending on the particular material) through a potential function $\phi_c=\phi_c(\sigma_{ij})$,

$$\epsilon^{e}_{ij} = \frac{\partial \phi_c}{\partial \sigma_{ij}} \tag{6}$$

If Eq.(6) can be inverted to yield σ_{ij} as a function of ε^{e}_{ij}, then Eq.(6) implies that a potential function $\Phi=\Phi(\varepsilon^{e}_{ij})$ exists with the property that

$$\sigma_{ij} = \frac{\partial\Phi}{\partial\varepsilon^{e}_{ij}} \tag{7}$$

where

$$\Phi = -\Phi_c + \sigma_{ij}\varepsilon^{e}_{ij} \tag{8}$$

Viscoelastic behavior is defined by the creep compliance, D. It may be observed that the notation $D(t,\tau)$ is often used instead of $D(t-\tau,t)$; but the notation is equivalent and allows for aging. Thermorheologically simple behavior, a form of temperature dependence commonly obeyed by polymers, is a special case of this representation for creep compliance, with constant or transient temperature. The modulus E_R is a free parameter which makes Eq.(5) dimensionally correct as Φ_c has the dimensions of modulus; E_R may be selected as desired to simplify the notation in fracture results. That Eq.(5) is a good approximation for many nonlinear viscoelastic materials is discussed in (1); also, it is shown in (1) that Φ_c may depend on certain important types of damage, such as distributed microcracks. If we assume $D(t-\tau,t)$ is proportional to $t-\tau$, Eq.(5) reduces the constitutive equation for a linear or nonlinear viscous material.

COPLANAR CRACK GROWTH IN POWER-LAW MATERIALS

By means of an elastic-viscoelastic correspondence principle established in (1) and approximations similar to those used in (16, Part II) for linear theory, it is found that if α is small compared to other relevant dimensions such as crack length,

$$2\Gamma = E_R D(\alpha/3\dot{a},t)J_v \tag{9}$$

where Γ, the intrinsic fracture energy, is the mechanical work that the continuum does on the failure zone when one unit of new surface is formed. The generalized integral, J_v, is defined as in Eq.(1), but Φ replaces W and pseudo-displacements, u^{e}_{i} (corresponding to pseudo strains, Eq.(6)) replace u_i. In deriving Eq.(9), it is assumed crack speed is essentially constant during the time $\alpha/\dot{a}$, which is that required for crack growth of an amount α. The time t in the argument of D reflects, for example, aging and transient temperature and/or moisture content; but such effects are assumed constant in the time interval $\alpha/\dot{a}$. For simplicity, these transient effects will be neglected in all subsequent discussion.

Let us now introduce a power law for creep compliance,

$$D(t-\tau) = D_1(t-\tau)^n \tag{10}$$

where D_1 and n are positive constants. Also, assume Φ is a homogeneous function of degree N+1 in pseudo strain,

$$\Phi(c\varepsilon^{e}_{ij}) = |c|^{N+1}\Phi(\varepsilon^{e}_{ij}) \tag{11}$$

where c and N are constants. The material defined by Φ may be anisotropic and physically nonhomogeneous.

In order to illustrate the significance of the exponent in Eq.(11), consider a uniformly stressed specimen under a time-dependent uniaxial stress σ (or, more generally, under multiaxial proportional loading). We find the strain in the direction of loading to be

$$\varepsilon = E_R D_1 \int_{0-}^{t} (t-\tau)^n \frac{d(\sigma/\sigma_o)^{1/N}}{d\tau}\, d\tau \tag{12}$$

where σ_o is a constant. If N is small, σ_o can be interpreted as a yield stress. In a creep test σ is constant and Eq.(12) reduces to

$$\varepsilon = E_R D_1 t^n (\sigma/\sigma_o)^{1/N} \tag{13}$$

Let us introduce temperature T and moisture M effects in standard notation for polymers by writing

$$E_R D_1 = a_{TM}^{-n}, \tag{14}$$

where $a_{TM}=a_{TM}(T,M)$ is the time-scale shift factor. Thus, the creep strain is,

$$\epsilon = (t/a_{TM})^n(\sigma/\sigma_o)^{1/N} \tag{15}$$

The requirement of a finite crack tip stress, whose magnitude at the point P_r in Fig.1 is denoted by σ_m, leads to the relation (1),

$$\alpha = C_1\left(\frac{\sigma_o}{\sigma_m}\right)^{1/N}\frac{J_v}{\sigma_m} \tag{16}$$

where C_1 is a dimensionless constant.

In general σ_m and Γ may depend on crack speed. If, however, they are constant, Eqs.(9), (10), (14), and (16) yield simply

$$\dot{a} = \frac{C}{a_{TM}}J_v^k \tag{17}$$

where C and k are positive constants, with

$$k = 1 + \frac{1}{n} \tag{18}$$

If Γ and α (instead of σ_m) are constant,

$$k = \frac{1}{n} \tag{19}$$

Finally, if α and crack opening displacement Δv_1 (at the left end of the failure zone in Fig.1) are constant (1),

$$k = \frac{1}{n(1+N)} \tag{20}$$

The constant C is different for each of these cases. It should be added that if the spacewise distribution of the stress in the failure zone varies greatly with speed, the change will be reflected as speed dependence of C; but this effect will be neglected here. Also, the assumption of constant σ_m and Δv_1 results in Eq.(18), and therefore does not represent another independent case.

For bodies on which surface tractions are specified, instead of displacements, J_v as a function of these tractions is the <u>same</u> as for an elastic material. For an isolated crack in a macroscopically homogeneous, nonlinear power law body under proportional loading (1), (assuming $\alpha<<a$),

$$J_v = aC_2\sigma_o\left(\frac{\sigma}{\sigma_o}\right)^{1+(1/\hat{N})} \quad , \quad \sigma > 0 \tag{21}$$

where C_2 is a dimensionless constant and $\sigma=\sigma(t)$ is the remote stress in a given direction; $\hat{N}$ is for the far-field, which may differ from N for the near-tip material.

Equations (17) and (21) yield

$$\dot{a} = C_3\frac{a^k}{a_{TM}}\left(\frac{\sigma}{\sigma_o}\right)^q \tag{22}$$

where C_3 is another constant and

$$q \equiv k(1+\hat{N})/\hat{N} \tag{23}$$

When the geometry of a body is that in Fig. 2, which is a sheet (or thick slab) that is loaded vertically through rigid clamps, the form of J_v is the same as in Eq. (21), except h replaces a. Assuming $\alpha<<a<h/2$, the coefficient C_2 is essentially constant, where σ is equal to the stress σ_∞ in the uniformly stressed portion of the strip; as a good approximation, at least if $\hat{N}=1$, σ may be taken as

the total vertical load P_v divided by the uncracked area (1). Thus,

$$\dot{a} = C_4 \frac{h^k}{a_{TM}} \left(\frac{\sigma}{\sigma_o}\right)^q \tag{24}$$

Given $\sigma(t)$ or $P_v(t)$, Eqs.(22) and (24) may be integrated to predict crack size. If the stress is applied for a long enough period, a failure time t_f is found. Suppose $k>1$ in Eq.(22); then $a \to \infty$ when

$$\int_o^{t_f} (\sigma^q/a_{TM})dt = C_5 \tag{25}$$

where C_5 is a constant proportional to a_o^{1-k}; a_o is initial crack size. The same type of result is derived from Eq.(24) but $C_5 \sim h^{-k}$, σ is to be replaced by P_v and failure occurs when $2a=L$. It should be added that Eqs.(21)-(25) are not restricted to plane stress or plane strain problems. The axisymmetric problem of a penney-shaped crack is also included, in which 2a and L are crack and sample diameters, respectively.

When the applied load is constant (creep test) and the physical environment is constant (constant value of a_{TM}), Eq.(25) yields $t_f \sim \sigma^{-q}$. Similarly, for a cyclic tensile fatigue test, $N_f \sim \sigma^{-q}$, where N_f is the number of cycles to failure and σ is stress amplitude; it is assumed for simplicity here that the wave shape and amplitude do not change with time. Thus, at least for the two idealized problems considered above, there is a simple relationship between the log-log slope q from crack speed, creep-rupture, or fatigue data and the basic material exponents, as given by Eq.(23).

We have compared the value of the exponent q found from crack growth and failure data in tests conducted on different polymeric materials. It is often found that the value corresponding to k in Eq.(18) agrees with the data. Some examples are discussed in the next section. In contrast, for metals undergoing viscous creep ($n=1$), Eq.(20) appears to provide the best agreement (1); typically for metals $N<<1$, and thus there is little difference between Eqs.(19) and (20).

EXAMPLES AND CONCLUDING OBSERVATIONS

The generalized J theory may be employed in different ways to characterize and predict failure behavior of materials (1). Also, as noted above, it provides a direct relation between fracture response and basic creep characteristics; only this aspect will be examined here.

Crack speed and overall specimen fracture was studied in (16, Part III) in which the linear theory was applied to a polyurethene rubber. For the material used, $n=0.5$, $\hat{N}=1$, and Eqs.(18) and (23) predict $q=6$; this value of q is in excellent agreement with the data, providing good evidence that Γ and σ_m are constant. The theory in (16) did not account for the local nonlinearity, as defined by N; as shown here, even though this exponent may not be unity, it has no effect on q (unless, of course, Eq.(20) were to apply).

Application of the theory to composite materials is not necessarily straightforward and, in fact, considerable additional analysis may be required to relate overall loads and deformations to J_v for microscale phenomena governed by Eq. (9) and more specifically by Eq.(17). This complexity is due in part to the fact that the creep compliance D in Eq.(5) for the neighborhood of crack tips may be different for the macroscale of a composite material. On the other hand, if the matrix constituent of a composite is homogeneous and obeys Eq.(5), and the reinforcement phase is essentially rigid, the creep compliance will be the same regardless of the scale of the deformation process. Stress and environment-induced phase changes (e.g., glass-to-rubber transition at crack tips) introduces additional complexity. Temporarily setting aside such concerns, let us consider the data in Figs.3 and 4. For the fatigue loading case, Fig.3, and using either a dominant flaw model, Eq.(25), or a matrix degradation model with uniformly distributed microflaws (23) (each of which obeys Eq.(25)) we anticipate that $q=2(1+1/n)$; it is assumed that any global nonlinearity is due to microcracking, and therefore $\hat{N}=1$. Inasmuch as the zero-time (glassy) compliance is neglected in this comparison, and the value of q is based on k in Eq.(18), we suggest that the cracking process is controlled by polymer matrix above the glass transition temperature; the very high stresses in the matrix around microcracks are thus assumed to lower the glass transition temperature below the local temperature (which may be elevated due to heat generation)(24). For a fiber-dominated laminate the value of q is larger than in Fig.3 (21, Phase III). As indicated in Fig.4, $q=2(1+1/n)$ for the solid propellant if the data are normalized to constant strain level through the function f; data actually obtained in constant strain tests obey $q=2(1+1/n)$ (22). It is believed the interaction of far-field microcracking with the macrocrack causes this strain-dependence (1).

Clearly, there are many factors that have to be accounted for in the development of models for micro- and macro-cracking of composites. But, it is believed that the fracture theory in this paper will prove useful in a systematic mechanics approach in view of the present encouraging results and the broader theoretical basis developed in (1).

ACKNOWLEDGMENT

Sponsored by the Air Force Office of Scientific Research, Office of Aerospace Research, United States Air Force.

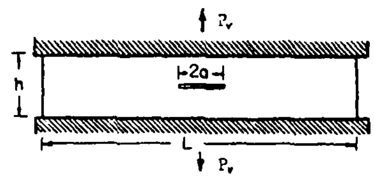

Fig.2 A cracked strip or slab. Also, an elementary model for microcracking in the soft matrix phase of a composite.

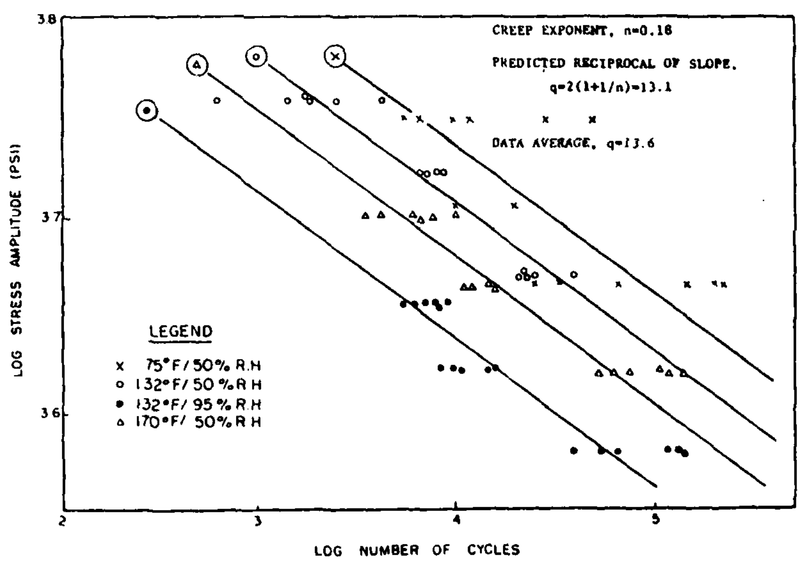

Fig.3 The S-N curve of $[\pm45/90_2]_s$ tensile fatigue coupons of graphite/epoxy (AS/3501-6); creep exponent from (21, Phase II). Specimen moisture and temperature levels are in equilibrium with indicated environments. Frequency = 3 HZ, stress ratio = 0.1. After (21, Phase III).

REFERENCES

1 Schapery, R. A., "Correspondence Principles and a Generalized J Integral Theory for Deformation and Fracture Analysis of Nonlinear Viscoelastic Media," In three parts. Texas A&M University Report Nos. MM 3724-81-1 through -3, 1981, College Station, TX.

2 Rice, J. R., "A Path Independent Integral and the Approximate Analysis of Strain Concentration by Notches and Cracks," J. Applied Mechanics, ASME, Vol. 35, 1968, pp. 379-386.

3 Rolfe, S. T. and Barsom, J. M., Fracture and Fatigue Control in Structures, Prentice-Hall, Englewood Cliffs, NJ, 1977.

4 Rice, J. R., "Elastic-Plastic Fracture Mechanics," in The Mechanics of Fracture, F. Erdogan, Ed., ASME-Pub. No. AMD-Vol. 19, 1976, pp. 23-53.

5 Knowles, J. K. and Sternberg, E., "An Asymptotic Finite-Deformation Analysis of the Elastostatic Field Near the Tip of a Crack," J. Elasticity, Vol. 3, 1973, pp. 67-107.

6 Eshelby, J. D., The Continuum Theory of Lattice Defects, Solid State Physics, Vol. 3, Academic Press, New York, 1956.

7 McMeeking, R. M., "Finite Deformation Analysis of Crack-Tip Opening in Elastic-Plastic Materials and Implications for Fracture," J. Mech. Phys. Solids, Vol. 25, 1977, pp. 357-381.

8 Rice, J. R., "The Mechanics of Quasi-Static Crack Growth," Proc. 8th U. S. National Congress of Applied Mechanics, Western Periodicals Company, North Hollywood, CA, 1978, pp. 191-216.

9 Landes, J. D. and Begley, J. A., "A Fracture Mechanics Approach to Creep Crack Growth," Mechanics of Crack Growth, ASTM STP 590, American Society for Testing and Materials, 1976, pp. 128-148.

10 Sakata, M. and Finnie, I., "Application of Fracture Mechanics to Creep Crack Propagation," Proceedings Japan Soc. Mech. Engrs. (in Japanese), 1972, pp. 177-180.

11 Ohji, K., Ogura, K., and Kubo, S., "Application of J-Integral to Creep Crack Problems," Proc. Japan Soc. Mech. Engrs. (in Japanese) No. 740-11, 1974, p. 270.

12 Kubo, S., Ohji, K., and Ogura, "An Analysis of Creep Crack Propagation on the Basis of the Plastic Singular Stress Field," Engineering Fracture Mechanics, Vol. 11, 1979, pp. 315-329.

13 Ohtani, R. and Taira, S., "Effects of Nonlinear Stress-Strain Rate Relation on Deformation and Fracture of Materials in Creep Range," ASME J. Eng'g Materials and Technology, Vol. 101, 1979, pp. 369-373.

14 Taira, S., Ohtani, R., and Komatsu, T., "Application of J-Integral to High-Temperature Crack Propagation-Part II-Fatigue Crack Propagation," ASME J. Eng'g Materials and Technology, Vol. 101, 1979, pp. 162-167.

15 Schapery, R. A., "A Theory of Crack Initiation and Growth in Viscoelastic Media: I. Theoretical Development," Int. J. Fracture, Vol. 11, 1975, pp. 141-159.

16 Schapery, R. A., "A Theory of Crack Initiation and Growth in Viscoelastic Media," Int. J. Fracture; Part II. "Approximate Methods of Analysis," Vol. 11, 1975, pp. 369-388; Part III. "Analysis of Continuous Growth," Vol. 11, 1975, pp. 549-562.

17 Knauss, W. G., "On the Steady Propagation of a Crack in Viscoelastic Sheet: Experiments and Analysis," In Deformation and Fracture of High Polymers, Edited by H. H. Kausch, J. A. Hassell, and R. I. Jaffee, Plenum Press, New York, 1973, pp. 501-541.

18 Knauss, W. G., "Fracture of Solids Possessing Deformation Rate Sensitive Material Properties," in The Mechanics of Fracture, F. Erdogan, Ed., ASME Pub. AMD-Vol. 19, 1976, pp. 69-103.

19 Brockway, G. S. and Schapery, R. A., "Some Viscoelastic Crack Growth Relations for Orthotropic and Prestrained Media," Eng'g Fracture Mechanics, Vol. 10, 1978, pp. 453-468.

20 Schapery, R. A., "A Method for Predicting Crack Growth in Nonhomogeneous Viscoelastic Media," Int. J. Fracture, Vol. 14, 1978, pp. 293-309.

21 Ho, T., "The Effect of Environment on the Mechanical Behavior of AS/3501-6 Graphite/Epoxy Material." Department of the Navy, Naval Air Systems Command, Contract Nos. N00019-78-C-0599 (Phase II) and N00019-79-C-0580 (Phase III). Vought Corporation Report (Phase II, Jan. 1980; Phase III, Jan. 1981), Dallas, TX.

22 Schapery, R. A., "Fracture Mechanics of Solid Propellants," in Fracture Mechanics, edited by N. Perrone, H. Liebowitz, D. Mulville, W. Pilkey, Univ. Press of Virginia, Charlottesville, 1978, pp. 387-398.

23 Schapery, R. A., "Deformation and Failure Analysis of Viscoelastic Composite Materials," Chapt. 5 in Inelastic Behavior of Composite Materials, C. T. Herakovich, Ed., ASME Pub. AMD-Vol. 13, 1975.

24 Struik, L. C. E., Physical Aging in Amorphous Polymers and Other Materials, Elsevier Press, 1978.

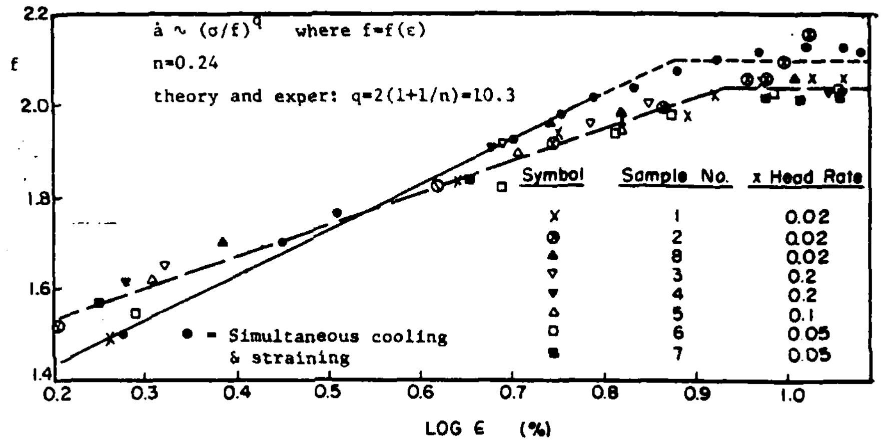

Fig.4 Crack propagation in strip-biaxial specimens of an HTPB propellant (ϵ is in percent and cross-head rate is constant and given in inches/min). After (22).

DATE
FILMED

8